The Messenger

No. 137 – September 2009

Astronomy in Austria
NACO Pupil-stabilised Coronography
Images from VLTI
Wandering in the Redshift Desert

ESO

Astronomy in Austria

Sabine Schindler[1]

[1] Institute of Astro- and Particle Physics, University of Innsbruck, Austria

Austria officially became the fourteenth ESO member in June 2009. A brief outline of the recent developments and scientific highlights of astronomical research in Austria is presented. Having started from a relatively low level a few years ago, astronomical research is now expanding very rapidly thanks to the accession to ESO.

Research in astronomy in Austria is conducted at three universities: the University of Vienna at the Institute of Astronomy; the University of Innsbruck at the Institute of Astro- and Particle Physics; and the University of Graz at the Institute for Physics. Some additional astronomy or related research is conducted at various other places such as the Institute for Space Research of the Austrian Academy of Sciences in Vienna. In total there are currently 27 staff members and many young people working at the three university institutes. The research topics cover a very wide range: from solar physics at Graz[1]; astroseismology, the late stages of stellar evolution, planetary systems, the interstellar medium, the Milky Way, structure of galaxies, galaxy clusters, the history of astronomy and participation in the CoRoT and Herschel missions at Vienna[2]; to planetary nebulae, novae, galaxy structure, galaxy clusters and astroparticle physics at Innsbruck[3].

Recent developments

For many decades it was the goal of Austrian astronomers to join ESO. Fortunately, accession to ESA was achieved in 1987, but accession to ESO proved to be more difficult. There were several attempts and a lot of effort spent by the scientists to convince the relevant authorities that ESO membership is a must for an active astronomical community. Several studies evaluating the quality of the institutes and the scientists were conducted. Astronomers have made increasing efforts over recent years to increase national and international visibility, working towards eventually securing a positive result. These efforts included the acquisition of an increasing number of grants (from national and international sources), of extending international collaborations, of enhancing public outreach activities and of increasing the publication rate (see Figures 2, 3 and 4). Eventually, the ESO accession document was signed in 2008 (see the ESO press release of 30 June 2008) and ratified in February 2009.

With Austria's new place in the international scientific community confirmed by its accession to ESO, further development is secured. In Innsbruck a new full professorship was recently filled in astroparticle physics, in Vienna two new full professors for astrophysics are in the process of being appointed and in Innsbruck two more astronomy(-related) full professorships are planned, to be announced in 2010. So from the low state in 2001, with just one full professorship in astronomy, with three more filled before the ESO accession and the five new ones in prospect, there will be nine full professors within a few years, i.e. an increase by a factor of nine over ten years. This development allows an optimistic view of the future of Austrian astronomy.

Furthermore, the number of science topics being pursued has developed in recent years. Previously the Austrian strength was mainly in stellar astrophys-

Figure 1. The Institute of Astronomy at the University of Vienna.

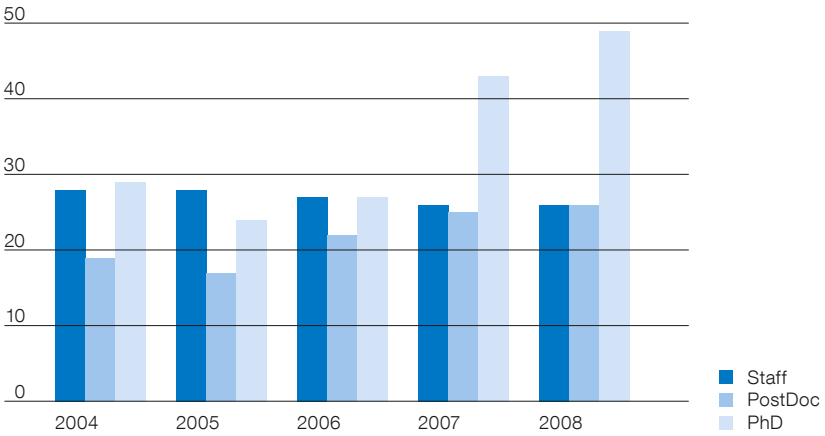

Figure 2. Growth in the total number of personnel at the three university astronomical institutes in Graz, Innsbruck and Vienna over the last five years. While the permanent staff numbers have stayed almost constant, there is a clear increase in the number of postdocs and PhD students. In 2009 an even greater increase in these numbers is expected.

ics, but there are now several active extragalactic groups, along with more connections to other fields such as mathematics and computer science, a natural extension because of the large numerical simulations performed by some groups. This year has also seen the establishment of astroparticle physics in Austria (including membership of the High Energy Stereoscopic System [HESS] collaboration).

As in the rest of Europe, the Bachelor/Master system was also introduced in Austria. While the Universities of Graz and Innsbruck offer a Bachelor of Physics and a Master of Physics, which include many astrophysics courses, the University of Vienna offers a Bachelor of Astronomy and a Master of Astronomy. All three universities also offer a PhD programme, partly in connection with doctorate schools.

The Austrian Society for Astronomy and Astrophysics

In order to adequately represent the Austrian astronomical community in pursuing the accession to ESO, the Austrian Society for Astronomy and Astrophysics (ÖGAA) was founded in 2002. This was an important step towards ESO membership, but, increasingly, it also serves many other purposes. This society holds an annual meeting, at which all Austrian astronomers meet to present new results and discuss new developments. The society performs joint public outreach activities, keeps in contact with amateur astronomers and supports young people.

Scientific highlights

Austrian astronomy can look back on a long history of astrophysics, including the Nobel laureate Victor Franz Hess, who discovered cosmic rays in 1911. Nowadays many modern science topics are addressed, of which a few recent highlights are selected and presented here.

Figure 3. Number of refereed publications resulting from the three university astronomy institutes in Austria over the last five years.

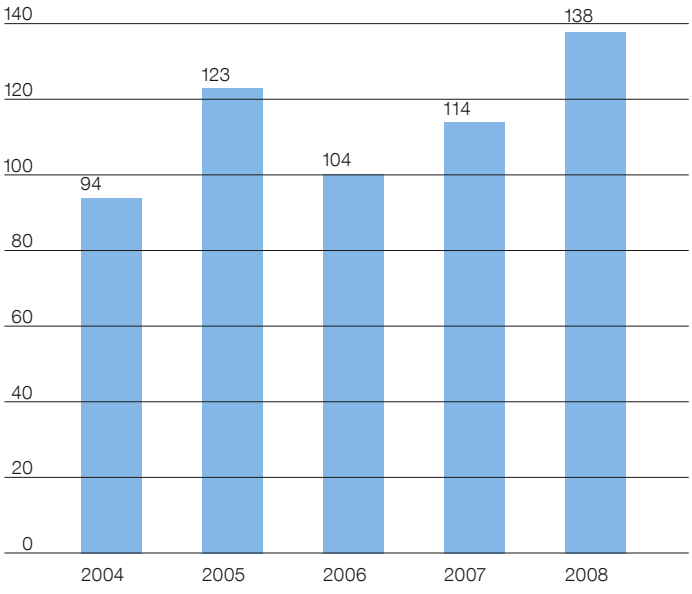

Figure 4. Acquired grants (in €) for the three Austrian university astronomy institutes over the last four years.

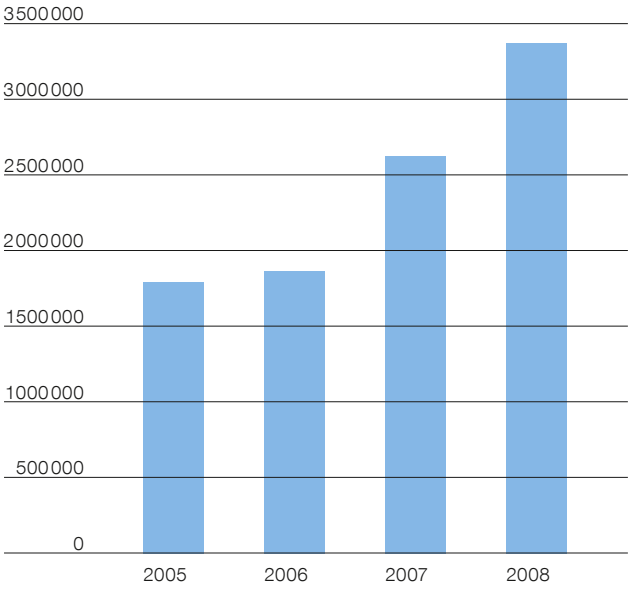

Towards a new Maunder Minimum?

The current solar activity minimum is longer lasting than previous ones (up to around 1900). Will there be a new prolonged phase of strongly reduced solar activity like that during the Maunder Minimum, which lasted from 1645–1715 and coincided with the peak of the "little Ice Age" in Europe? The activity of the Sun is monitored and "space weather", which is strongly influenced by solar activity, is studied. Solar activity influences the ionisation of the upper atmosphere and the propagation of radio signals and GPS signals can be severely disturbed (see the depiction in Figure 5). Due to the expanding atmosphere, satellite orbits can become unstable and the radiation can endanger human activities in space. At the solar monitoring observatory at Kanzelhöhe, data are taken and used in combination with other observations to predict the upcoming solar activity maximum. The first predictions for the new maximum (2011) were revised and the next maximum is expected to occur two or three years later, and its amplitude is predicted to be lower than the previous one. Applying methods of nonlinear dynamics, it has been shown that solar activity behaves regularly on a longer term basis, but is affected by the onset of chaos on smaller scales (Brajša et al., 2009). For these calculations solar activity proxies have been used (such as cosmogenic isotopes).

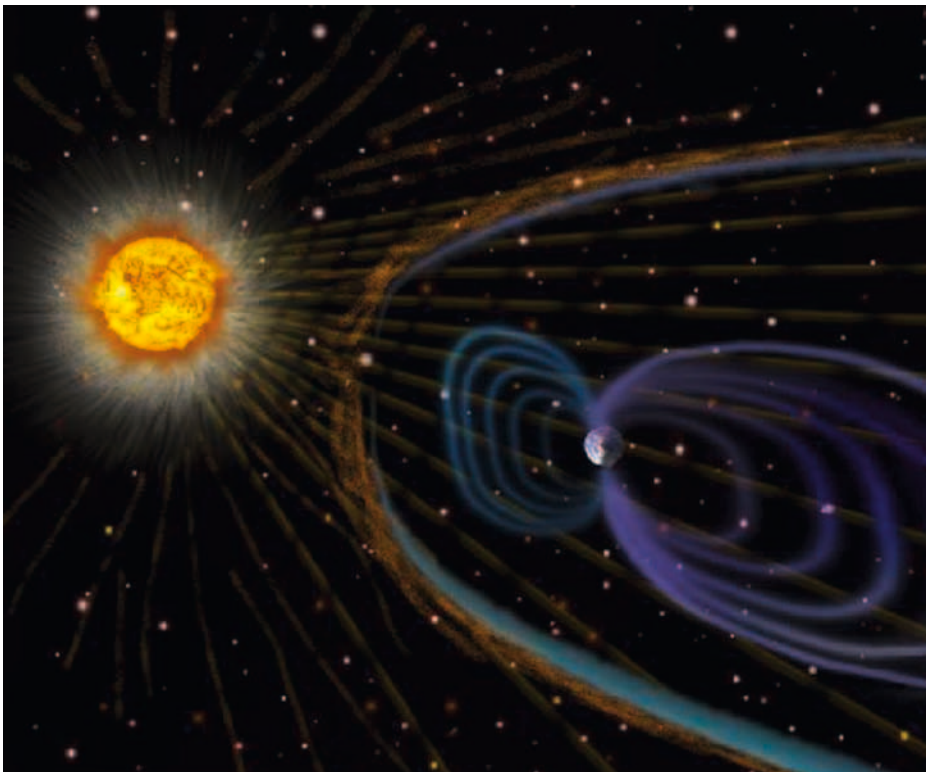

Figure 5. The solar wind interacting with the Earth's magnetosphere. It compresses the magnetosphere on the side facing the Sun. This can cause magnetic storms and, during strong solar events, such as flares or coronal mass ejections, even power lines on Earth can fail.

Star formation between galaxies

While it was thought previously that galaxy evolution is mainly determined by internal processes, it is now clear that the environment plays an important role. Ram-pressure stripping of galaxies in clusters (removal of the interstellar medium by the pressure of the intracluster medium) in particular has turned out to be much more efficient than previously thought (Rödiger & Hensler, 2005; Schindler et al., 2005; Domainko et al., 2006). Therefore numerical simulations of spiral galaxies moving through the intracluster medium have been performed. It was found that gas is stripped, not simply dispersed, into the intracluster medium, and it becomes clumpy, due to external pressure and radiative heating (Figure 6). In this clumpy gas new stars can form, so that the star formation rate is increased considerably by the stripping process, and in extreme cases the increase in star formation can even be up by a factor of ten (Kronberger et al., 2008). Interestingly the stars not only form in the disc, but also in the wake behind the galaxy. Many of these stars are not bound to the galaxy, so that we have found a process that produces a population of new stars in

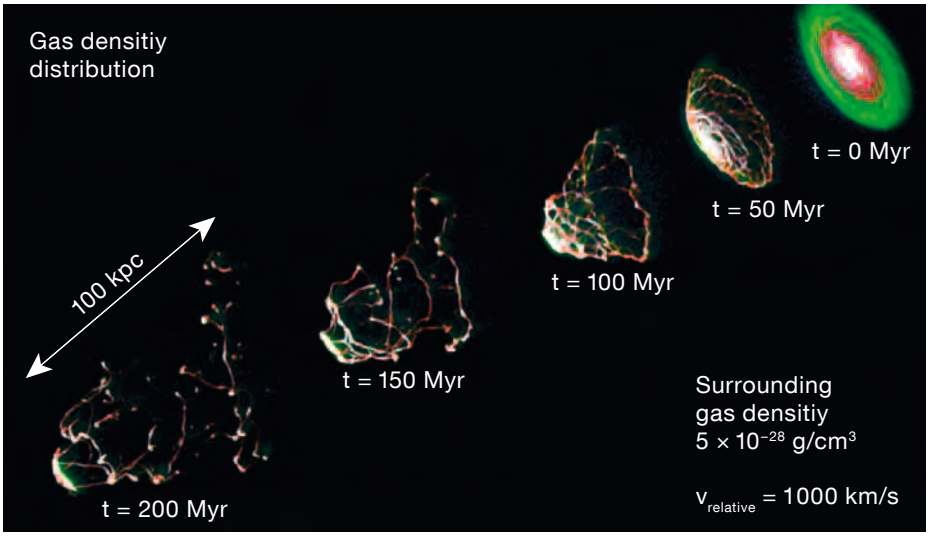

Figure 6. Simulation of a galaxy moving through the intracluster gas. The interstellar medium is stripped off by ram pressure and forms clumpy structures behind the galaxy. In these structures stars, which are no longer bound to the galaxy, can form.

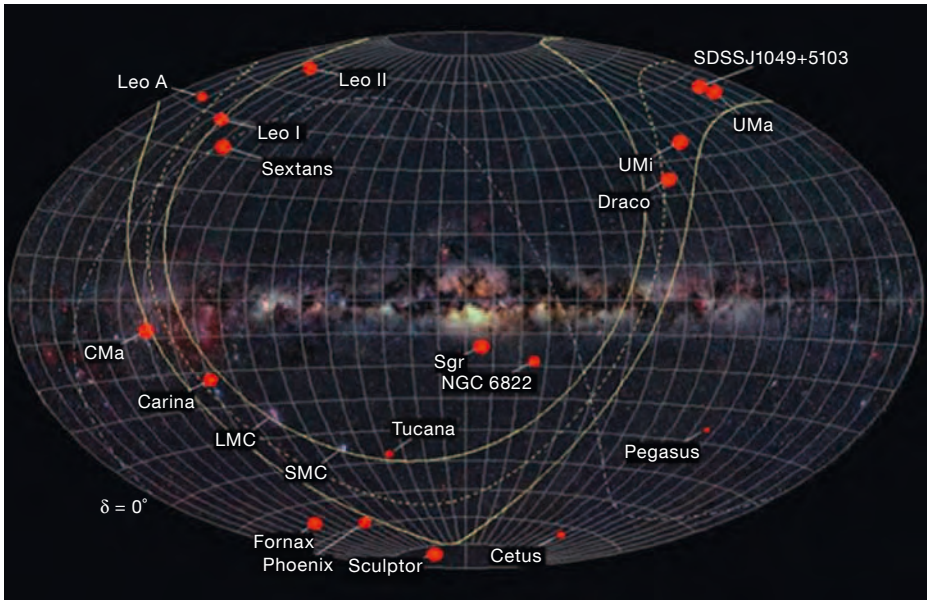

Figure 7. The disc of satellites around the Milky Way.

the space between the galaxies (Kapferer et al., 2009). The required densities for this process to take place are not as high as expected: ram pressure with star formation can also take place at distances of 1 Mpc from the cluster centre, i.e. it is expected that this is a very common process.

Galaxy mergers and the origin of satellite galaxies

Gravitational tides are widely understood to strip and destroy galactic substructures. In the course of a galaxy merger compressive tides may develop and prevent star-forming regions from dissolving, after they have condensed to form clusters of stars. A statistical study of such compressive modes of the galaxy merger in NGC 4038/39 (the Antennae) showed that around 15 % of the disc material undergoes compressive tides at the pericentre (Renaud et al., 2008). In addition, secondary structures form when gas-rich galaxies interact: conservation of angular momentum and energy leads to expanding tidal arms which fragment and form star clusters of varying size up to dwarf galaxy type objects. The formation of such "tidal dwarf galaxies" is therefore an inherent part of any cosmological structure formation theory. Detailed modelling of the evolution of such tidal dwarf galaxies in their host's potential shows that they are not easily destroyed by the host tide or their own internal energy release due to star formation (Hensler et al., 2004; Recchi et al., 2007). This issue combines two effects seen in the satellite galaxies surrounding our Milky Way: first, there are far fewer than expected from the Lambda Cold Dark Matter (ΛCDM) cosmology; and, secondly, the eleven brightest satellites of the Milky Way lie more or less in the same plane (see Figure 7 and Kroupa et al., 2005) and rotate with the same spin direction as the orbit vector. This phenomenon leads one to argue that it can only be explained if the satellites were created a long time ago through collisions between younger galaxies, i.e. be of tidal origin (Metz et al., 2009). As a very strong but logical consequence, the satellite galaxies should also be free of dark matter, a finding that stands in fundamental conflict with kinematically derived total masses for these dwarf galaxies.

Detection of non-radial oscillation modes with long lifetimes in giant stars

Towards the ends of their lives, stars like the Sun expand greatly to become red giant stars. Such evolved stars can provide stringent tests of stellar theory, as many uncertainties in the internal stellar structure accumulate with age. Important examples are convective overshooting and rotational mixing during the central hydrogen-burning phase that determine the mass of the helium core, but which are not well understood. The analysis of radial and non-radial stellar oscillations can be used to constrain the mass of the helium core. Although all giants are expected to oscillate, it has hitherto been unclear whether non-radial modes are observable at all in red giants, or whether the oscillation modes have a short or a long mode lifetime, which determines the observational precision of the frequencies. Using data from the CoRoT mission, radial and non-radial oscillations were detected in more than 300 giant stars (De Ridder et al., 2009). For at least some of the giants, the mode lifetimes are of the order of a month. So far, no satisfactory theoretical explanation currently exists for these observations.

Public outreach

To "share exciting discoveries and the beauty of the Universe with the broad public" (as phrased by ESO), has been, is and will, of course, be an important goal for Austrian astronomers in the future. Promotion of astronomy to the Austrian public will be enhanced by membership of ESO through the, already widespread, activities that have taken place, partly within the framework of the International Year of Physics 2005, the International Heliophysical Year 2007 and the International Year of Astronomy 2009. Such activities comprise: lectures at various types of adult education centres, elementary and secondary schools (see Figure 8), universities and clubs (like Rotary Clubs, Lions Clubs, etc.); advanced training courses for school teachers; regular (and irregular) guided tours, including public use of telescopes at our institutes; various open air activities, partly in cooperation with amateur astronomers; indoor activities at, say, shopping centres, fairs and the like; an annual Austrian astronomy day; popular articles for newspapers and magazines; exclusive interviews for the press, as well as for radio and TV stations; and last, but not least, answering the widely varied questions sent in by telephone or e-mail on phenomena in the night and day sky.

This list of outreach activities could easily be extended. It is expected that this kind of work will certainly "wax, rather than wane". Austrian astronomers are pleased to react to their new membership at ESO, not only with respect to an improved scientific output, but also in regard to an increased interaction with the public. After all, Austrian taxpayers (also) have the right to know what happens when their money is spent on "heavenly matters".

Figure 8. Children at a 3D presentation of simulated galaxies.

References

Brajša, R. et al. 2009, A&A, 496, 855
De Ridder, J. et al. 2009, Nature, 459, 398
Domainko, W. et al. 2006, A&A, 452, 795
Hensler, G., Theis, C. & Gallagher, J. S. 2004, A&A, 426, 25
Kapferer, W. et al. 2009, A&A, 499, 87
Kronberger, T. et al. 2008, A&A, 481, 337
Kroupa, P., Theis, C. & Boily, C. M. 2005, A&A, 431, 517
Metz, M. et al. 2009, MNRAS, 394, 2223
Recchi, S. et al. 2007, A&A, 470, L5
Renaud, F. et al. 2008, MNRAS, 391, L98
Rödiger, E. & Hensler, G. 2005, A&A, 433, 875
Schindler, S. et al. 2005, A&A, 435, L25

Links

[1] http://www.uni-graz.at/igamwww
[2] http://astro.univie.ac.at
[3] http://astro.uibk.ac.at

Adriaan Blaauw, the former ESO Director General (1970–1974), paid a return visit to ESO Headquarters on 16 July 2009. He is shown here seated in the library where he was consulting the Oort Library, donated by the late Jan Hendrik Oort to ESO. Adriaan Blaauw, now aged 95, is the author of *ESO's Early History* and set up the ESO Historical Archives collection, which is housed at ESO headquarters. During his visit he reviewed the collection and was able to include some additional historical documents.

A section of the 130-metre-long VLTI tunnel showing the tracks on which carriages for the reflectors of the delay lines run and adjustment work taking place.

Direct Imaging of Exoplanets and Brown Dwarfs with the VLT: NACO Pupil-stabilised Lyot Coronagraphy at 4 µm

Markus Kasper[1]
Paola Amico[1]
Emanuela Pompei[1]
Nancy Ageorges[2]
Daniel Apai[3]
Javier Argomedo[1]
Nick Kornweibel[1]
Chris Lidman[1]

[1] ESO
[2] Max-Planck-Institut für extraterrestrische Physik, Garching, Germany
[3] Space Telescope Science Institute, Baltimore, USA

NACO is the versatile adaptive optics assisted near-infrared instrument at the VLT. Among its many modes it offers spectral differential imaging that efficiently enhances the contrast in searches for faint companions. Recently, an additional method to calibrate quasi-static speckles through angular differential imaging has been developed, offering the option to operate NACO in a pupil-tracking mode. Using this new mode, in combination with Lyot coronagraphy and an optimal choice of observing wavelength in the thermal infrared around 4 µm, allows NACO to reach unprecedented sensitivities for masses of companions for all but the hottest exoplanets, beginning to open up the mass domain targeted by future instruments such as SPHERE.

For about half a decade surveys for planetary-mass companions have been carried out in the near-infrared (near-IR) by three methods: broadband imaging (e.g., Chauvin et al., 2003; Masciadri et al., 2005); spectral differential techniques in narrowband filters inside and outside the *H*-band, using the methane absorption features to subtract speckle noise efficiently (called spectral differential imaging [SDI]; see, for example, Biller et al., 2007); and using angular differential imaging techniques (ADI; see Lafrenière et al., 2007). In addition, specialised instruments (e.g., NICI at Gemini South and HiCiao at Subaru) that even combine *H*-band SDI with ADI recently began operation and are expected to produce first results very soon. The improved understanding of the high-contrast imaging problem and corresponding improvements in ground-based instrumentation and observing strategies have recently led to the first direct images of planetary-mass companions around the early-type (around A5) stars HR8799 (Marois et al., 2008) and Beta Pic (Lagrange et al., 2009). Table 1 lists possible planetary-mass companions discovered by ground-based direct imaging, together with their separation and the contrast in magnitudes to their host stars in various bands.

Table 1. Possible planetary-mass companions discovered by direct imaging.

Object	Contrast (mag)	Separation (arcsec.)	Discovery instrument and reference
2M1207 b	ΔJ = 7 ΔH = 5.7 ΔK = 5 ΔL = 3.6	0.77	NACO Broadband (Chauvin et al., 2005)
GQ Lup b	ΔH = 6 ΔK = 6.2 ΔL = 5.8	0.73	NACO Broadband (Neuhäuser et al., 2005)
Beta Pic b	ΔL = 7.7	0.41	NACO *L'* (Lagrange et al., 2009)
HR 8799 b	ΔJ = 13.9 ΔH = 12.6 ΔK = 11.8 ΔL = 10.5	1.73	Keck NIRC2/Gemini NIRI Broadband, ADI (Marois et al., 2008)
HR 8799 c	ΔJ = 12.2 ΔH = 11.6 ΔK = 10.9 ΔL = 9.5	0.95	Keck NIRC2/Gemini NIRI (Marois et al., 2008)
HR 8799 d	ΔJ = 12.9 ΔH = 11.6 ΔK = 10.9 ΔL = 9.4	0.63	Keck NIRC2/Gemini NIRI (Marois et al., 2008)

The advantages of the thermal infrared, especially the long end of the *L*-band, have only recently been realised (e.g., Kasper et al., 2007; Janson et al., 2008). This wavelength range offers considerable advantages compared to shorter wavelengths, the most important one being the improved contrast of planetary-mass companions with respect to their host stars. Models predict *H–L* colours of around 2 mag for a 1000 K companion (a 5 Jupiter mass [M_J] object at an age of 30 Myr or a 30 M_J object at 1 Gyr) and an *H–L* colour ~ 4.5 mag for a 350 K companion (1 M_J at 30 Myr or 5 M_J at 1 Gyr). Obviously, the *L*-band offers tremendous gains for observing lower mass and older objects. As an example, the planetary-mass companion to the brown dwarf 2M1207, or the companions of HR 8799 (see Table 1), have an *L*-band contrast with respect to their host stars which is about 2 magnitudes more favourable than in the *H*-band! An additional advantage of adaptive optics (AO) assisted *L*-band over shorter wavelength observations is the better and more stable image quality, with Strehl ratios well above 70 %, and sometimes as high as 85 %, thus reducing speckle noise and facilitating point spread function (PSF) subtraction. All these advantages more than compensate for the increased sky background in the thermal infrared.

In the following, we describe the science requirements for high-contrast imaging and the technical tests that were carried out with NACO in pupil-tracking mode using the NB4.05 filter with and without the 0.7-arcsecond diameter stop of the Lyot coronagraph. This combination of NACO instrument settings (Pupil Stabilised Coronagraphy at 4 µm, hereafter denoted PSC4Mu) is identified as the currently most sensitive mode for planetary-mass companion detection in the close vicinity of bright stars, worldwide. Using it, NACO is even sensitive to mass regimes similar to the ones that will be become accessible with SPHERE, albeit at larger orbital separations. Hence, NACO PSC4Mu will be able to nicely complement detections with SPHERE in the thermal IR.

Science requirements

Burrows et al. (2003) explored the spectral and atmospheric properties of brown

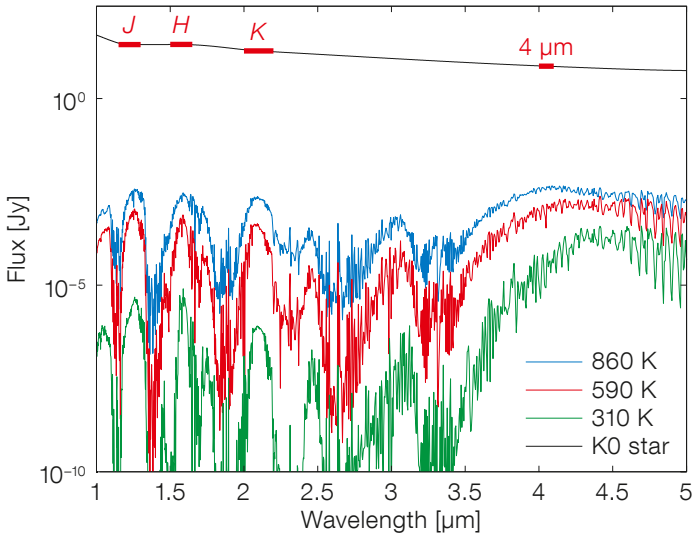

Figure 1. Absolute flux density of giant exoplanets in the near- to mid-IR. For reference, the black lines indicate the flux of a K0 star located at 10 pc in several filters (see Table 2).

Filter	λ_1 [μm]	λ_2 [μm]
J	1.20	1.25
H	1.55	1.60
K	2.05	2.15
L′	3.50	4.10
4 μm	4.0	4.10

Table 2. Filter widths assumed for the contrast analysis. The filters are assumed to transmit all radiation between limits λ_1 and λ_2 and block it completely outside these limits.

dwarfs cooler than the latest known T dwarfs. Their focus was on the yet-to-be-discovered free-floating brown dwarfs in the T_{eff} range from ~ 800 to ~ 130 K and with masses from 25 to 1 M_J. Evolutionary models were used to determine T_{eff} as a function of age and mass, and atmospheric models were used to calculate the resulting spectra. Burrows et al. (2003) concluded that studies in the mid-infrared could assume a new, perhaps transformational, importance in the understanding of the coolest brown dwarfs and giant exoplanets. The modelled spectral energy distributions (SEDs) provided by Burrows were used for the analysis and conversion between point spread function contrast and detectable planet mass.

Since the radius of a giant planet rapidly converges to around 1 Jupiter radius (R_J) and surface gravity effects play only a minor role, the planet's spectrum is primarily determined by the planet's effective temperature, which is a function of its mass and age. Figure 1 shows the absolute flux of giant exoplanets in the near- to mid-IR for different effective temperatures. The red lines indicate the flux of a K0 star located at 10 parsecs (pc) in several filters for reference. The non-blackbody SED with pronounced absorption in the H_2O, CH_4 and NH_3 molecular bands is striking. It is also apparent from this figure that the flux contrast between star and planet at 4 μm is greater than in the near-IR, hence this wavelength is more favourable for planet detection. This contrast advantage increases towards lower effective temperatures and thus toward older and lower mass planets.

Based on these simulated spectra, the contrasts were calculated for the spectral regions/filters listed in Table 2. For each near-IR band, the regions with the most favourable possible contrasts (unaffected by molecular absorption) are used in the comparisons. While the planet/star contrast ratio is fairly similar in the near-IR (*J, H, K*) for all values of T_{eff}, it is clear that the contrast at 4 μm is always superior to that in the near-IR by factors between ~ 5 (at 800 K) and ~ 50 (at 300 K), as evident from Figure 2.

The price to be paid when observing in the thermal IR is the reduced sensitivity because of the increased sky background. On Paranal, for example, the typical instrumental background (sky + telescope)[1] in the *H*-band is 14.4 mag arcsecond^{-2}, while the background in *L*-band is 3.9 mag arcsecond^{-2}. Using the NACO exposure time calculator (ETC), background-limited 5σ detection of magnitude 16.3 point sources is possible in 2 hours using the NB4.05 filter (i.e. the red end of *L′* filter, which is best for exoplanet detection), while in the same time in the NB1.64 filter (*H*-band, SDI-like filter width), sources as faint as 21.7 mag can be detected. As shown in Figure 3, *H*-band and 4 μm filters have a similar background-limited sensitivity for ~ 300 K objects, while the *H*-band is more sensitive for warmer objects (i.e. the *H*–4-μm colour varies between 4.5 for T_{eff} = 300 K and 2 for T_{eff} = 850 K). Objects with temperatures around 300 K would be detectable in both filters up to about 10 pc distance (the absolute magnitude is similar to the background-limited detectivity), while a 600 K planet would be detected up to a distance modulus of ~ 3 mag or 40 pc at 4 μm and up to a distance modulus of 5.7 or 140 pc in

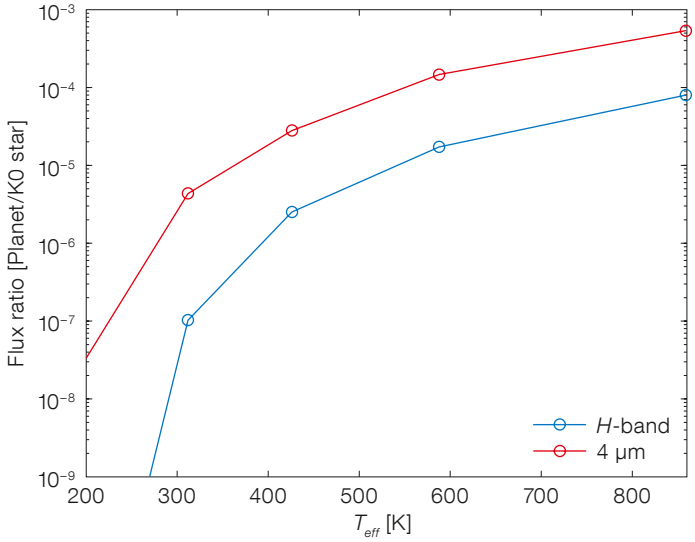

Figure 2. Contrast ratio of a planet to host K0 star as a function of the planet's effective temperature for *H*-band, shortwards of the CH_4 absorption (in blue) and 4 μm observations (in red).

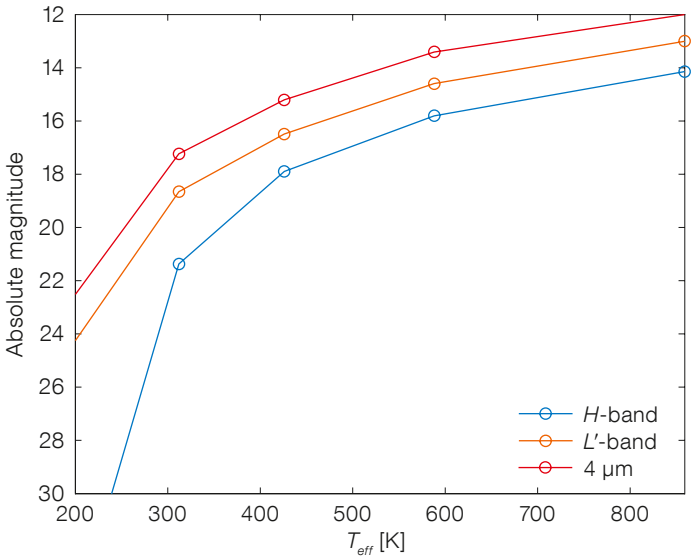

Figure 3. Absolute magnitudes of exoplanets in different filters as a function of effective temperature in the *H*, *L′* and 4 µm bands.

H-band. Thus, isolated warm planets are more easily detected in the near-IR because of the lower sky background. Figure 3 also shows the absolute magnitude of exoplanets in *L′* to demonstrate the 1–1.5 magnitude advantage of the 4 µm filter. The 4 µm filter is at a favourable wavelength to cover just the peak of the spectrum (see Figure 1), while the shorter end of *L′* does not capture much flux from an exoplanet.

NACO pupil-stabilised imaging at 4 µm

One of the main impediments to reaching the highest contrasts is the presence of quasi-static speckles that cannot easily be distinguished from a faint companion in a long-exposure image. These quasi-static speckles are created by imperfections or aberrations of the telescope and instrument optics and persist over time spans covering an observation. Hence, their intensity integrates in the same way as the exoplanet's flux and no improvement of contrast signal-to-noise ratio (SNR) in an ordinary image can be obtained with increase in the observing time.

However, efficient methods exist to calibrate quasi-static speckles and to improve contrast. SDI exploits the fact that speckles show spectral features of the star, while a reasonably cool exoplanet shows strong molecular bands that allow it to virtually disappear at certain wavelengths. Subtracting an image taken inside the molecular band from one taken in the adjacent continuum leaves the image of the planet, while removing the speckles. ADI is another method that can be used if the field of view, and hence the image of the exoplanet, is allowed to rotate with respect to the telescope/instrument configuration and hence the quasi-static speckle pattern. The difference between two images with relative field of view rotation would efficiently remove quasi-static speckles, while leaving the exoplanet (provided that the rotation is large enough to avoid overlap between the exoplanet's images at the desired angular separation). ADI is rather simple to implement for non-rotating instruments mounted at the Cassegrain focus of an alt-azimuth telescope, because only the field would rotate with the parallactic angle. The situation at the Nasmyth focus (where NACO is mounted) is more complex, since a stationary instrument would see both pupil and field rotating during observations. NACO is mounted instead on the adaptor-rotator that itself rotates the whole instrument in order to keep the field orientation fixed. An alternative rotation mode called pupil-tracking has recently been implemented to allow NACO to rotate with the pupil, effectively freezing the telescope/instrument relative orientation and hence the quasi-static speckle pattern. In this mode, the instrument field of view again rotates with the parallactic angle and true ADI is possible.

While SDI relies on a "known" spectrum of quasi-static speckles, ADI relies on temporally static aberrations. This is a strong assumption, especially because NACO still de-rotates the pupil with telescope altitude and so may experience significant variations of the gravity vector, leading to instrument flexure during an observation. ADI is most effective when observing an object passing through the meridian, because pupil rotation rate is a minimum while field *v.* pupil rotation rate is a maximum there.

The efficiency of the pupil-tracking mode of NACO was tested on a bright star close to the meridian in favourable DIMM seeing of 0.6–0.7 arcseconds. The AO performance with the 14 × 14 lenslet array was very good, delivering Strehl ratios higher than 80 % in the NB4.05 filter. While the fixed position of the pupil is demonstrated by the well-defined, unsmeared diffraction of the telescope spider arms, the parallactic angle changed and hence the field of view (FoV) rotated by almost 70 degrees over the 30-minute observation.

Individual 30-second exposures (DIT 0.2s, NDIT 150) were recorded on a dither pattern that allowed us to remove the sky background. Then the images were high-pass filtered to remove smooth PSF structures (atmospheric speckle halo) and increase the speckle contrast. Figure 4 shows a sequence of three 30-second exposures where the second image was taken 5 minutes and the third image 30 minutes after the first one. The speckle pattern shows a remarkable stability over a period of 30 minutes.

The rate of parallactic angle change is an important parameter for ADI image reduction. In order to avoid the overlap of a λ/D-sized object at 5 λ/D separation (λ/D ~ 0.1 arcseconds at 4 µm wavelength and the VLT), a minimum field rotation of 11.4° between two images is required. Typically, the rate of change of rotation for an object of declination –40° near the meridian observed from Paranal (latitude –24°) is of the order 0.015°/s. Hence, ADI reduction typically needs

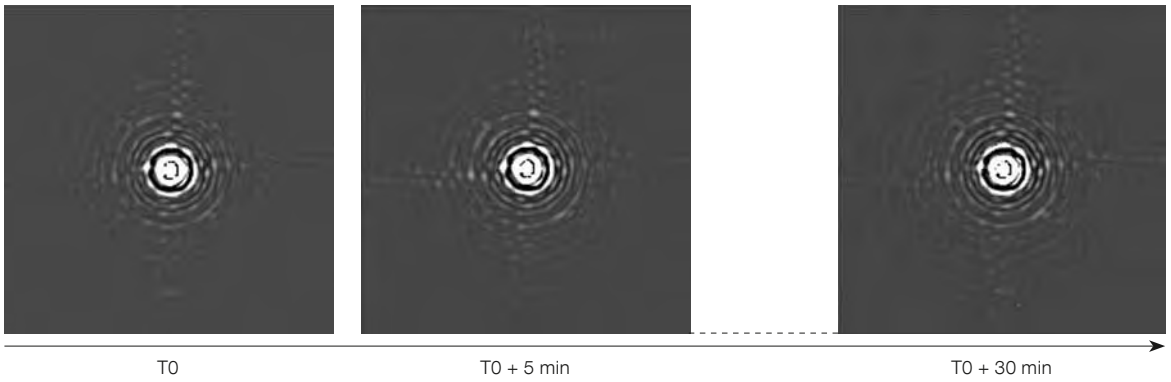

Figure 4. Sequence of three 30-second exposures in pupil-tracking mode, where the second was taken 5 minutes and the third 30 minutes after the first. The images were high-pass filtered to enhance the contrast of the speckle pattern.

image pairs separated by 11.4/0.015 seconds or at least 10 minutes in time.

The ADI reduction of the individual 30-second exposures now consists of the following major steps:
i) Images separated in time as close as the parallactic angle change allows (criterion, for example, > 11.4°) are re-centred and subtracted from each other. Here the normalisation can be quite difficult, since the intensity of the quasi-static speckle pattern scales with the AO-corrected Strehl ratio (better correction means stronger speckles!) and its determination is not always an easy task (e.g., when the stellar PSF core saturates the detector). Alternatively, one could also try to determine the normalisation factor that leads to minimum intensity in the subtracted image or in annuli of certain radii from the centre. Due to the stable seeing conditions and corresponding AO correction, no image normalisation was necessary here.
ii) The subtracted images are de-rotated by the parallactic angle offset to the first image of the pair and summed up.

The output of the ADI processing steps described above is given in Figure 5. For reference, artificial benchmark planets were inserted into the unprocessed data to verify the contrast levels calculated from the residual speckle pattern. Without a coronagraph, the PSF contrast of 4-μm ADI imaging beyond 0.5-arcsecond separation is already better than can be achieved with SDI, even without considering the additional contrast gain in planetary mass provided by the favourable planet-to-star contrast at 4 μm compared to the near-IR (Figure 2).

NACO pupil-stabilised coronagraphy at 4 μm

Even further contrast improvements can be expected from coronagraphy. The reduction of the Airy pattern by a coronagraph brings two major benefits:
i) It reduces the so-called “pinned” speckles that result from interference between light from the speckle and from the Airy rings. Since the intensity of a pinned speckle is proportional to the Airy intensity, the small classical Lyot coronagraph of NACO (0.7 arcsecond diameter mask and a Lyot stop undersized to 90 % of the pupil diameter) should reduce the intensity of pinned speckles by a factor of a few tens.
ii) It reduces the intensity of speckles originating from the optics after the coronagraphic mask (i.e. all optics inside CONICA) by the coronagraphic suppression of the PSF core, which is better than a factor of 100 in the case of the NACO small Lyot coronagraph.

To confirm the positive effect of the coronagraph, individual 1-minute exposures (DIT 1 s, NDIT 60) were recorded using NACO in pupil-tracking mode with the small Lyot coronagraph and the NB4.05 filter (PSC4Mu method), that will turn out to be most effective for exoplanet detection with NACO. One drawback of coronagraphy is that dithering is no longer possible and sky background has

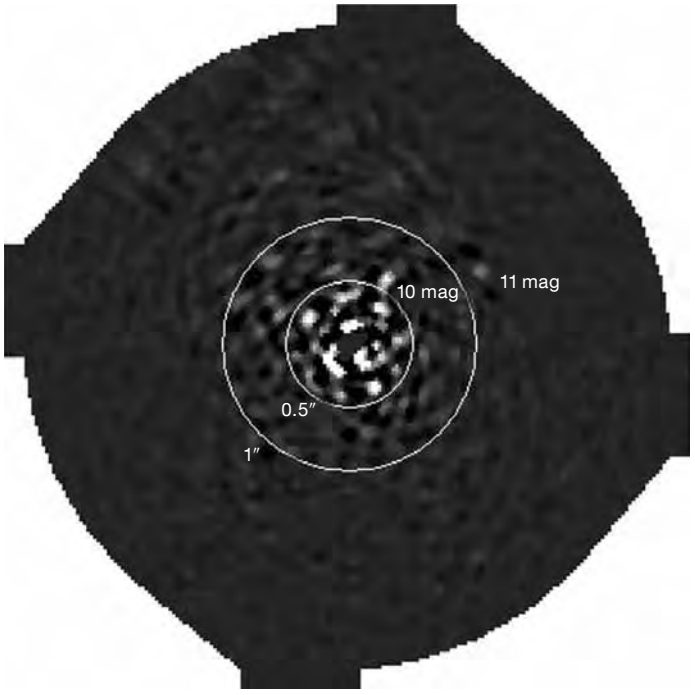

Figure 5. Final ADI processed non-coronagraphic image. Two artificial benchmark planets of delta magnitude 10 and 11, were inserted into the unprocessed data to verify the contrast level calculated from the residual speckle pattern.

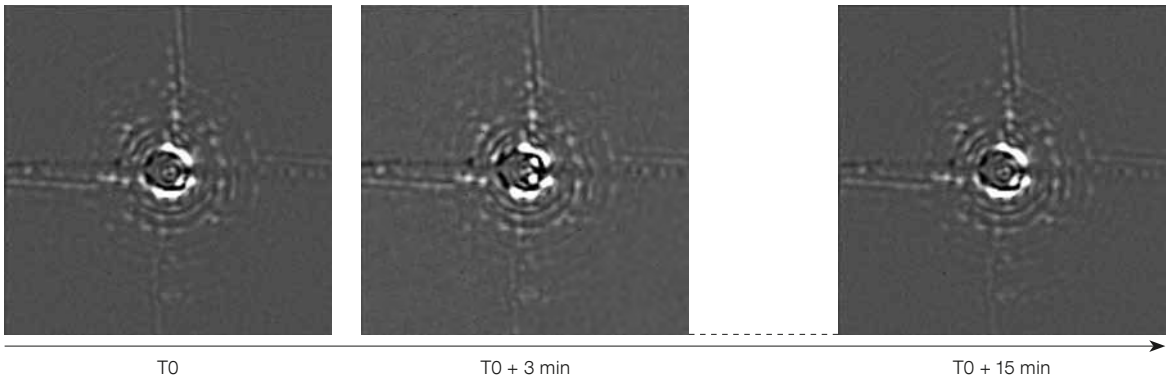

Figure 6. Sequence of three 1-minute exposures in pupil-tracking mode with coronagraphy, where the second was taken 3 minutes and the third 15 minutes after the first. The images were high-pass filtered to enhance the contrast of the speckle pattern.

to be recorded separately, thus decreasing the on-source efficiency. However, for small-field high-contrast imaging observations, the impact of a variable sky background mainly consists of constant offsets that can be removed very efficiently by the data reduction. Another complication is the movement of the star image relative to the coronagraphic mask (possibly introduced by an unstable mask position) that currently requires frequent manual adjustment of the star's position to keep it centred on the mask.

Figure 6 shows a sequence of three 1-minute exposures where the second image was taken 3 minutes and the third 15 minutes after the first image. Again, the speckle pattern shows a remarkable stability over 15 minutes. In addition, the intensity of quasi-static speckles is dramatically reduced in comparison to the non-coronagraphic images (Figure 4) as expected.

Following similar ADI data reduction steps as described above for the non-coronagraphic imaging, the final image shown in Figure 7 results. The same two artificial planets have again been inserted and now appear at a much better contrast SNR. Actually planets that are even more than 11 magnitudes fainter than the central star could be detected, with sufficient confidence, at separations larger than about 0.5 arcseconds. For angular separations smaller than 0.5 arcseconds, the achievable contrast quickly deteriorates and is worse than with non-coronagraphic imaging. At such separations, the impact of edge effects at the coronagraphic mask, which vary strongly with the precise centring of the star, dominate over residual speckle intensity and degrade the achieved contrast.

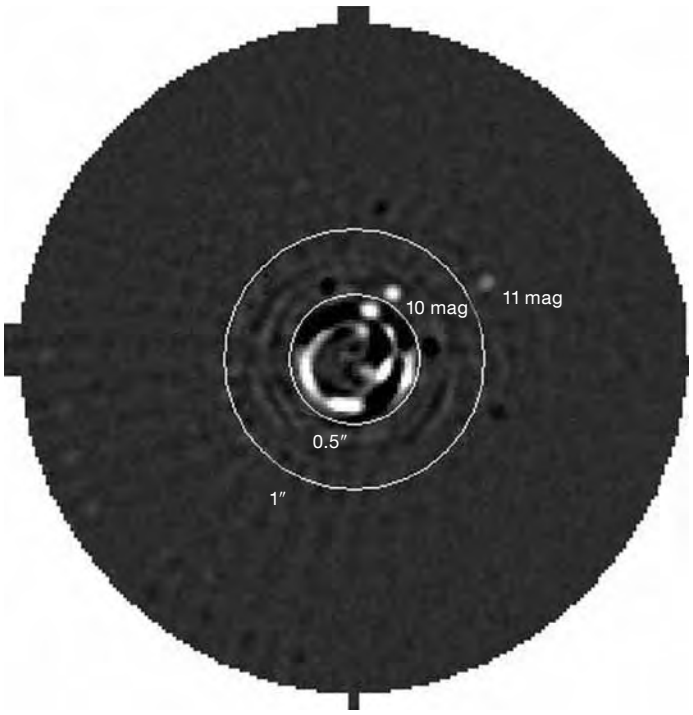

Figure 7. Final ADI processed coronagraphic image. Two artificial benchmark planets were inserted into the unprocessed data to verify the contrast levels calculated from the residual speckle pattern are indicated (c.f. Figure 5).

Residual radial contrast curves of the non-coronagraphic and the coronagraphic images after spatial filtering (SF) and ADI correction (Figure 5 and Figure 7) have been derived from the standard deviation of the intensity fluctuations in a 2 pixel-wide annulus centred on the star. The contrast was normalised to unit intensity of the peak of the non-coronagraphic image, and the reduced off-axis throughput of the coronagraph (90 % undersized pupil stop) has been taken into account. Figure 8 shows the derived 1σ contrast as well as a theoretical Airy pattern and the profile of the non-coronagraphic PSF (saturated in the centre) with an estimated Strehl ratio of 85 %. At 0.5 arcsecond separation, the ADI-reduced coronagraphic image achieves a 1σ contrast performance of about 7×10^{-6}. Assuming that 5σ is sufficient for a safe ADI detection, the achievable contrast at this separation is better than 11 magnitudes, as demonstrated by Figure 7. This mode of NACO is efficient enough to ensure that the contrast beyond 1 arcsecond is essentially limited by sky background, and therefore similar to an isolated object.

Using the exoplanet evolutionary and atmospheric models of Burrows et al. (2003) referred to earlier, the measured PSF contrast can be converted into an exoplanet mass sensitivity, assuming a given stellar brightness and age. Figure 9 shows the result of this analysis

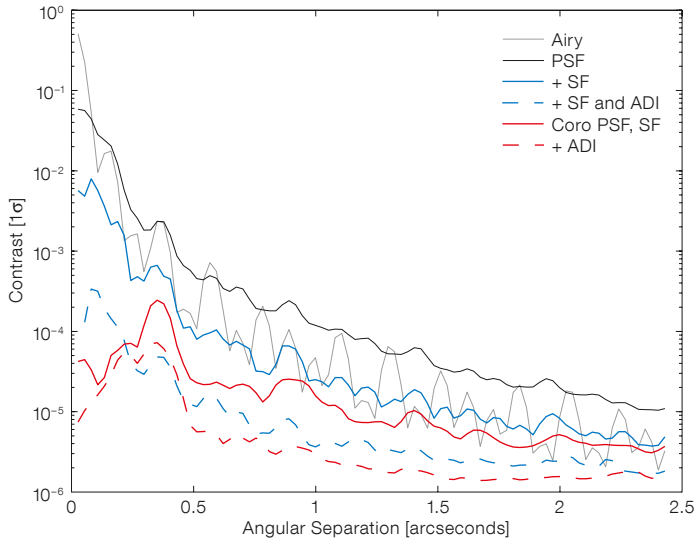

Figure 8. Contrasts measured on the non-coronagraphic (blue) and coronagraphic (red) images after different steps of the data reduction (spatial high-pass filter – SF and ADI).

assuming a K0 type star and ages of 100 and 316 Myr. For comparison, the same analysis was carried out with the best SDI contrasts reported by Biller et al. (2007) and the NICI contrast obtained during commissioning (Chun et al., 2008). While NACO–SDI contrast appears to lag behind, it must be noted that SDI could also be combined with and benefit from coronagraphy and pupil-tracking; a quantitative evaluation of such an observing strategy remains to be done.

Pupil-stabilised coronography at 4 μm is a very sensitive observing method for detection for all but the hottest exoplanets, delivering unprecedented mass contrasts. Excitingly, this mode of NACO already begins to open up the mass domain targeted by future instruments, such as SPHERE. However, the background-limited point-source sensitivity in the thermal IR makes it optimal for relatively nearby targets with distances up to a few tens of pc. The advantage of the method could be extended even further by installing a new astronomical filter in CONICA that would increase the bandwidth by about a factor of five over the one provided by the currently installed NB4.05 filter. With such a new filter the observing times required would be reduced by the same factor of five and a much greater efficiency in direct imaging of giant exoplanets would be reached.

References

Biller, B. et al. 2007, ApJS, 173, 143
Burrows, A., Sudarsky, D. & Lunine, J. I. 2003, ApJ, 596, 587
Chauvin, G. et al. 2003, A&A, 404, 157
Chauvin, G. et al. 2005, A&A, 438, L25
Chun, M. et al. 2008, Proc. SPIE, 7015, 49
Janson, M. et al. 2008, A&A, 488, 771
Kasper, M. et al. 2007, A&A, 472, 321
Lafrenière, D. et al. 2007, ApJ, 670, 1367
Lagrange, A.-M. et al. 2009, A&A, 493, 21
Masciadri, E. et al. 2005, ApJ, 625, 1004
Marois, C. et al. 2008, Science, 322, 1348
Neuhäuser, R. et al. 2005, A&A, 435, L13

Links

[1] http://www.eso.org/gen-fac/pubs/astclim/paranal/skybackground/

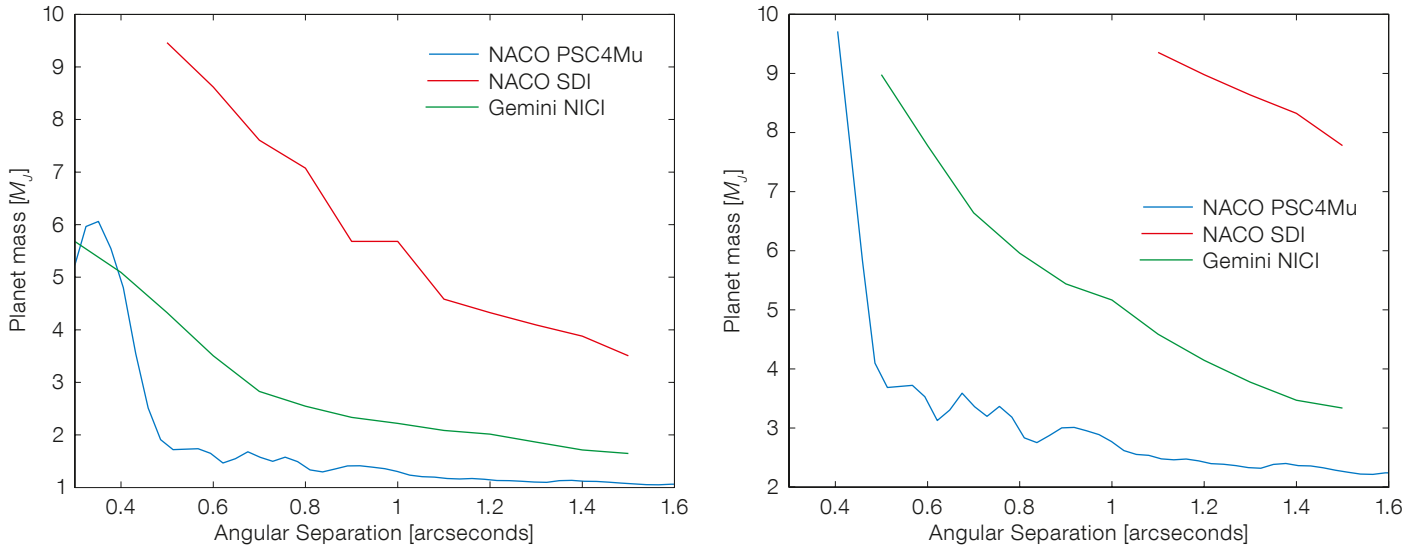

Figure 9. Detectability expressed in planet mass (assuming K0 host star) of the NACO PSC4Mu mode, compared to NACO SDI and GEMINI NICI using modelled exoplanet spectra for 100 Myr age (left) and 316 Myr age (right). A 3σ detection criterion was used for all instrument contrasts.

The AstraLux Sur Lucky Imaging Instrument at the NTT

Stefan Hippler[1]
Carolina Bergfors[1]
Wolfgang Brandner[1]
Sebastian Daemgen[1,2]
Thomas Henning[1]
Felix Hormuth[1,4]
Armin Huber[1]
Markus Janson[1,3]
Boyke Rochau[1]
Ralf-Rainer Rohloff[1]
Karl Wagner[1]

[1] Max-Planck-Institut für Astronomie (MPIA), Heidelberg, Germany
[2] ESO
[3] Department of Astronomy, University of Toronto, Canada
[4] German–Spanish Astronomical Center at Calar Alto (CAHA), Spain

Lucky Imaging is an observational technique that aims to achieve nearly-diffraction-limited image quality from the ground on 2–4-metre-class telescopes. While diffraction-limited observations from the ground are usually accomplished with the help of adaptive optics in the near-infrared spectral range at almost all 8–10-metre-class telescopes, Lucky Imaging aims for a similar imaging performance at shorter wavelengths, in particular from 0.7–1.1 microns. AstraLux Sur, a visitor instrument for the NTT, built at the Max-Planck-Institute for Astronomy, is described and some early results are presented.

Matter of luck: optical turbulence statistics

The working principle of Lucky Imaging is fairly simple and passive when compared to conventional adaptive optics systems with actively controlled deformable mirrors. The Lucky Imaging technique exploits the temporal behaviour of atmospheric turbulence. By selecting only the best few percent of several tens of thousands of short exposure images, it is possible to recover the full angular resolution of medium-sized telescopes at visible wavelengths. This can be realised with a fraction of the instrumental effort and cost that is needed for adaptive optics.

In his 1978 paper, David Fried showed that the probability of finding an image with a Strehl ratio ≥ 37 %, i.e. a wavefront variance < 1 rad^2, depends on the exponential of the ratio of the telescope diameter, D, to the square of the Fried parameter r_0. The Strehl ratio is an empirical measure of image quality, defined as the ratio of the peak height in an image to that expected for a diffraction-limited image. The Fried parameter is a direct measure of the length scale of atmospheric turbulence and is related to the seeing. For D = 2.2 m and r_0 = 0.3 m (this corresponds to a good I-band seeing of 0.55 arcseconds), the probability of obtaining an image with Strehl ratio > 37 % is about 0.0013. For a 3.5-metre telescope under the same conditions, the corresponding probability is about 3.5×10^{-9}. In a series of 20 000 images one would therefore expect 26 and 0 Lucky Images, for a 2.2-metre and a 3.5-metre telescope respectively. It is important to stress that this is the probability of obtaining nearly-diffraction-limited (Strehl ≥ 37 %) images at a wavelength of 800 nm, and with an angular resolution of 90 milliarcseconds (mas; for D = 2.2 m) and 47 mas (for D = 3.5 m).

In fact, the probability increases if we look for images with Strehl ratios < 37 %. Baldwin et al. (2001) could show that using exposures with the highest 1 % of Strehl ratios can result in a final image with a Strehl ratio of 0.3. All this of course only works if the exposure time is short enough to freeze the atmospheric turbulence, i.e., shorter than the speckle coherence time, τ_e. According to Robert Tubbs, τ_e depends on the ratio of the Fried parameter to the average wind velocity, v. This dependence requires an exposure time of about 30 ms for r_0 = 0.1 m and v = 10 m/s. Fortunately, CCD detectors with sub-electron read noise that can be operated at frame rates of 30 Hz and above are nowadays available. These electron multiplication CCD detectors are, in this respect, the cornerstone for the Lucky Imaging technique, combining very high quantum efficiency and very low noise at high speed.

The sequence of images in Figure 1 a–e shows how Lucky Imaging works. From a series of 50 000 images taken in z-band (central wavelength: 912 nm) at a speed of almost 40 images per second with the Calar Alto 2.2-metre telescope, five different long-exposure images have been created:

– The first image (Figure 1a) is just the sum of all 50 000 images, which is almost the same as the 21-minute (50 000/40 seconds)-long exposure, seeing-limited image. It looks like a typical star image, but slightly elongated. The full width at half maximum (FWHM) of the seeing disc is around 0.9 arcseconds.
– The second image (Figure 1b) is the sum of all 50 000 single images, but here with the centre of gravity (centroid) of each image shifted to the same reference position. This is the tip-tilt corrected — or image-stabilised — long-exposure image. It already shows more detail — two objects — than the seeing-limited image in Figure 1a.
– The third image (Figure 1c) shows the 25 000 (50 % selection) best images added together, with the brightest pixel in each image used to shift to the same reference position. In this image, the object is resolved into a triple system.
– The fourth image (Figure 1d) shows the 5000 (10 % selection) best images added together, with the brightest pixel in each image again used as the reference position. The surrounding seeing halo is further reduced and an Airy ring around the brightest object becomes clearly visible.
– The last image (Figure 1e) shows the 500 (1% selection) best images added together, with the brightest pixel in each image used for registration. The seeing halo is further reduced from the result in Figure 1d. This image provides the maximum signal-to-noise ratio of the five images.

The difference between the seeing-limited image and the result of selecting the best 1% of the images is quite remarkable: a triple system can be detected. The brightest component, to the west, is a V = 14.9 magnitude M4V star. This component is the Lucky Imaging reference source. The weakest — tertiary — component is an M7–M8 spectral type star. The distance of the system is known to be about 45 parsecs. Airy rings can be seen, which indicate that the diffraction limit of the Calar Alto 2.2-metre telescope, 86 mas, was reached. The signal-

Figure 1. Pictorial representation of the image selection process of Lucky Imaging. The image in Figure 1a is the sum of 50 000 *z*-band images each of 25 ms duration. Figure 1b shows the result of combining the 50 000 images, but with shifting to align the centroid of each image. Figures 1c through 1e show the results of selecting the best 50, 10 and 1 % of the images according to the Strehl ratio. See text for details.

to-noise ratio of the point sources increases with stronger selection. On the other hand, the seeing halo is more suppressed. The separation between the two brighter objects is around 0.55 arcseconds and between the two fainter objects less than 0.15 arcseconds. At a distance of 45 parsecs this corresponds to 6.75 astronomical units (AUs), around 10^9 km.

Lucky, well not always, but well-earned

In July 2006 we installed the Lucky Imaging instrument ASTRALUX at the 2.2-metre telescope of the German–Spanish Astronomical Center at Calar Alto (Hormuth et al., 2007; 2008). The simplicity, robustness and great success of this instrument — around 10 publications so far[1] — resulted, in autumn 2007, in the idea of building a copy of the instrument for the 3.5-metre New Technology Telescope (NTT) at the La Silla Observatory in Chile.

In May 2008, eight months after the starter's gun fired, we shipped the heaviest piece of the instrument, now christened AstraLux Sur, to Chile. The 225 kg adapter flange was especially designed for the NTT adapter/rotator counterpart. Accompanied by the camera mount, filter wheel, Barlow lens, an electron multiplying, thinned and back-illuminated CCD (model Andor iXon+), four computers and an electronic rack, everything arrived safely at the observatory. The instrument is sensitive in the visible spectrum and deploys the Lucky Imaging technique with nearly-diffraction-limited performance (~ 0.1 arcseconds) in *I′*-band and *z′*-band. The instrument provides a field of view of 16 × 16 arcseconds with a pixel scale of 31 mas.

First light of AstraLux Sur took place on the night of 19 July 2008. The first light target was the ~ 0.7 arcsecond binary system γ Lupi. Even though the observing conditions were rather poor and the NTT was closed for most of the night, with the exception of about half an hour, we could perform basic instrument tests. The opto-mechanical interface with the telescope, as well as our computing equipment, worked as expected. After some adjustments, the AstraLux Sur online data pipeline and the communication with the NTT control system via pctcs (a special telescope control system software module) ran smoothly. Pointing and focusing worked nicely. The image orientation, image scale and optical throughput were determined and the first photometric data could be obtained. Apart from one 25-minute window during the first night, no observations were possible in the first three nights due to high wind speeds and snowstorms. On the fourth night, the telescope could be opened during the second half of the night, and on the fifth night observations were able to start about two hours after sunset. Observing conditions were non-photometric for most of the time, and the seeing (DIMM) varied between 1 arcseconds and 2.5 arcseconds. Because of the high wind speed, the observations were also subject to very short coherence times.

In summary, after the first two observing runs in 2008, the performance of AstraLux Sur is as expected, in terms of Strehl ratio, but obviously slightly worse than its sister instrument at the 2.2-metre telescope on Calar Alto on account of the larger telescope diameter. The full diffraction limit was reached in *I′*-band with a FWHM of ~ 50 mas. In general an angular resolution of around 150 mas was achieved in *I′*-band and *z′*-band. This is slightly worse than our result on the 2.2-metre telescope at Calar Alto. To understand this behaviour, one should ask if there is an ideal combination of telescope diameter, seeing and filter bandpass for Lucky Imaging. It has been shown by Hecquet & Coupinot (1985) that the Strehl resolution, *R,* reaches its maximum at $D/r_0 = 7$ if the best 1 % of short exposures are selected. The Strehl resolution is defined as the product of the Strehl ratio and the ratio of the telescope diameter to the wavelength squared. The Strehl resolution is a measure of the image quality, including both the Strehl ratio and the

Figure 2. The AstraLux Sur commissioning team, from left to right: Stefan Hippler, Wolfgang Brandner and Boyke Rochau in July 2008. The AstraLux Sur instrument is attached to the aluminum adapter flange, which itself is connected to the NTT Nasmyth adapter/rotator.

image resolution, roughly corresponding to terms like contrast and sharpness. Both higher and lower values for D/r_0 than the supposed optimal value of 7 lead to a loss of image quality. If the telescope diameter is increased at a fixed r_0, equivalent to fixed wavelength and seeing conditions, then the probability for a Lucky Image will decrease, leading to a smaller resulting Strehl ratio. If the telescope diameter is decreased, the higher resulting Strehl ratio is achieved at the cost of image resolution.

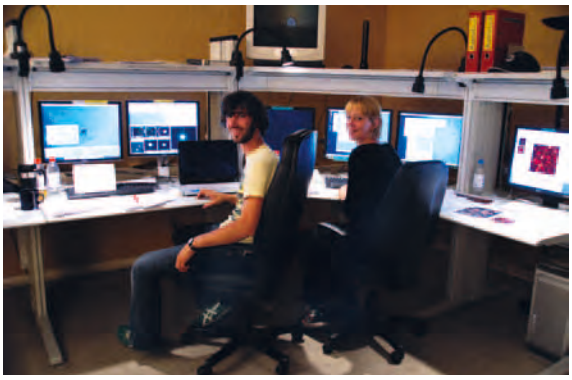

Figure 3. Since November 2008 — with the second AstraLux Sur observing run — observations with AstraLux Sur have been carried out from the La Silla remote control building, the RITZ. The remote operations include control of the instrument, as well as online data reduction and inspection. Observers Sebastian Daemgen and Carolina Bergfors are shown.

Science programmes: Lucky Imaging survey for binary M dwarfs

With the AstraLux Sur instrument at the NTT visitor focus, we achieved nearly-diffraction-limited imaging performance in the SDSS *I′*- and *z′*-band filters, a wavelength range not accessible with other ground-based high-resolution (adaptive optics) instruments.

In Period 81 we initiated three science programmes at the NTT with AstraLux Sur. The first programme is a second epoch follow-up of T Tauri binary and multiple systems, which were originally discovered some 15 to 20 years ago. The second epoch observations obtained with AstraLux Sur test if the individual components of each system have a common proper motion, and hence are gravitationally bound. In addition we will derive first estimates of orbital periods and system masses of a statistically significant sample of T Tauri stars. The final observations for this programme were obtained in March 2009, and the analysis has just been completed and we are preparing the findings for publication. A survey of about 800 young, active M dwarfs in the Solar Neighbourhood aims at improving binary statistics, identifying very low-mass and substellar companions, finding systems suitable for dynamical mass determination, and establishing a sample of M dwarf binaries suitable for future astrometric exoplanet searches with GRAVITY at the VLT Interferometer. The final observing run for this programme is scheduled for Jan/Feb 2010. A third observing programme surveys transiting exoplanet host stars with the aim of identifying close binary companions. If unresolved, such binary companions bias the determination of planetary parameters from the light curve (see, e.g., Daemgen et al., 2009, for first results obtained with the Northern AstraLux camera). A number of previously unrecognised binary companions were indeed discovered with AstraLux Sur, and the data are currently being analysed.

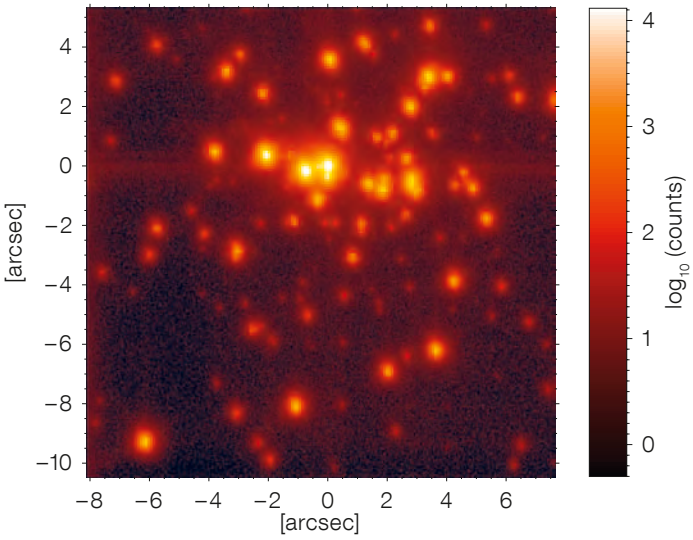

Figure 4. The core of the Galactic starburst cluster in the giant HII region NGC 3603, which serves as one of our astrometric calibration targets, as seen by AstraLux Sur in the SDSS *z′*-band at the NTT. The 1 % image selection (100 out of 10 000 frames) yields a resolution (FWHM) of 120 mas.

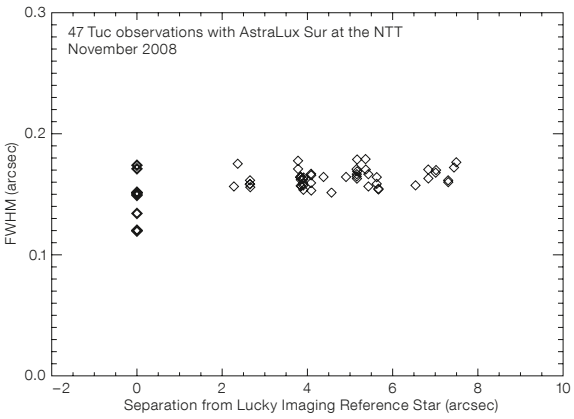

Figure 5. The measured point source full width at half maximum, FWHM, is shown at different separations from the Lucky Imaging reference star in observations of the globular cluster 47 Tuc. We analysed 9 *z′*-band images with a single frame integration time of 30 ms and used a 10 % selection process (1 000 out of 10 000 frames). The ASM (DIMM) seeing varied between 0.8 and 1.8 arcseconds. Hence, even under worse than median seeing conditions, Lucky Imaging can deliver images with resolutions below 200 mas.

Lucky future!

Two new science projects planned for Period 84 are a study of the binary properties of massive young stars in the Carina Nebula, and the analysis of the light curves of eclipsing binaries located in the centres of starburst clusters. We

are also very open to collaborations with other research groups who want to take advantage of the high angular resolution and fast time resolution facilitated by Lucky Imaging at the NTT. The NTT on La Silla is the only readily accessible place in the Southern Hemisphere for applying the Lucky Imaging technique under almost optimal conditions.

With the availability of the so-called burst mode offered by quite a few VLT instruments (e.g., VISIR, NACO and ISAAC, see Richichi, 2008), individual readouts, rather than simply the co-added frames, can now be stored and made available to the astronomer for post-processing. Thus Lucky Imaging-like procedures such as image selection and re-registration of individual frames before co-adding are becoming more and more common and help to further optimise angular resolution and sensitivity of observations. NACO observations in *J*- and *H*-bands benefit most, as the decreasing atmospheric coherence time at shorter wavelengths makes it harder for the adaptive optics system to keep up with the atmospheric variations. Experiments carried out with a Lucky Imaging camera in combination with adaptive optics at the Palomar 5-metre telescope (Law et al., 2009) appear highly promising. A Lucky Imaging camera like AstraLux Sur attached to the visitor port of the VLT NAOS instrument could achieve an angular resolution of 20 mas at a wavelength of 900 nm.

References

Baldwin, J. E. et al. 2001, A&A, 368, L1
Daemgen, S. et al. 2009, A&A, 498, 567
Fried, D. L. 1978, JOSA, 68, 1651
Hecquet, J. & Coupinot, G. 1985, Journal of Optics, 16, 21
Hormuth, F. et al. 2007, A&A, 463, 707
Hormuth, F. et al. 2008, SPIE, 7014, 48
Law, N. et al. 2009, ApJ, 692, 924
Richichi, A. 2009, The Messenger, 135, 32
Tubbs, R. N. 2003, PhD Thesis, University of Cambridge

Links

[1] http://www.mpia.de/ASTRALUX/Publications.html

Credit: L. Knee/ALMA

Two ALMA antennas at the Operations Support Facility (OSF) pointing to the same source in the sky.

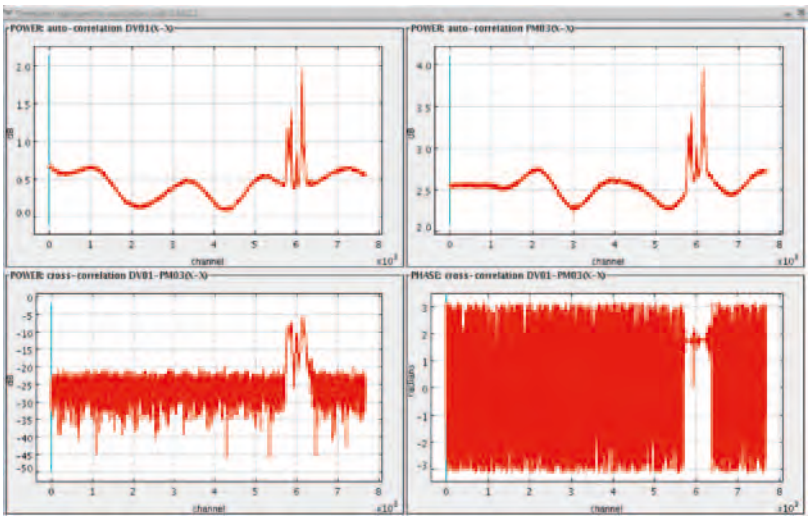

Following the initial success of the first fringes between two ALMA antennas at the OSF (see release ESO 18/09), the system has been undergoing further tests, software upgrades and debugging. In early June 2009, stable fringes under computer control were routinely achieved. An example of the tests on an SiO maser source is shown. The top two panels show the autocorrelation signal from each of the two antennas and the bottom panels show the amplitude and phase of the cross-correlation signal.

Fringes with three telescopes, including closure phase, at the 5000 m high site are expected toward the end of the year. This event will be a major milestone toward the first Early Science observations with sixteen telescopes in 2011.

Halftoning for High-contrast Imaging: Developments for the SPHERE and EPICS Instruments

Patrice Martinez[1]
Christophe Dorrer[2]
Emmanuel Aller-Carpentier[1]
Markus Kasper[1]
Anthony Boccaletti[3]
Kjetil Dohlen[4]

[1] ESO
[2] Aktiwave, Rochester, New York, USA
[3] LESIA, Observatoire de Paris, France
[4] Laboratoire d'Astrophysique de Marseille, France

Controlling the amplitude of light is crucial for many scientific applications, such as in imaging systems, astronomical instruments or laser physics. We provide a brief overview of recent R&D activities at ESO using halftoning, the process of presenting a continuous image through use of dots. Customised filters with spatially varying transmission are produced using a binary array of metal pixels that offers excellent control of the local transmission. Applications to the production of an apodiser for the VLT SPHERE instrument and a mask for E-ELT EPICS are presented.

High-contrast instruments, such as SPHERE, the Spectro-Polarimetric High-contrast Exoplanet Research instrument (the planet-finder instrument under construction for the ESO Very Large Telescope or VLT), or EPICS (the planet-hunter project for the future European Extremely Large Telescope or E-ELT), will require customised components with spatially varying transmission. A typical example is a stellar coronagraph, which is an optical element that is capable of reducing the contrast between a companion and its parent star. The goal of these subsystems is to control the spatial transmission, either in a pupil plane (pupil apodisation), or in a focal plane of the instrument (occulting mask, i.e. low frequency filter). Reliably producing these components with spatially varying transmission is not trivial, and different techniques have already been investigated for application to astronomy (e.g., metal deposition with spatially varying thickness, or high energy beam-sensitive glass treated by electron beam lithography). We present some results related to the recent development of components with spatially varying transmission using a relatively simple technique analogous to the digital halftoning process used for printing applications.

Halftone dot process principle and applications

Halftoning has been used for hundreds of years in the printing industry as a way of generating continuous tone images with only black or white dots. The so-called halftone image, seen from a distance, should resemble the original continuous tone image as much as possible, based on human visual perception. Following this idea, the continuous transmission of an optical filter can be generated with a specific implementation of opaque and transparent pixels as presented in Figure 1.

The microdot filter is an array of dots (i.e. pixels) that are either opaque (0 % transmission) or transparent (100 % transmission). It is fabricated by lithography of a light-blocking metal layer deposited on a transparent glass substrate. The technique has several advantages: relative ease of manufacture, achromaticity, reproducibility and the ability to generate continuous and rapidly varying transmission functions, without introducing wavefront errors. The technique can be applied in many areas, such as laser beam shaping (Dorrer et al., 2007), intensity modulation in projection and illumination systems, coronagraphy, apodisation (soft-edged apertures) and optical testing. It allows customised filters to be generated with specific and rapidly varying transmission shape, e.g., Gaussian, prolate, sinusoidal-like functions and test zones with calibrated transmissions.

Key parameters

In order to specify a microdot filter, several application-dependent parameters must be carefully defined. Microdot filters are arrays of pixels with binary transmission, and thus light propagating through them has a continuously varying intensity after free space propagation, or after filtering in the far field. Therefore, these filters have a power spectrum different from the power spectrum of an ideal continuous filter. The way the dots are distributed, the size of the dots, and the density of the dots in the pattern directly impact the power spectrum of the filter, and these parameters must be carefully tuned according to the application.

Distribution of the dots

The error diffusion algorithm provides excellent continuous tone rendering and only produces noise at high frequencies in the power spectrum. Unlike many other halftoning algorithms, the error diffusion algorithm has the advantage of only introducing high frequency noise, i.e. the low and middle range of frequencies in the generated transmission have little or no noise due to pixellation and the binary nature of the dot transmission. The error diffusion technique is very simple to describe. The algorithm sets the transmission of a given pixel (either 0 % or 100 %) by comparing the transmission required at this location to a 50 % threshold. The transmission is set to zero if the required transmission is less than 50 % and to one otherwise. The induced transmission error is diffused to adjacent pixels that have not yet been processed by biasing the transmission required at the corresponding locations. This locally cancels the error of the binary optics introduced by the process of translating the required

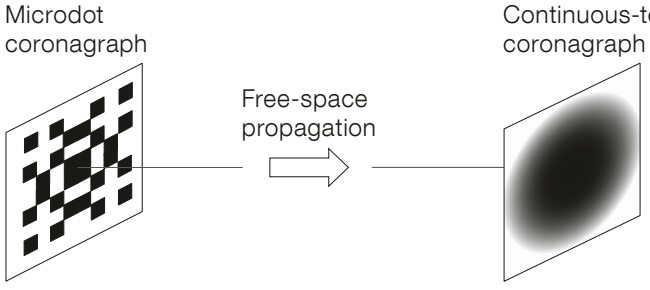

Figure 1. Principle of the generation of a continuous modified intensity transmission using a microdot filter after Fourier filtering.

continuous tone transmission into binary values. This procedure is used for gray level reproduction with black and white printing techniques, and has been used for laser beam shaping (Dorrer et al., 2007).

Characteristics of the microdot filters

On account of the pixellation and binary transmission of the pixels, high frequency components are generated in the power spectrum of a microdot filter. The smaller the dots are, the higher the spatial frequencies at which the light is scattered. With smaller pixels, the agreement between the required transmission and the obtained transmission improves (Martinez et al., 2009a; 2009b). This issue is formally equivalent to a sampling problem. Better results are obtained when increasing the sampling rate (i.e. more binary dots are used to reproduce the continuously varying transmission). In the specific case of coronagraphs, theoretical derivations of the impact of the dot size in the science image for pupil apodiser-type components have been developed (Martinez et al., 2009a), and verified experimentally (Martinez et al., 2009b), as well as for focal plane masks (Martinez et al., 2009c).

One must generally avoid dots with sizes comparable to the wavelength of the light with which they are designed to operate. In such a regime, it is difficult to predict how the field will react to such filters, and the transmission might be strongly dependent on the wavelength. Typical pixel sizes that are useful for astronomical applications range from a few tens of microns to a few microns.

Coronagraphs fabricated for pupil plane apodisation do not require a high opacity. However, the opacity of the metal layer (the optical density [OD], which is wavelength dependent) is an important parameter for focal plane masks, whether they are fabricated with microdot filters or other technologies. High OD specification is required for focal plane mask coronagraphs, at least OD > 6 (transmission $< 10^{-6}$) in order to avoid starlight leaking on to the detector.

Application of halftoning to SPHERE

The Apodised Pupil Lyot Coronagraph (APLC) is one of the three coronagraphic concepts for the SPHERE IRDIS, (Infra-Red Dual beam Image and Spectrograph) instrument, which will enable direct images, and spectra to be obtained for warm, self-luminous Jovian planets. A recent study also points out its potential application to E-ELT instruments (Martinez et al., 2008), such as EPICS, the extreme adaptive optics planet imager. The APLC combines an apodiser in the entrance aperture with a small opaque mask in the focal plane. Manufacturing an accurate apodiser is critical for such a coronagraph, as for any other concept using pupil apodisation (e.g., a dual zone coronagraph, or for conventional pupil apodisation concepts).

The definition of the prototype profile has been optimised (Martinez et al., 2007) for its use on HOT, the High Order Test bench at ESO (Aller Carpentier et al., 2008), and is roughly similar to the one defined for SPHERE. The main characteristics of the microdot version of the APLC apodiser are summarised in Table 1. The main difference with SPHERE is the size of the pupil to apodise (18-mm diameter for SPHERE, while in HOT it is only 3 mm, increasing the difficulty of producing the apodiser because smaller pixels are required). The size of the square chrome dots of our prototype is 4.5 µm; see Figure 2, where metrology inspection of the microdot apodiser is illustrated. The dot spatial distribution across the pupil was analysed using a shadowgraph (contour profile projector for quality control) and compared with a simulation map, demonstrating extremely good agreement. The principle of the shadowgraph inspection consists in placing the specimen on a glass stage that is illuminated from below, and the resulting image is picked up by a microscope objective and projected onto a large projection screen, where only the details of the contour and profile are seen. The shadowgraph is a powerful tool for controlling dot size and spatial distribution, which can be easily compared to specification maps.

Figure 3 shows the good agreement between the measured and required profiles. The transmission error is approximately 3 %. The achromaticity of the transmission profile is also demonstrated: the profile error increases by only about 2 % between the narrow *H*-filter and the broadband *J*-filter. Figure 4 shows a laboratory experiment where we have analysed the effect of the dot size in the coronagraphic image. Different microdot filters were fabricated to approximate the same coronagraph with dot size specified as 15, 30, 60, 120 and 240 µm, corresponding to masks 2 to 6 respectively.

Coronagraphic images exhibit speckles with intensity and position in the field that were confirmed to be a function of the dot size, and the agreement with the theoretical derivation is very good (Martinez et al., 2009b). When the dots are sufficiently small, a usable field of view free of speckles appears and reveals the residual diffraction from the VLT-like pupil (spider vane diffraction spikes). Overall the prototype has excellent quality and meets the specifications.

Application of halftoning to EPICS

Even though the APLC is considered as well, for EPICS (an instrument that is planned to enable direct images and spectra for both young and old Jupiter-mass planets in the infrared), several

Table 1. Summary of the main characteristics of the prototype halftone components for SPHERE and EPICS.

	Prototype	
	Pupil apodiser (APLC)	Focal plane mask (BLC)
Function	Prolate-like function	(1-sinc)
Metal layer	Chrome	Aluminium
OD (dot opacity)	4+ (Visible)	8+ (near-infrared)
Dot size	4.5 µm	5/10 µm
Diameter of the pattern	3 mm	12.0 mm
Diameter of the substrate (BK7)	12.7 mm	12.7 mm
Accuracy of the profile	3 %	5 %

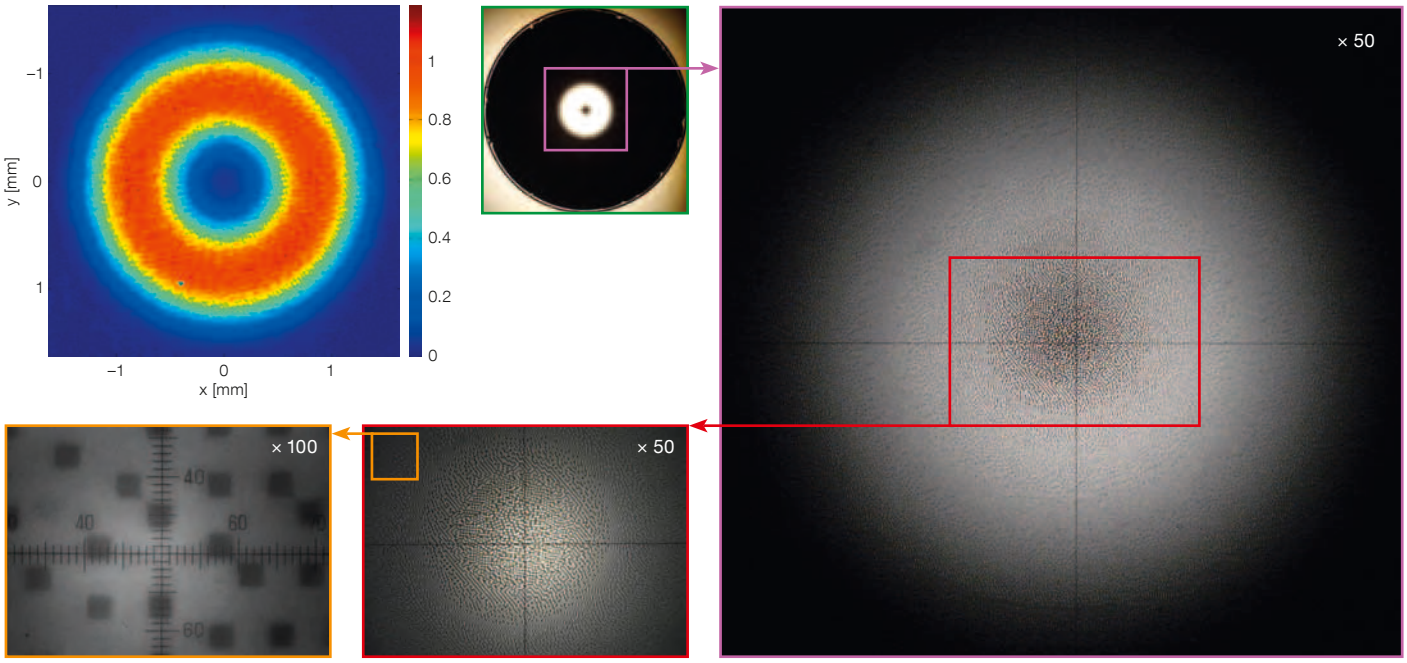

Figure 2 (above). Metrology inspection of the final prototype using a camera (green box), a shadowgraph (purple and red boxes), a microscope (orange box), and the corresponding spatially resolved transmission (top-left).

Figure 3 (below). Left: Apodiser azimuthally averaged from centre to edge using different filters (*J*- and *H*-band) with width indicated compared to the specification (black curve). Right: Corresponding average amplitude error as a function of radius.

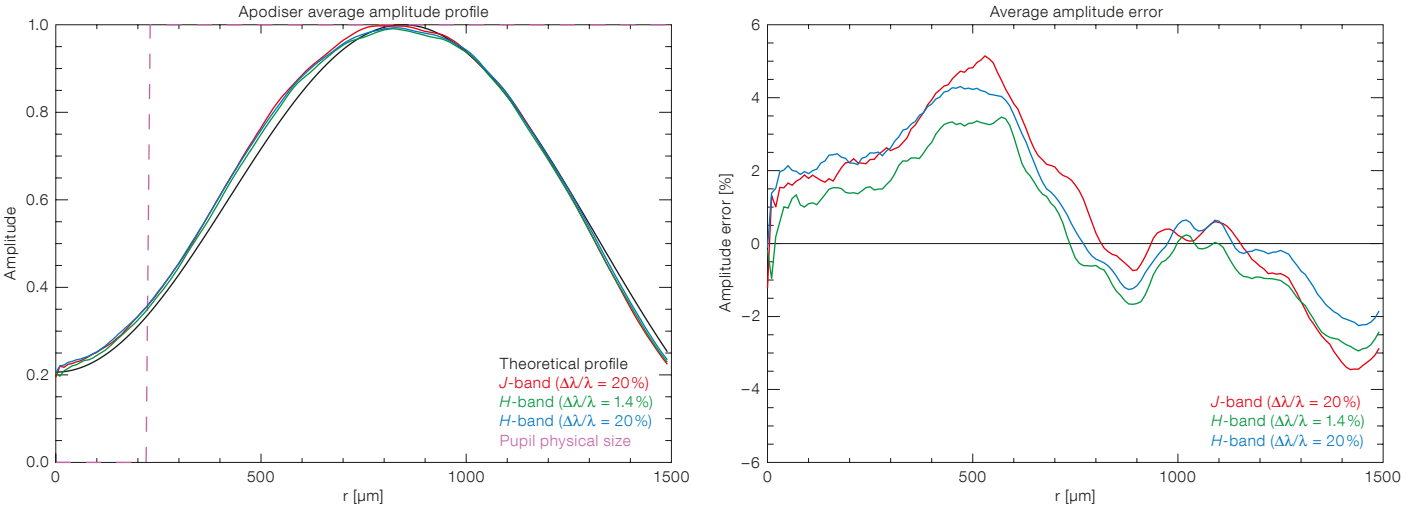

other coronagraphic concepts are under investigation. Some of them require the microdot technique for pupil apodisation (conventional pupil apodisation coronagraph or dual zone coronagraph), while the band-limited coronagraph (BLC) requires an accurate filter with a spatially varying transmission (e.g., a sinusoidal function such as 1-sinc) in the focal plane of the instrument. A theoretical analysis of the design issues (different from the APLC) is detailed in Martinez et al. (2009c).

We produced several prototypes (Figure 5) based on the same function, but with different dot sizes (indicated as a and b in Figure 5, where a corresponds to a 5-µm dot size and b to a 10-µm dot size) and function bandwidth (BL5 and BL10). The main characteristics of the prototypes are detailed in Table 1. Qualitative and quantitative descriptions of the resulting prototypes are shown in Figures 5 and 6. The accuracy is about 5% in the high transmission part (recently improved to an accuracy of 2 % with new prototypes). Accuracy in the low transmission part (centre of the mask) is extremely good.

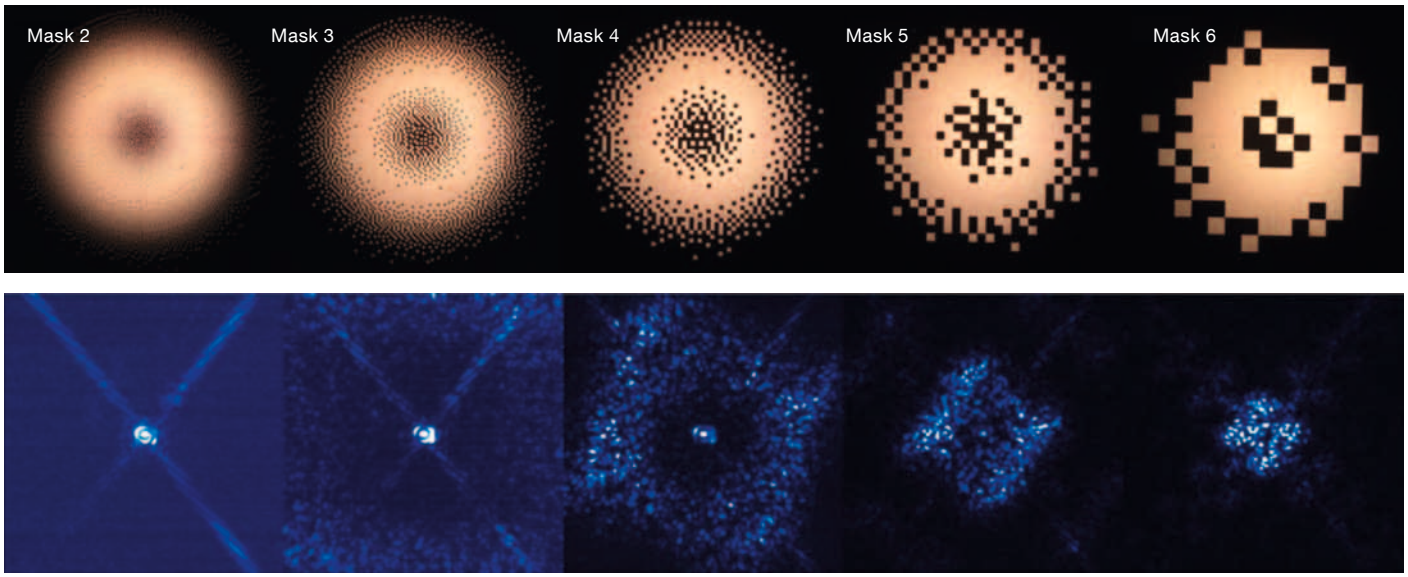

Figure 4 (above). Top row: Shadowgraph inspection (× 50) of different masks based on the same profile, but differing dot size. Bottom row: The coronagraphic images (with narrowband illumination, $\Delta\lambda/\lambda$ = 1.4 %) corresponding to the different masks.

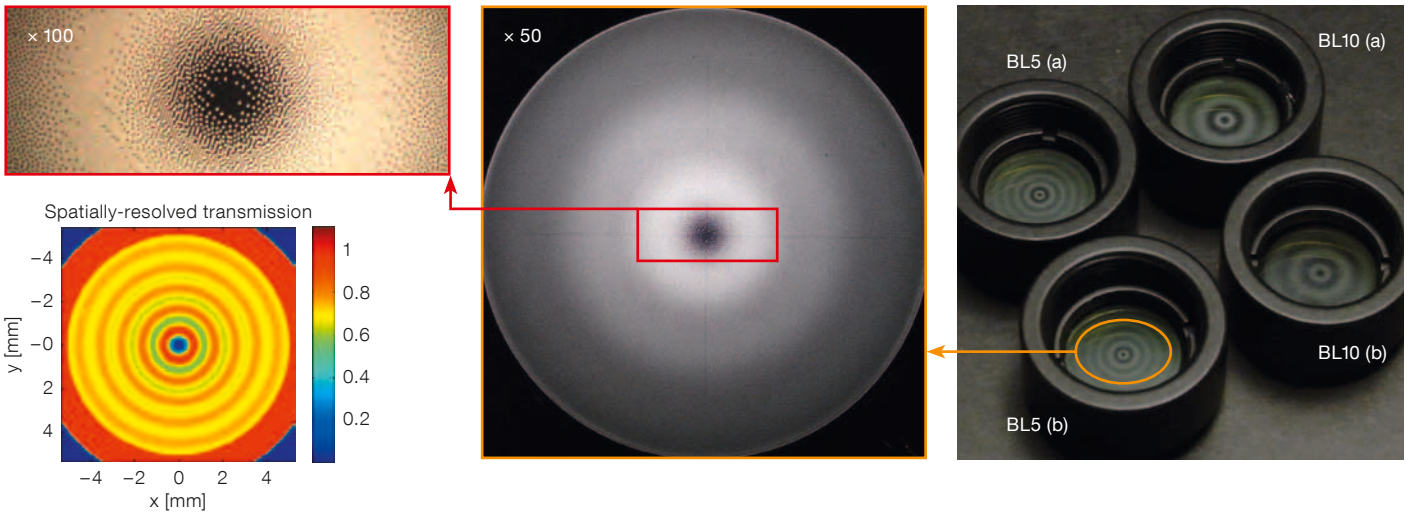

Figure 5 (below). Metrology inspection of the band-limited coronograph prototypes. From right to left: The four prototypes in their integration mounts, shadowgraph image (× 50), shadowgraph image (× 100) and spatially resolved transmission of BL5 (b), with 5 µm dot size.

Results obtained with APLC and BLC

We tested our prototypes first in a near-infrared coronagraphic transmission bench developed at ESO (turbulence-free and AO-free, operating in *H*-band). APLC demonstrates the ability to reduce the on-axis starlight by a factor of 700 on the peak, and to reach a contrast of 5×10^{-5} and 10^{-6} at 3 and 20 λ/D offset (0.12 and 0.8 arcseconds for an 8-metre telescope) respectively (Figure 7, and Martinez et al. [2009a] for more details). BL5 demonstrates a peak reduction of 2500, and a contrast of 3×10^{-5} and 2.7×10^{-8} at 5 (inner working angle), i.e. offset angle below which a companion cannot be resolved and 20 λ/D respectively (i.e. 0.2 and 0.8 arcseconds), while BL10 yields a peak reduction of 83 000 and a contrast of 1.3×10^{-7} and 1.3×10^{-8} at 10 (inner-working angle) and 20 λ/D respectively (Martinez et al., 2009c). The theoretical limits of the coronagraph have not been reached. Limitations originate from alignment issues, and from the static aberrations of the optical bench. Contrast levels reached are similar (APLC) or better (BLC) than the quasi-static speckle halo level expected after adaptive optics (AO) correction in a real instrument (10^{-5}–10^{-6}).

We further investigated the APLC performance on HOT, which is a high-contrast imaging eXtreme Adaptive Optics (XAO) bench developed at ESO. Its objective is to test and optimise different techniques and technologies (e.g., wavefront sensors, coronagraphs,

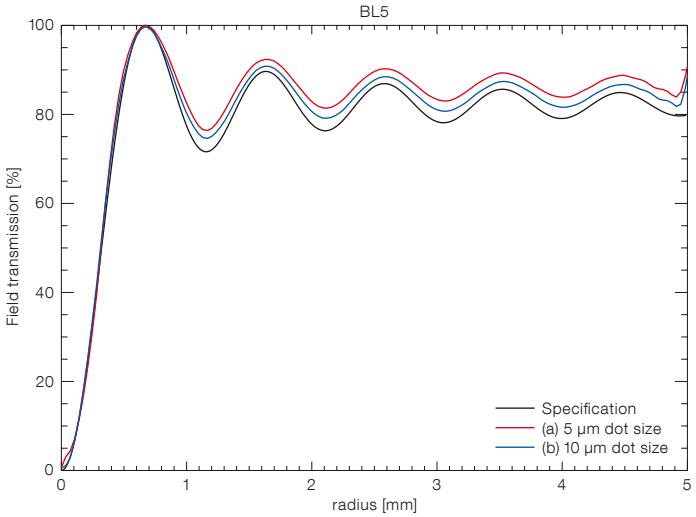

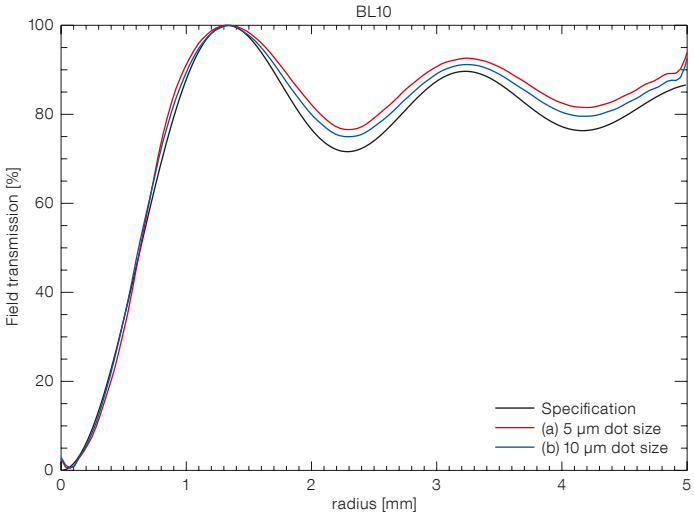

Figure 6 (above). Azimuthally averaged profiles (from centre to edge) of the band-limited coronographs BL5 (left) and BL10 (right) with 5 and 10 µm dot sizes.

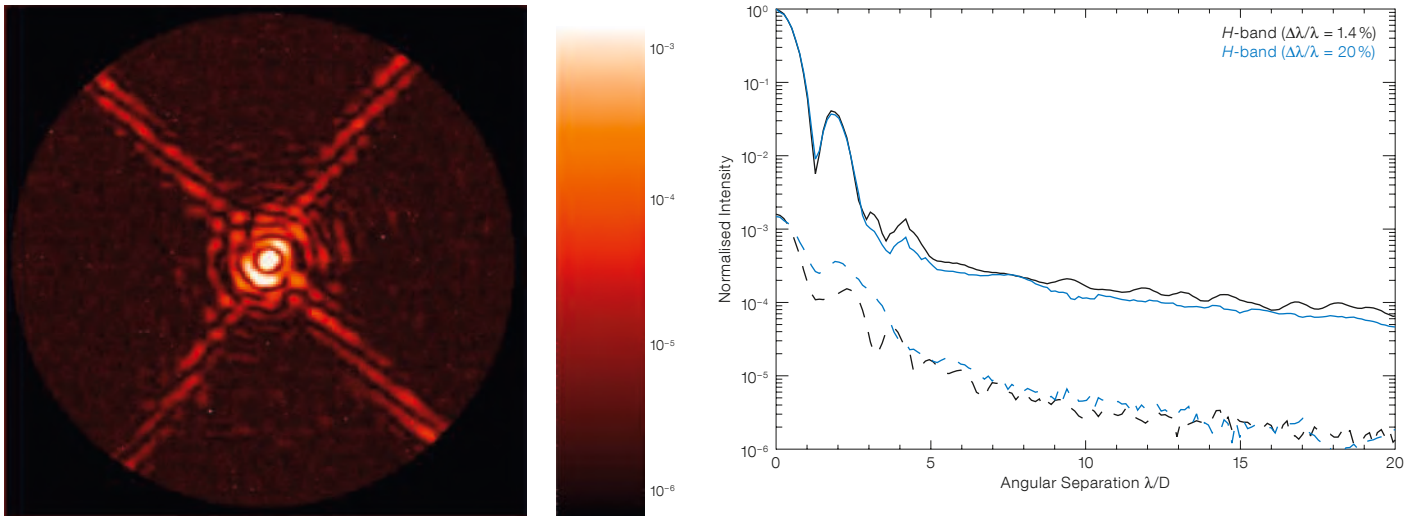

Figure 7 (below). Apodised pupil Lyot coronograph (APLC) results obtained in *H*-band (94 % Strehl optical bench assuming the VLT-pupil without turbulence or AO correction). Left: Coronagraphic image. Right: APLC contrast profiles (dashed lines) compared to the PSF contrasts, i.e. without the coronagraph (full lines), for two bands.

speckle calibration methods, image post-processing). HOT mimics the conditions occurring at a real telescope (e.g., the VLT), including turbulence generation, XAO, and various near-infrared (near-IR) coronagraph concepts. The experiment was performed under 0.5-arcsecond seeing, with real-time AO-correction using a 31 × 31 DM (15 λ/D AO cut-off frequency, i.e. 0.6 arcseconds in *H*-band) and a Shack–Hartman wavefront sensor. Recently, we have also experimented with differential imaging (DI) tests, using sequential coronagraphic image subtraction in between closely spaced narrowband filters in *H*-band (1.56 µm and 1.60 µm, *H1* and *H2* respectively).

Figure 8 qualitatively describes the different steps of the experiment.

1. The AO-corrected (apodised) point spread function (PSF) reveals the diffraction pattern of the VLT pupil by achieving a high (90 %) Strehl ratio. The apodisation of the PSF helps in reducing the intensity level of the PSF wings.
2. The coronagraphic images recorded in *H1* and *H2* both confirm the effect of the APLC, where images exhibit atmospheric speckles with lower intensity in the AO correction domain (from the second or third wing of the PSF to the rise of the AO cut-off frequency clearly seen in the images), while the central core of the coronagraphic PSF being brighter, appears dominated by diffraction residuals and pinned-speckles.
3. The differential image, where the speckle contrast has been improved by removing the atmospheric speckle halo and a part of the instrumental speckle contribution. The image has been high-pass filtered to remove smooth structures, leaving the small-scale higher frequency objects unaffected (e.g., faint companion).

The raw contrasts achieved after the APLC (Figure 9, red and green curves) are in good agreement with the SPHERE simulations. When removing the atmospheric speckle halo with a high-pass filter

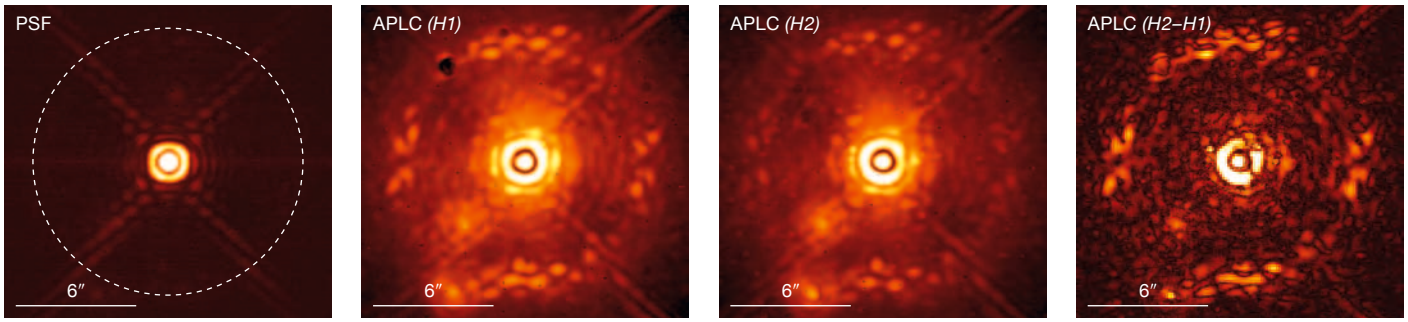

Figure 8. From left to right: AO-corrected and apodised PSF is shown (white-dashed circle indentifies the AO cut-off frequency in the field); APLC coronagraphic images recorded with *H1* and *H2* near-IR filters (middle images); and (right) subtraction of the two coronagraphic images, after high-pass filtering.

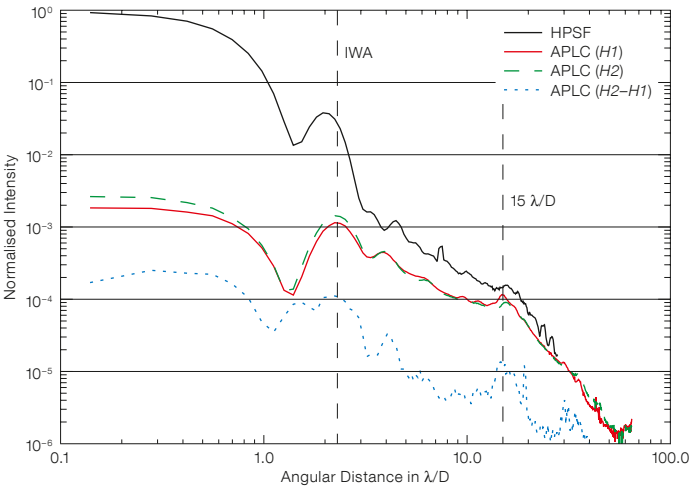

Figure 9. Azimuthally averaged profiles of the AO-corrected PSF (black curve), APLC raw coronagraphic images in filters *H1* and *H2* (red and green curves), and 1σ contrast after differential imaging and low frequency content suppression (blue curve). IWA is the inner working angle.

Table 2. Some of the next instruments that can benefit from the use of the halftoning process for producing (at least) their coronagraphs (in blue). FQPM and PIAA refer to Four Quadrant Phase Mask and Phase Induced Amplitude Apodisation respectively.

Instrument	In service by	Coronagraph type
SPHERE/VLT	2011	FQPM/APLC/Lyot
GPI/Gemini	2011	APLC
HCIAO +	2010	Lyot/APLC/PIAA
JWST	2013	Band-limited/FQPM
EPICS/E-ELT	> 2018	CPA (baseline)
PFI/TMT	> 2020	APLC

applied either on *H1* or *H2* images (not plotted in Figure 8), the contrast curve nicely fulfilled the SPHERE expectation as well. High-pass filtered APLC images demonstrate a 5σ detectability of 2.5 × 10^{-4} and 2.2 × 10^{-5} at 0.1- and 0.5-arcsecond offsets respectively, without Spectral Differential Imaging (SDI) or Angular Differential Imaging (ADI) techniques, i.e. a factor of 25 and 45 at 0.1 and 0.5 arcseconds respectively from the goal contrast of SPHERE (after SDI and/or ADI). The 1σ contrast provided after differential imaging (blue dashed curve) demonstrates atmospheric speckle suppression (1 order of magnitude gain), while slightly improving the speckle noise. Improvement of these results is foreseen with a simultaneous implementation of the DI tests (implemented in a sequential way so far). These results provide confidence in the expected performance of SPHERE.

The halftoning process presented has been validated for pupil apodisers (APLC for SPHERE and for the Gemini Planet Imager, GPI), and is defined as the baseline technique for EPICS (for producing a conventional pupil apodisation coronagraph [CPAC], the concept baseline). Space-based telescopes can also benefit from the halftoning process, such as the JWST NIRCam coronagraphic masks for which microdot band-limited coronagraphs are being manufactured. Table 2 summarises some of the future instruments that can take advantage of the halftoning technique at least for coronagraphs. Its interest has been recently extended in the context of the manufacture of the apodisation mask for the BIGRE Integral Field Spectrograph for SPHERE (Antichi et al., 2009).

Acknowledgements

We deeply thank Sebastien Tordo and Christophe Dupuy from ESO for their support with the Infrared Test Camera and metrology aspects. We are indebted to Precision Optical Imaging and Aktiwave (Rochester, New York) for the high quality manufactured prototypes, and for the numerous open discussions about the technique.

References

Aller Carpentier, E. et al. 2008, Proc. SPIE, 7015, 108
Antichi, J. et al. 2009, ApJ, 695, 1042
Dorrer, C. & Zeugel, J. D. 2007, J. Opt. Soc. Am. B, 24, 1268
Martinez, P. et al. 2007, A&A, 474, 671
Martinez, P. et al. 2008, A&A, 492, 289
Martinez, P. et al. 2009a, A&A, 495, 363
Martinez, P. et al. 2009b, A&A, 500, 1281
Martinez, P. et al. 2009c, ApJ, accepted

Colour image of the Sd spiral galaxy NGC 7793, a member of the Sculptor group, at 3.4 Mpc distance. NGC 7793 has a very large HII disc as is apparent from the many Hα emitting regions (visible in red). This colour composite is formed from *B*, *V*, *I* and *Hα* images taken with VLT FORS. See ESO Press Photo 14b/09 for details.

First Images from the VLT Interferometer

Jean-Baptiste Le Bouquin[1]
Florentin Millour[2]
Antoine Merand[1]
VLTI Science Operations Team[1]

[1] ESO
[2] Max-Planck-Institut für Radioastronomie, Bonn, Germany

The ESO Very Large Telescope Interferometer has recently produced its first images, achieving a spatial resolution of a few milliarcseconds. The published images reveal the precise astrometry of close massive binaries (θ^1 Ori C and HD87643), the presence of material close to the surface of an old, variable star (T Lep), and the dusty environment of an active galactic nucleus (NGC 1068). However, this is only a first step and additional results and numerous improvements are expected in the forthcoming years.

The stars with the largest apparent size in the sky are of the order of ten milliarcseconds. This is much smaller than the resolving power of the largest world-class telescopes, such as the Unit Telescopes (UTs) of the ESO Very Large Telescope (VLT). In the coming decades, the Extremely Large Telescopes (ELTs) will deliver better resolving powers thanks to their larger apertures and the use of new generation adaptive optics (AO). However, even the ELTs will only be able to image a few of the largest stars of the sky, such as Betelgeuse (α Orionis), whose diameter is about 30 milliarcseconds. To resolve solar-like stars, interacting binaries, or the inner part of planet-forming discs requires a telescope of at least 150 m in diameter. At optical wavelengths, building and co-phasing such a telescope will remain out of reach of our technical and financial capabilities for decades yet.

Interferometric aperture synthesis is the only currently available solution. This technique mixes the light collected by several small, independent telescopes separated from each other by tens or even hundreds of metres, and so recovers the resolving power of a virtual telescope of equivalent size (see Figure 1).

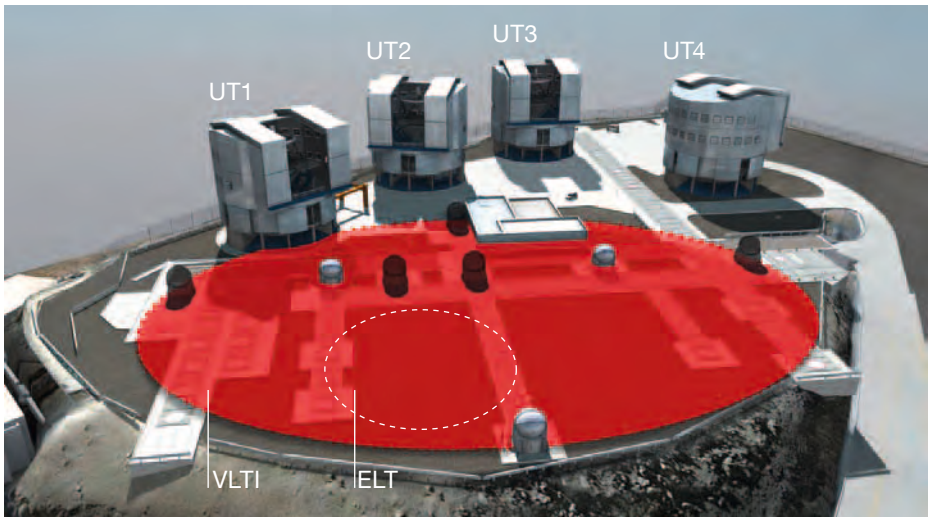

Figure 1. Overview of the Paranal Observatory platform, showing the four Unit Telescopes (UTs) and the three relocatable Auxiliary Telescopes (ATs). The three ATs are the small white telescopes arranged in an equilateral triangle. Combining them together and moving them to different positions (black shadows) emulates the resolving power of a virtual giant telescope, represented here as the red area. It is important to note that the interferometric technique only reproduces the resolving power of the virtual giant telescope, not its sensitivity. The size of the ELT is represented for comparison.

Optical long-baseline interferometry has been used by a steadily growing community, as shown by the publications graph in Figure 2. Since 2003, the rate of increase has been higher due to the introduction of "user-friendly" interferometers such as the Keck Interferometer (Keck-I), the ESO Very Large Telescope Interferometer (VLTI) and CHARA. Even so, for the general astronomer, optical interferometry still appears as a technical engineering playground, instead of an attractive high-angular-resolution observing method. This can be explained by the fact that general users have little intuition about how interferometric observables, called visibilities, behave as a function of the object shape. In order to bridge the gap for general users, optical interferometry has to step into an "imaging era", as was done for radio interferometry decades ago.

We present the first images from the ESO VLTI (Haguenauer et al., 2008), showing that we are just entering the long-waited "imaging era" of this facility. The instruments are now working better than ever, and the requisite image reconstruction

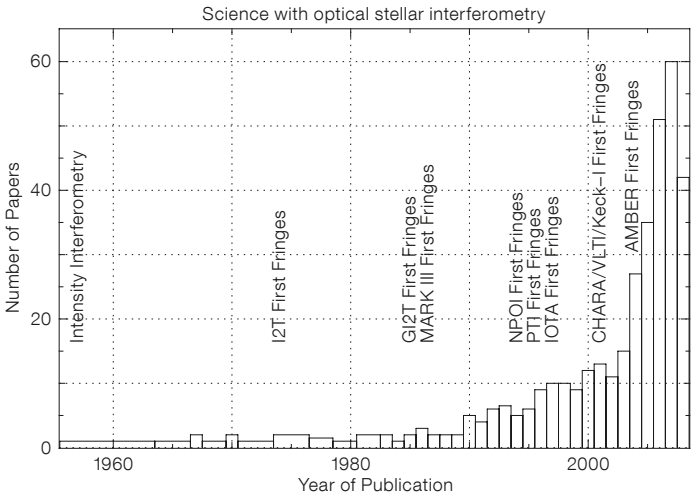

Figure 2. Publications made with optical interferometers, only including scientific results (source OLBIN[1]). We see a steadily increasing number of publications.

software exists. However, this is only a first step, as numerous aspects still need polishing. We will therefore also describe improvements expected to take place in the near future.

Image reconstruction

When light beams coming from two distant telescopes are overlapped they form an interference pattern; and by measuring the contrast and position of this pattern, information about the morphology of the observed astronomical source can be determined. Mathematically, the fringe contrast and position (amplitude and phase) define a complex number, V, linked to the Fourier Transform of the observed brightness distribution (Image) at the spatial frequency B/λ, given by:

$$V(B) = FT\{Image\}\ (B/\lambda)$$

In this equation, B is the geometrical vector joining the telescopes of the interferometer projected into the plane of the sky, generally called the projected baseline. λ is the wavelength of the observation, typically between 1 and 10 microns for the VLTI. FT denotes the Fourier Transform operator, normalised to 1 when B = 0. An interferometer measures some discrete values of the Fourier Transform of the observed image and not a continuous image.

When only a few pairs of telescopes are available, model fitting must be used to convert these observables, the visibilities V(B), into astrophysical quantities. In particular, only the spatial extent — the size — and the level of asymmetry can be constrained, but at a precision unachievable with classical single telescopes. Until recently, this was the method used for the major discoveries made by the VLTI. Among them, we recall the precise radius and limb-darkening measurements of different kinds of stars (see ESO PR 14/03 and ESO PR 25/04), the characterisation of discs surrounding young stars (ESO PR 29/05) and hot Be stars (ESO PR 35/06), the astrometry of close spectroscopic binaries, the study of mass-loss events around evolved stars or novae (ESO PR 22/08), the direct size determinations of small asteroids (ESO PR 04/09), and the unique probe inside the dusty environments of a few nearby active galactic nuclei (AGN).

When large numbers of observations of the visibilities, V(B), of a given target are available, it becomes possible to invert the Fourier Transform of the visibilities (*viz.* $FT^{-1}\{V(B)\}$) to produce an Image of the source. Performing such a computation is called "image reconstruction" because it has to deal with several difficulties. Firstly the spatial sampling of the points V(B) is anything but regular or homogeneous, as shown by the example in Figure 3. Secondly each observation is corrupted by random noise, whose amplification should be avoided during the inversion process. Finally, the phase information cannot be estimated independently for each point V(B), but only along closing triangles of observations (called closure phase). The use of the incomplete phase-closures, instead of the exact phases, makes the inversion problem non-convex (meaning hard to solve).

Several algorithms are now available to reconstruct an image from sparse and noisy V(B) datasets: MIRA, BSMEM, WISARD, BBM and MACIM. These algorithms were the challengers in the series of Optical/IR Interferometric Imaging Beauty Contests, which have quantitatively compared the results of various image synthesis methods every two years since 2004. See Cotton et al. (2008) for the latest results and winners. All the reconstruction methods attempt somehow to adjust an image to the data according to some additional knowledge about the shape of the object. At the least, this additional *a priori* information is that the reconstructed image is positive everywhere. But the reconstruction is strongly aided, and the result more accurate, if additional information can be supplied. Is the image composed of unresolved components (such as a multiple system)? Does the image contain some background level? Is all the flux concentrated inside an area of some known size? All these pieces of information can, and should, be injected into the (choice of the) reconstruction algorithm.

Figure 3. Coverage of the uv-plane obtained after observing with nine different pairs of telescopes made with four configurations of three ATs. Each telescope pair creates an arc since the projected baseline B changes with the Earth's rotation during the night. An estimation of the complex fringe contrast has been obtained for each point. The poor and irregular sampling of the spatial frequencies represents a real challenge for the reconstruction algorithms. The dotted ellipse is the shape of the virtual telescope emulated by these observations.

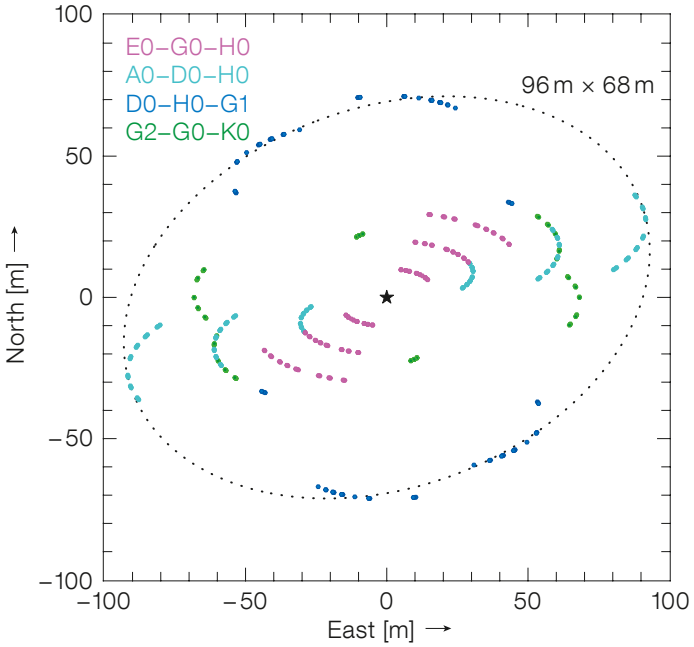

Imaging multiple stars

The first reconstructed image produced by the VLTI is of the binary θ^1 Ori C (see the article in the last *Messenger* issue, Kraus et al., 2009b; and Kraus et al., 2009a), located in the well-known dense Orion Trapezium Cluster. To create an image of this object, the investigators had to observe the system for several nights, using the movable 1.8-metre Auxiliary Telescopes (ATs) and the AMBER instrument (Petrov et al., 2007). The ATs were combined in different groups of three, and were also moved to different positions, creating more new interferometric configurations. Taken together the configuration emulates a virtual telescope approximately 130 m across. AMBER's continuous spectral coverage across the *H*- and the *K*-bands at a spectral resolution of R = 35 allowed better filling of the so-called uv-plane, thanks to the $1/\lambda$ term in the spatial frequency term in the equation. However, because observations were not simultaneous enough, the authors had to artificially rotate the uv-plane between each configuration to account for the binary rotation. The authors employed the Building Block Mapping software (BBM). Starting from an initial single δ-function, this algorithm iteratively adds unresolved components to the image, which is convolved finally with a clean beam that reflects the elongation of the sampled uv-plane.

θ^1 Ori C is one of the youngest and closest high-mass (O5–O7) stars and is also a binary. The resulting interferometric image separates the two components of the system. The observations themselves have a spatial resolution of about 2 milliarcseconds. Figure 4 compares the images of θ^1 Ori C obtained with the VLTI and with the 6-metre Russian Big Telescope. The evident increase of resolving power in the VLTI image directly translates into a much better astrometric accuracy. From these, and several other speckle and interferometric observations, the authors could precisely derive the orbital parameter of this binary system (Kraus et al., 2009a). They concluded that the total mass of the two stars is 47 $M_\odot$ and their distance from us is 415 parsec (pc).

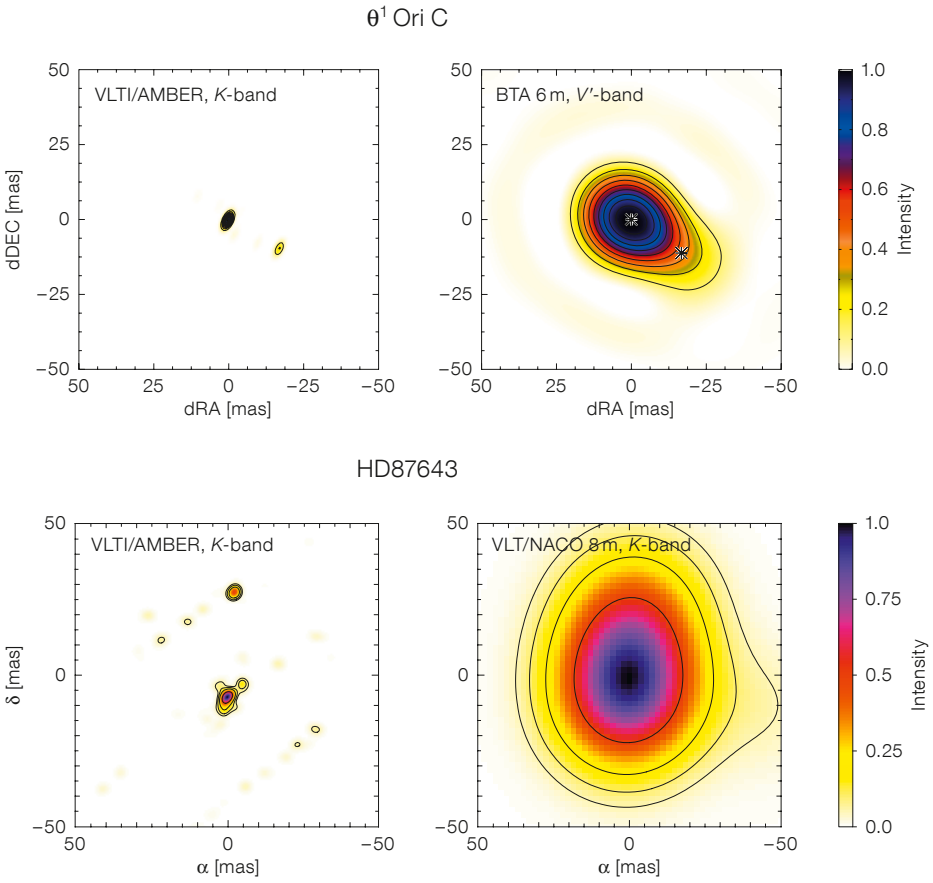

Figure 4. Top: Images of the θ^1 Ori C binary from Kraus et al. (2009). Shown at left is the interferometric image reconstructed with VLTI/AMBER emulating a telescope of around 130 m in diameter. Shown right is the de-convolved image obtained at the 6-metre Russian Big Telescope. For each image, 10 % intensity level contours are shown and the fitted component positions are marked with an asterisk. Bottom: Images of HD87643 from Millour et al. (2009). Shown left is the AMBER interferometric image of the system, with roughly the same spatial resolution as for θ^1 Ori C, and right is a de-convolved image obtained with the AO-assisted NACO instrument at UT4.

The same instrument and method was used by Millour et al. (2009) to reconstruct the image of the binary star HD87643. This star is an extreme example of the B-type stars that show the B[e] phenomenon (*viz.* a B-type star with emission lines). These stars exhibit a spectrum of emission from light element recombination and metallic forbidden line transitions, as well as infrared excess associated with dust emission. Figure 4 shows the images of HD87643 obtained by Millour et al. (2009) with the VLTI and with the NACO camera on UT4. The interferometric image has been built with the MIRA software, employing the "smoothness" and "positivity" constraints only. We have compared the resulting image with that produced by other existing software packages (BBM and BSMEM), which gave substantially the same results.

Interestingly, very little was understood about this B[e] star before our interferometric observations. The evident increase in resolving power in the VLTI image, compared to the NACO image, permitted a clear detection of the binary nature of this system. In addition, the image allowed us to resolve the circum-primary dust shell, which was unattainable at the resolution of single telescope observations. Therefore our new view of HD87643 is: 1) a B[e] star, enshrouded by its dusty circumstellar disc, and whose inner dust-sublimation rim can be seen in the images; 2) a very compact and

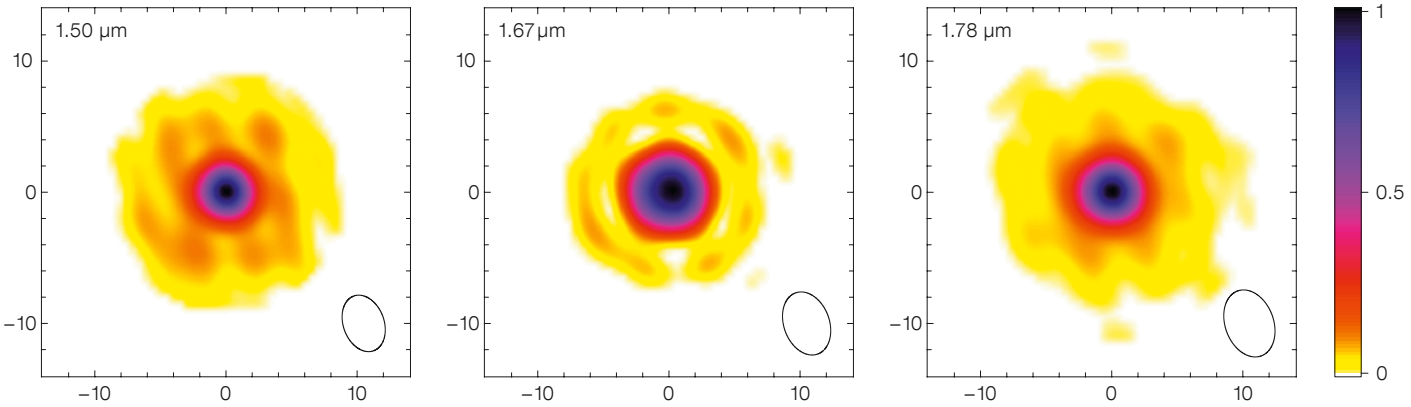

Figure 5. Images of the Mira star T Lep obtained with VLTI/AMBER emulating a telescope of around 100 m in diameter (Le Bouquin et al., 2009). These images in three narrow bands have been extracted from a position-wavelength datacube of around 30 images. Spatial scale is in milliarcseconds. As a comparison, the full image displayed here would fit inside a single pixel of VLT NACO.

dust-enshrouded companion star; 3) the binary system itself immersed in a cocoon of warm silicate dust.

Imaging the surfaces of stars

Mira stars are favourite targets of amateur variable star observers because of their huge variability in the visible wavelength range. These are giant stars that have almost extinguished their nuclear fuel and are losing mass at a high rate before entering the cooling track as white dwarfs. They pulsate with periods of several hundred days and molecules and dust are formed in the layers of the atmosphere immediately surrounding the central star. The Sun will become a Mira star in a few billion years, engulfing the Earth in the dust and gas. Although Mira stars are among the biggest factories of molecules and dust in the Universe, the exact shape, density and composition of the expelled material is still debated.

The classical Mira star T Leporis, in the constellation of Lepus (the Hare), is located at 170 pc and pulsates with a period of 380 days. Although it is a giant star, it is so far away that only facilities like the VLTI can obtain a resolved image of it. We achieved this recently by using the data from four configurations of three ATs (Le Bouquin et al., 2009; ESO PR 06/09). Instead of combining all spectral channels together, as in the case of θ^1 Ori C or HD87643, we were able to build an independent image at each wavelength bin, as shown in Figure 5. We employed the MIRA software (Thiebaut, 2008) with a specific two-step strategy. The first step consisted of building a radially symmetric image from the data. This supposition was supported by a previous analysis of the data, showing no obvious difference in apparent size along different directions. The main interest is that we could make use of relatively simple *a priori* constraints (smoothness) for this first guess image. As a matter of fact, the reconstructed ring-like structure is highly trustworthy. On the other hand the smoothness of the central star is not necessarily a correct assumption and the star could have normal, sharper edges. The second step uses these initial brightness distributions as support for a quadratic regularisation of the 2D images, allowing the software finally to map the asymmetries.

Although only a few pixels across, the reconstructed images shows an extreme close-up of a star about one hundred times larger than the Sun, corresponding roughly to the distance between the Earth and the Sun. The star appears encircled by a sphere of material, which is about three times as large again. Such images unambiguously demonstrate that an envelope of dust and gas, whose aspect ratio and opacity is changing with the wavelength, surrounds a Mira star.

Imaging the innermost part of AGNs

Raban et al. (2009) recently presented interferometric observations of the nucleus of NGC 1068, using the VLTI MIDI instrument. They obtained extensive uv-plane coverage with 16 baselines with a maximal resolution of 120 m (corresponding to 7 milliarcseconds at 10 microns). In common with other AGNs, NGC 1068 is so faint that it could not be observed with the relocatable ATs, but only with the 8-metre UTs. As a consequence, the distribution of the tracks is concentrated in the second/fourth quarter of the uv-plane, with only one observation on a perpendicular baseline, reflecting the fixed physical placement of the UTs. On account of the near-zero declination of NGC 1068, the tracks are parallel to the u-axis.

The authors were able to reconstruct an image of the nucleus using maximum entropy (ME) methods by combining all the 16 observations. The ME methods guarantee that the resulting image will be the most statistically probable reconstruction given the information in the data and considering positivity as the unique constraint (together with the implicit smoothness criterion of ME). One of the main advantages of the ME method is that few prior assumptions about the source are needed to obtain good results from the algorithm. According to Raban et al. (2009), the reconstructed image confirms the basic properties of the source in a completely model-independent way, but it does not provide a more detailed picture than previously known.

Feedback from first images

About six months after obtaining the first images, we can already draw some

general conclusions concerning image reconstruction at the VLTI:
1) The published results demonstrate nicely the capability of this ESO facility to deliver images at a spatial resolution of a few milliarcseconds, although on bright targets only. We recall that such a spatial resolution is unattainable by classical single telescopes, even when considering the ELT era.
2) Up to now, only rather simple objects have been imaged: binaries, simple circumstellar environments, or images with a small field-of-view (perhaps 5 by 5 pixels in size, at maximum).
3) The main results have been obtained in Visitor Mode, with at least three different telescope configurations, so typically over three observing (half-)nights.
4) While it has often been said that the VLTI is too slow, a sampling speed of approximately 25 minutes per calibrated point sounds sufficient.
5) The poor quality of the calibrated visibilities is an important limitation.
6) Finally all existing datasets suffer from a poorly populated uv-plane, especially in the North–South direction.

The two last points cover the majority of the VLTI user complaints, and should receive careful attention from the Science Operations team in the future.

Several other imaging projects are in progress concerning B[e] stars, young stellar objects and supergiants. The investigators generally conclude that the reconstructed images validate the basic properties of the targets in an independent manner for the first time. However, for the moment, the images do not provide a more detailed picture than parametric models. This hurdle could only be overcome by increasing the number and the quality of the visibility measurements, as previously mentioned. However models will always be needed to provide quantitative constraints and to test consistently the physics underlying the images.

Positioning the VLTI in the current international context is rather easy. The VLTI does not yet provide the best imaging capabilities: the MIRC instrument at the CHARA array already combines four telescopes and is being upgraded to six (see, for instance, the image of the surface of Altair by Monnier et al., 2008). The VLTI does not yet provide the best dynamic range: the FLUOR instrument at CHARA, although combining only two telescopes, provides precision below 1%. In terms of limiting magnitude, Keck-I and the VLTI with the UTs have similar performance. However, the VLTI and its instruments do provide a unique spectral coverage, from 1 to 10 microns and a unique spectral resolution up to R = 12 000. It does provide the unique capability of relocatable telescopes (the ATs) that allows both compact (~ 16 m) and large (~ 130 m) interferometric arrays to be built within a few days. Finally, it is the only interferometer with real Service Mode scheduling and a high level of user support, resulting in a large number of refereed publications (more than 200 to date).

Prospects

In the forthcoming years, we believe that improvements in the imaging capability of the VLTI will mainly lie in an enhancement of the data quality, as well as an increase in the number of offered interferometric baselines. Background work by the Science Operations team at the Paranal Observatory is ongoing on these two points. For instance, it is planned to increase the number of offered AT triplets from four (current period) to more than ten (goal for Period 86). Opening and offering new triplets and new telescope stations however requires an intensive effort both from the Engineering and Science Operation teams.

In 2012, the VLTI is expected to receive the second generation instruments MATISSE (Lopez et al., 2008) and GRAVITY (Eisenhauer et al., 2008). These instruments will make use of four telescopes. Combining four telescopes simultaneously, instead of three, simply doubles the number of possible simultaneous visibility measurements (six instead of three): with only one additional telescope, the interferometer is twice as fast at collecting enough points to build up an image. We believe it will be possible to reconstruct a simple image within about two observing nights instead of about four as of now. At that time, getting six ATs could be a decisive step towards allowing routine imaging within the ESO Service Mode framework. Regarding the UTs, the main challenge is to reduce their mechanical vibrations to an acceptable level for interferometry; if achieved, important gains in interferometric efficiency can be expected. The VLTI should then be able to reconstruct simple images of 11th magnitude objects when combining the four UTs together.

In 2015, the VSI instrument (Malbet et al., 2008) is planned to allow six telescopes (15 visibility points) and eventually even eight telescopes (28 visibility points) to be combined simultaneously. Associated with real-time data processing, eminently feasible within the standard ESO observation framework, it would provide a realistic snapshot imaging capability. Ideally a visiting astronomer to the VLTI will see the image of the observed object being reconstructed in real-time at the console.

References

Cotton, W. et al. 2008, Proc. SPIE, 7013, 70131N
Eisenhauer, F. et al. 2008, IAU Symposium, 248, 100
Haguenauer, P. et al. 2008, Proc. SPIE, 7013, 70130C
Kraus, S. et al. 2009, A&A, 497, 195
Le Bouquin, J.-B. et al. 2009, A&A, 496, L1
Lopez, B. et al. 2008, Proc. SPIE, 7013, 70132B
Malbet, F. et al. 2008, Proc. SPIE, 7013, 701329
Millour, F. et al. 2009, A&A, accepted
Monnier, J. et al. 2007, Science, 317, 342
Petrov, R. et al. 2007, A&A, 464, 1
Raban, D. et al. 2009, MNRAS, 394, 1325
Thiébaut, E. 2008, Proc. SPIE, 7013, 70131I

Links

[1] http://olbin.jpl.nasa.gov

Constraining Quasar Structural Evolution with VLT/ISAAC

Jack Sulentic[1,2]
Paola Marziani[3]
Giovanna Stirpe[4]
Sebastian Zamfir[1]
Deborah Dultzin[5]
Massimo Calvani[3]
Paolo Repetto[5]
Radoslav Zamanov[6]

[1] University of Alabama, Tuscaloosa, USA
[2] Instituto de Astrofisica de Andalucia, Granada, Spain
[3] INAF – Osservatorio Astronomico di Padova, Italy
[4] INAF – Osservatorio Astronomico di Bologna, Italy
[5] Instituto de Astronomía, UNAM, Mexico
[6] Bulgarian Academy of Science, Sofia, Bulgaria

We describe a VLT–ISAAC spectroscopic survey of the Hβ region for more than 50 quasars at redshifts between 1 and 3. We use the width of Hβ as a virial estimator of black hole mass and the Eddington ratio. The minimum observed width of Hβ increases from ~ 500–1000 km/s at low luminosity to ~ 3500 km/s in the high luminosity domain. This trend is consistent with the virial assumption and a broad line region size-luminosity relation with exponent α ~ 0.65. Broader lined sources show a second very broad and redshifted Hβ line component, which should be removed for reliable black hole mass estimation.

Forty-five years after their discovery we have a widely accepted idea about the nature of quasars, although much of a fundamental empirical understanding is still lacking. The standard paradigm sees all active galactic nuclei (AGN) as driven by gravitational accretion onto a supermassive black hole. This has led to the impression that all AGN are phenomenologically similar — a view reinforced by the low signal-to-noise (S/N) of most published source spectra. Future advances in understanding quasars will likely come from high S/N spectroscopic studies of broad emission line spectra because such measures provide the most direct clues about the kinematics and geometry of the central broad line region (BLR). They offer the only way to "resolve" the BLR in significant numbers of sources.

We reported in the June 2001 *Messenger* (Sulentic et al., 2001) on how spectroscopic observations with 1–3-metre-class telescopes were improving our understanding of quasar phenomenology through the development of a surrogate H–R diagram (now called 4-Dimensional Eigenvector 1 space: 4DE1) for these sources. The centrepiece of 4DE1 involves four parameters that emphasise correlations and differences between the quasar (defined as sources showing broad emission lines and optical FeII emission) population (Sulentic et al., 2000ab; 2007). 4DE1 studies reveal a source dichotomy that we call Population A–B where the two populations distinguish: a) sources with "narrower" broad lines (FWHM Hβ = 500–4000 km/s) including Narrow Line Seyfert 1s (NLSy1), called Population A; and b) sources with broader lines (> 4000 km/s) including almost all radio-loud quasars, called Population B. We now report on a campaign of VLT–ISAAC spectroscopy (Sulentic et al., 2004; 2006; Marziani et al., 2009) for higher redshift quasars that enable us to extend our low-*z* results out to $z \sim 2$–3. Our VLT programme was designed to derive black hole masses using a single virial estimator (the full width at half maximum [FWHM] of the Hβ line). It was also designed to test the Population A–B concept that arose from our 4DE1 studies at low *z*.

Black hole masses (M_{BH}) and Eddington ratios (L/L_{Edd}) are fundamental parameters of interest to astrophysicists and cosmologists. The Eddington luminosity is that at which the gravitational force is balanced by radiation pressure. We think that M_{BH} and the Eddington ratio are also the principal drivers of source occupation in 4DE1 space, implying that Pop. A sources host the smallest M_{BH} (highest L/L_{Edd}) values and Pop. B the opposite (Marziani et al., 2003). But how are these key parameters measured — especially in high-*z* sources? The width of broad emission lines is considered a reliable indicator of velocity dispersion in the BLR gas surrounding the central black hole. FWHM Hβ is the measure of choice because the line is strong, relativelly symmetric and less uncontaminated by other lines. But how can we compare inferred properties of low-*z* quasars with higher redshift sources where Hβ cannot be observed in the optical domain? One solution was to use other low (MgII 2798 Å) or higher ionisation (CIV 1549 Å) line measures. However it is more difficult to extract reliable FWHM measures for these lines due to strong FeII contamination in the former case and because there is reason to doubt that the latter line is a valid virial estimator.

A more modern solution is twofold: 1) use low-*z* samples to obtain a better understanding (in the 4DE1 context) of source phenomenology; and 2) use VLT–ISAAC infrared spectroscopy to measure FWHM Hβ in high-*z* sources. The former involves estimating the effects of source orientation on line profiles as well as isolating the virial component of Hβ. M_{BH} determinations also require an estimate for the radius of the BLR (r_{BLR}) — only a small sample of low-*z* sources have reasonable estimates from reverberation mapping (Kaspi et al., 2005). We must therefore rely upon — and perhaps constrain — the correlation between r_{BLR} and source luminosity (i.e. the Kaspi relation).

Infrared observing strategy

There is a long history of infrared (IR) quasar spectroscopy (e.g., Kühr et al., 1984), but it has only recently become possible to obtain high S/N spectra of the Hβ region for significant numbers of high-*z* sources. ISAAC is the IR (1–5 μm) imager and spectrograph at the Nasmyth B focus of the VLT Unit Telescope 1 and high S/N spectra of $z = 1$–3 quasars can be obtained when Hβ is shifted into one of the IR "windows". Each spectrum corresponds to a wavelength range (IR windows *Z*, *J*, *H*, *K*) that covers all or, most often, part of the region involving Hβ, the FeII 4570 Å blend and/or the FeII 5130 Å blend. Accuracy in wavelength calibration is especially important and we obtain root mean square (rms) residuals of less than 20 km/s in all windows, which is comparable to the accuracy achieved for low redshift optical spectra with resolution $\lambda/\Delta\lambda \sim 1000$.

VLT–ISAAC spectra collected in four observing seasons have enabled us to measure emission-line parameters for more than 50 quasars in the range z = 0.9–3.2. The sample size now permits a meaningful analysis of luminosity trends and source occupation in 4DE1 space. We chose ESO–Hamburg quasars (Wisotzki et al., 2000) as ISAAC targets, which ensured a well-defined colour-selected sample of sources brighter than m_B = 17.5. We used two large comparison samples of low-z quasars: 1) our atlas of 215 moderate S/N spectra (Marziani et al., 2003); and 2) the 450+ brightest quasars in SDSS (Zamfir et al., 2008). Figure 1 shows examples of both ground-based optical and VLT–ISAAC spectra over the full redshift range of our study.

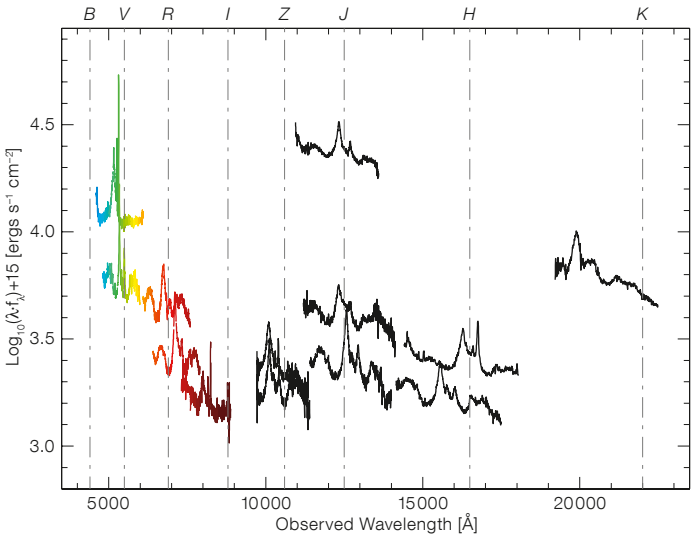

Figure 1. Sample VLT–ISAAC (in black) and optical ground-based spectra of the Hβ region plotted at their redshifted wavelengths. Photometric windows are labelled at the top.

Do quasar spectra change with z and luminosity?

Our samples are ideal for comparing spectra over 6 dex in source luminosity. Figure 2 shows median composite spectra for six luminosity bins (log L_{bol} = 43–49, L_{bol} in units of ergs^{-1}). We find no luminosity correlations in our low redshift samples — consistent with earlier results (Boroson & Green, 1992; Sulentic et al., 2000a; 2004; 2007) that source luminosity is orthogonal to Eigenvector 1 correlations involving FWHM Hβ. Figure 2 shows Pop. A and B composite spectra separately and in fact this 4DE1-inspired distinction is necessary in order to reveal the most significant change in Hβ. Without such a distinction the only luminosity trend that we find involves a systematic weakening of narrow emission lines ([O III] 4959, 5007 Å) with increasing luminosity (see also Netzer et al., 2004 and Marziani et al., 2009, for a few striking exceptions). While narrow line measures are not part of the 4DE1 parameter set, this line decrease raises the question of whether we are seeing a luminosity or redshift (i.e. source evolution) trend. Previous 4DE1 work (Sulentic et al., 2000ab) motivated the suggestion that Pop. A (and especially NLSy1) represent a young quasar population. This interpretation is favoured because we also observe weaker narrow lines in low-z NLSy1 sources. But why then do we see the same diminution in Pop. B composites?

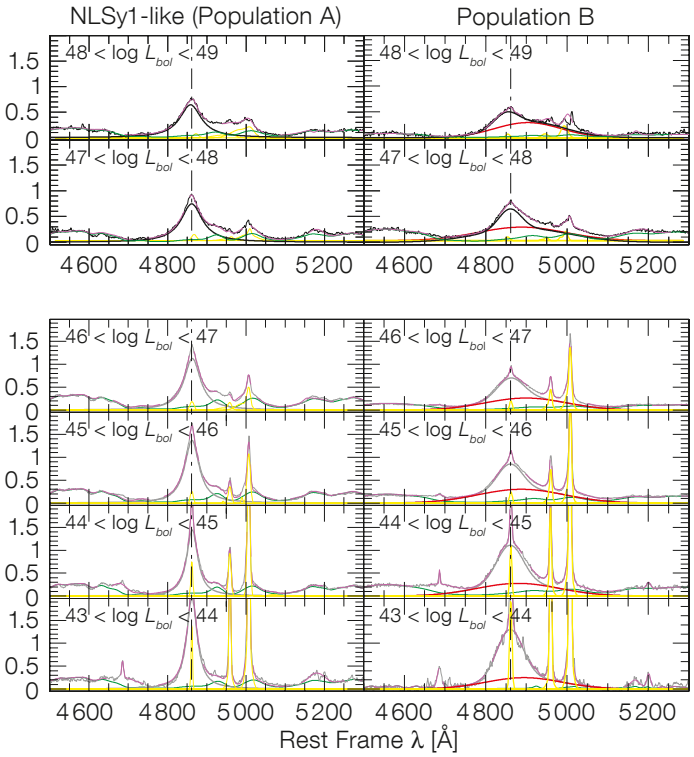

Figure 2. Median composite spectra binned in six integer luminosity intervals. The upper two and lower four bins show the VLT–ISAAC and optical ground-based composites respectively. Population A and B composites are shown for each bin. Fe II contamination (green lines) is always stronger in the Pop. A spectra and a very broad Hβ component (thick red line) is always present in Pop. B spectra.

We find a large spread in FWHM Hβ measures at all redshifts with a well-defined lower boundary that increases from FWHM Hβ ~ 500–1000 km/s at L_{bol} = 48–49. No clear change is observed in the upper FWHM boundary. The change in the lower boundary can be seen in Figure 3 where we plot the distribution of FWHM Hβ measures against log L_{bol}. An increase in minimum FWHM with luminosity is expected if Hβ line broadening is dominated by virial motions and if the emissivity-weighted r_{BLR} depends on luminosity following a power-

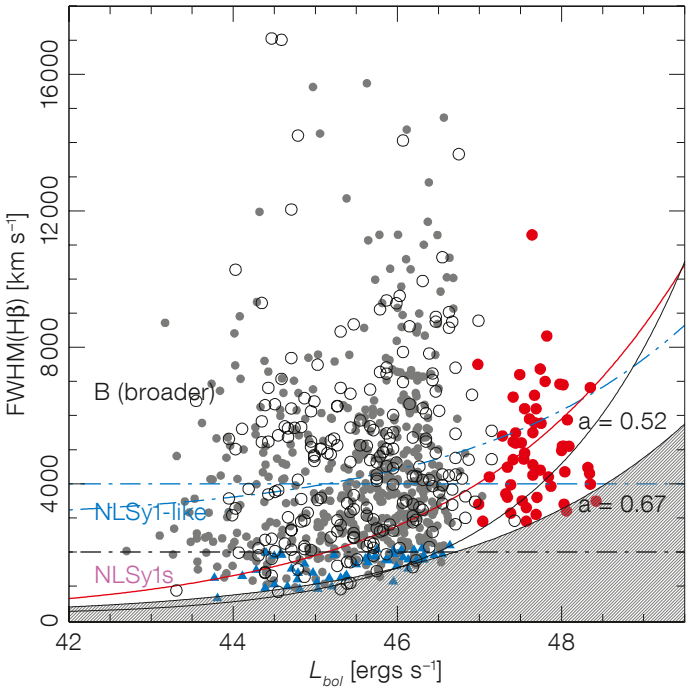

Figure 3. Source FWHM Hβ as a function of bolometric luminosity. Grey dots and open circles show our two low-redshift source samples while red dots indicate the VLT–ISAAC sample. Blue triangles represent additional NLSy1 sources found by Zhou et al. (2006). Horizontal dot-dash lines indicate Pop. A–B and canonical NLSy1-broader source boundaries. Blue dot-dash curve shows modified Pop. A–B boundary based on sources with Lorentzian and Gaussian profiles respectively (Marziani et al., 2009). Two labelled curves show Kaspi relations with exponents $\alpha = 0.52$ and 0.67. The thick red line indicates FWHM increase with L expected for $L/L_{Edd} = 0.15$ (assuming $\alpha = 0.67$). Shaded area is an apparent zone of avoidance for broad-line AGN.

law ($r_{BLR} \propto L_{\alpha}$; Kaspi et al., 2005). The exact value of the index is uncertain, but a more pronounced trend is expected in Figure 3 for $\alpha \approx 0.5$, especially at high luminosity (see caption to Figure 3). Irrespective of the correct value for α, the observed trend is one of the few independent lines of evidence supporting the assumption that broadening of Balmer lines is predominantly virial.

Median spectra in Figure 2 show that Pop. A sources retain very similar (Lorentzian) Hβ line profiles, while the same cannot be said for Pop. B sources, where a red asymmetry grows with increasing source luminosity. There is evidence (Marziani et al., 2009) that this asymmetry is a distinct, redshifted component (we call it the very broad line region or VBLR). This extra line component represents a challenge for both physical models of the BLR and for the use of FWHM Hβ as a virial estimator. Could this be the long-sought evidence for infall onto the central engine? Whatever the origin of the VBLR component, our VLT spectra reinforce the evidence that it is real, and that the Pop. A–B dichotomy has a physical meaning, likely involving changes in the structure of the BLR. This dichotomy has a direct implication for the computation of black hole masses — FWHM Hβ is a reliable virial estimator only for Pop. A sources. Only the core (BLR) part of the line appears to be a reliable virial estimator in Pop. B sources (see also Collin et al., 2006).

Comparing black hole masses and Eddington ratios

Figure 4 shows the distribution of M_{BH} as a function of redshift. M_{BH} estimates for the low-z samples span 4 dex and the VLT sample does not increase that range. The yellow region below the curve is inaccessible to useful observations at this time. Measures of $M_{BH} > 5 \times 10^9\ M_{\odot}$ are problematic if the M_{BH} *v.* M_{BULGE} relation is valid at high-z. $M_{BH} \sim 10^{10}\ M_{\odot}$ would imply stellar velocity dispersions ~ 700 km/s and resultant $M_{BULGE} > 10^{10}\ M_{\odot}$, which are not observed. Recent results on the fundamental plane of elliptical galaxies, and on the most massive spheroids at $z < 0.3$, confirm that stellar velocity dispersion measures are always

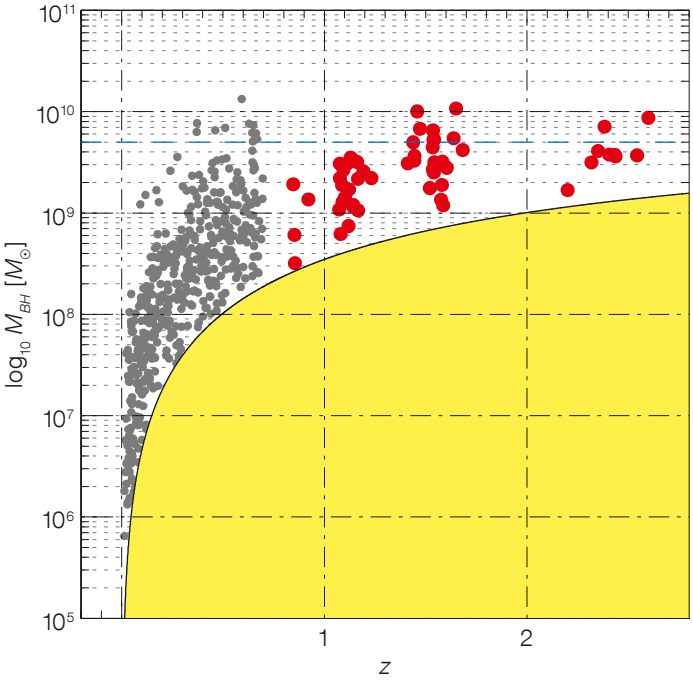

Figure 4. M_{BH} estimates derived from single-epoch FWHM Hβ measures. Red and grey dots represent VLT and low-z SDSS sources respectively. The yellow region is not accessible in our magnitude-limited surveys. The horizontal blue line shows the expected upper limit to the black hole mass of $5 \times 10^9\ M_{\odot}$.

< 500 km/s (Bernardi et al., 2005). Is there real evidence for log M_{BH} values greater than about 9.7?

If we place our confidence in Hβ as the virial estimator, then Figure 2 points toward a way to reduce large M_{BH} values. Our past work, now reinforced by the VLT sample, suggests that all, or most, of these values are overestimates. The VBLR component in Pop. B Hβ profiles shows a large redshift, immediately raising doubts that it arises from a virialised medium. It is safer to assume that the relatively unshifted BLR component is the virial estimator that corresponds most closely to the one used in Pop. A sources. Alternatively one can consider the width of the line part that is responding to continuum changes, which has been estimated for low-*z* sources (see also Sulentic et al., 2000c). If we use either of these two approaches to infer M_{BH} then most values fall below log M_{BH} = 9.7 (blue dashed line indicated in Figure 4). This would remove any serious challenge to the bulge mass–BH mass relation out to $z \sim 3$.

A fixed bolometric correction to the specific luminosity of each quasar provides the luminosity-to-mass ratio or, equivalently, L/L_{Edd}. This approach is very crude, but a bolometric correction is relatively stable for most sources, with the obvious exception of core-dominated radio-loud quasars. Figure 5 shows the distribution of derived L/L_{Edd} estimates as a function of *z*. At $z \sim 1$ we start losing quasars with low L/L_{Edd} that are abundant at low *z*. The loss of sources becomes very serious at $z > 2$ where we are sampling only the highest L/L_{Edd} radiators, which should be equivalent to the low-*z* NLSy1 sources. Low L/L_{Edd} sources should be present at high-*z* (numerous if they are young quasars) but an increasing fraction are unobservable. This effect must be carefully considered when studying L/L_{Edd} evolution in any flux-limited sample.

We note that small populations of Eddington or even super-Eddington radiators are present in our sample. We have previously interpreted the low-*z* sources as oriented near face-on. If line emission arises from a flattened cloud distribution (or accretion disc) where rotational motions dominate, then FWHM Hβ will underestimate virial motions and consequently M_{BH} in sources oriented near face-on. They will appear to be extreme L/L_{Edd} radiators. Reasonable corrections for an assumed face-on orientation will move all of these sources safely below log $L/L_{Edd} \sim 1$ (Sulentic et al., 2000a; Marziani et al., 2003; Ryan et al., 2007). But what of the high-*z* VLT sources at or near log $L/L_{Edd} \sim 1$ seen in Figure 5? The simplest interpretation places them as high luminosity analogues to lower-*z* NLSy1s.

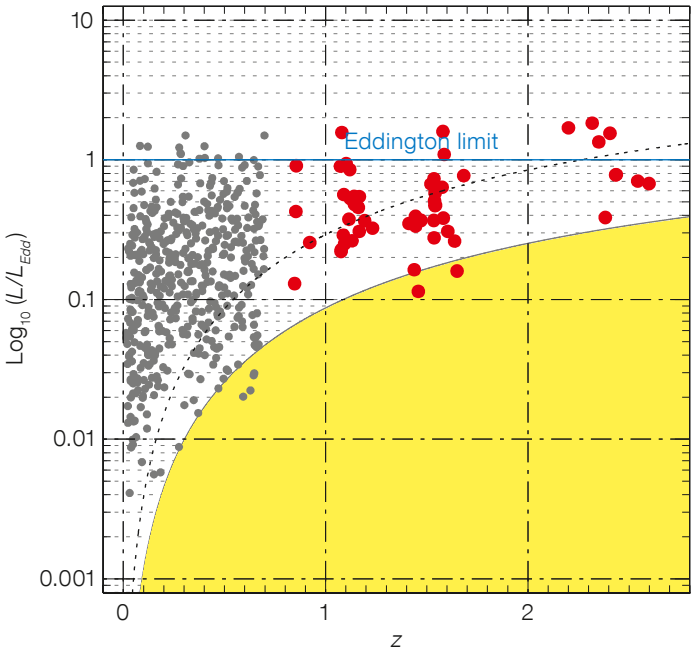

Figure 5. L/L_{Edd} estimates derived from the M_{BH} estimates shown in Figure 4. Red and grey dots represent VLT–ISAAC and low-*z* SDSS sources respectively. The yellow region is not accessible in our magnitude-limited surveys. Dotted and filled curves represent minimum detectable values of L/L_{Edd} (fixed log M_{BH} = 9.6) for magnitude-limited surveys to m_B = 16.5 and 17.5 respectively.

A modest investment of observing time (equivalent to a single run of 6–7 nights) provided data with unprecedented S/N and resolution and in a redshift range where they were completely absent. The data enabled us to identify several interesting luminosity trends that were not evident in large low-*z* samples. The ISAAC data reinforce the significance of the Pop. A–B dichotomy by showing that the redshifted VBLR Hβ is the stronger Hβ component in the most luminous Pop. B sources. They also permited a more reliable comparison of M_{BH} and L/L_{Edd} estimates out to $z \sim 3$. The observation of large black hole masses at $z \sim 3$ and beyond (Kurk et al., 2007) suggest that either: a) at least some supermassive black holes grow early in the history of the Universe; or b) rotational motions no longer dominate the Hβ line profile. Since iron enrichment and black hole growth require predictable timescales, extension of observations to high-*z* may eventually provide intriguing tests of the current cosmological scenario. It is premature to say whether the lack of spectral evolution poses problems for the concordance cosmology.

References

Bernardi, M. et al. 2005, AJ, 129, 61
Collin, S. et al. 2006, A&Ap, 456, 75
Kaspi, S. et al. 2005, ApJ, 629, 61
Kühr, H. et al. 1984, ApJ, 284, L5
Kurk, J. et al. 2007, ApJ, 669, 32
Marziani, P. et al. 2003, MNRAS, 345, 1133
Marziani, P. et al. 2009, A&Ap, 495, 83
Netzer, H. et al. 2004, ApJ, 614, 558
Ryan, C. et al. 2007, ApJ, 654, 799
Sulentic, J. W. et al. 2000a, ApJ, 536, L5
Sulentic, J. W. et al. 2000b, ARA&A, 38, 521
Sulentic, J. W. et al. 2000c, ApJ, 545, L15
Sulentic, J. W. et al. 2001, The Messenger, 104, 25
Sulentic, J. W. et al. 2004, A&Ap, 423, 121
Sulentic, J. W. et al. 2006, A&Ap, 456, 929
Sulentic, J. W. et al. 2007, ApJ, 666, 757
Zamfir, S. et al. 2008, MNRAS, 387, 856
Zhou, H. et al. 2006, ApJS, 166, 128

Velocity Fields of Distant Galaxies with FORS2

Bodo Ziegler[1]
Elif Kutdemir[2]
Cristiano Da Rocha[1]
Asmus Böhm[3]
Wolfgang Kapferer[3]
Harald Kuntschner[1]
Reynier Peletier[2]
Sabine Schindler[3]
Miguel Verdugo[4]

[1] ESO
[2] Kapteyn Institute, Groningen, the Netherlands
[3] University of Innsbruck, Austria
[4] University of Göttingen, Germany

We describe a method of obtaining two-dimensional velocity fields of distant, faint and small, emission-line galaxies efficiently with FORS2 at the VLT. The fields are examined for kinematic substructure to identify possible interaction processes. Numerical simulations of tidal interactions and ram pressure effects reveal distinct signatures observable with our method. We detect a significant fraction of galaxies with irregular velocity fields both in the field and cluster environments.

Galaxy formation and evolution are still principal research topics in modern astrophysics, and have been investigated since objects outside the Milky Way were recognised after the Great Debate between Shapley and Curtis. The main questions include: When and how did galaxies form? Why are there different morphological types? What is the role of environment? The models used to answer these questions range from single epoch to continous creation scenarios. The current theoretical paradigm of a cold dark matter (CDM) dominated Universe predicts a hierarchical bottom-up structure evolution from small entities towards bigger systems through merging. During such a process spiral galaxies can be transformed into ellipticals. However, the disc component can be regained through subsequent new gas accretion and star formation. Many irregular and peculiar galaxies are observed in clusters of galaxies, in which they may experience interactions in addition to merging and accretion.

Much progress has been achieved in recent years by deep photometric surveys (like GOODS) finding galaxies and quasars at high redshift ($z \sim 6$) corresponding to an epoch just a billion years after the Big Bang. These surveys have revealed a dichotomy between blue, star-forming and red, passive galaxies at later times, with an evolutionary transition between the two groups. Spectroscopic surveys (like the Canada France Hawaii Redshift Survey, CFHRS) have additionally produced evidence that there is a sharp decline in the overall star formation activity in the cosmos within the last eight billion years. However, all these results are based on measurements of the luminosity as produced by the stars, while the total mass of a galaxy is mainly composed of dark matter. Because the triggering and process of star formation contains complicated physics, we need to make many assumptions and simplifications in our modelling, and, in addition, we do not clearly understand the scaling between the baryonic and dark matter. Therefore, it would be more favourable if we could determine observationally the total mass of galaxies and compare its evolution directly to the predicted structure assembly.

Such measurements of the dynamical mass of even faint and small, very distant galaxies were achieved recently by a number of research groups using the largest telescopes. Through spectroscopy they derive the internal kinematics (motions) of the stellar systems that are subject to the whole gravitational potential. In the optical wavelength regime, we can conduct these measurements out to redshifts of one. For spiral galaxies, we can determine the rotation curve from gas emission lines (like [O II] at 372.7 nm restframe wavelength). If the galaxy is undisturbed, the rotation curve rises in the inner part and turns over into a flat plateau dominated by its dark halo and we can calculate the maximum rotation velocity V_{max}. In such a case the assumption of virialisation holds, so that we can use the Tully–Fisher relation (TFR; Tully & Fisher, 1977) as a powerful diagnostic tool that scales the baryonic matter (parameterised, e.g., by stellar luminosity) to the dark matter (as given by V_{max}). Our group, for example, has found that the TFR of 130 distant ($z = 0.5$, on average) field galaxies has a shallower slope than the local one if restframe *B*-band luminosities are considered, so that the brightening of a slow rotator is much larger than that of a fast rotator (Böhm & Ziegler, 2007). This result can be interpreted principally in two ways: either the majority of distant galaxies are much more scattered around the TFR and we do not see enough regular spirals at the faint end; or, there is a mass-dependent evolution with low-mass objects exhibiting on average a stronger effect over the last five billion years. The latter scenario is supported by modelling the chemical evolution of our galaxies that has revealed less efficient, but extended, star formation for slow rotators (Ferreras et al., 2004) and is consistent with other observational evidence for a mass-dependent evolution (often called “downsizing”).

For a correct application of the TF analysis a galaxy must be undisturbed, so that the assumption of virial equilibrium is fulfilled and, therefore, the rotation curve shows a very regular shape. If this is not the case, can we then still learn something? In the CDM structure formation theory, galaxies evolve by merging and accretion, so that we can look for kinematic signatures of such events and whether there is an increase in the abundance of such types with redshift. To investigate a possible environmental dependence, we need to disentangle such collisions from the numerous other interaction phenomena that galaxies can experience in groups and clusters.
The gas content of spirals reacts to the ram pressure exerted by the intracluster medium, a hot plasma permeating the whole structure. Part of the gas can also be stripped off by tidal forces (sometimes called “strangulation”). Other processes like harassment can even remove stars from galaxy discs, so that the overall morphology is altered. However, (irregular) rotation curves from slit spectroscopy do not contain unique information to reveal a specific interaction process unambiguously. In addition, peculiar shapes can sometimes be caused artificially by observational and instrumental effects when long slits are used (Ziegler et al., 2003; Jäger et al., 2004). A more favourable observation would, therefore, be that of a two-dimensional velocity field.

FORS2 spectroscopy to obtain velocity fields

Many large telescopes today offer 3D-spectroscopy and most future facilities (like the European Extremely Large Telescope) will provide such instrument modes. At the VLT, for example, VIMOS and FLAMES offer integral field unit (IFU) spectroscopy in the optical regime. For our specific purpose, however, we conceived a different method of obtaining velocity fields that has many advantages for our science case: matched galaxy sizes, good spatial resolution, long wavelength range and high efficiency through a large number of simultaneous targets and economic exposure times (see Kutdemir et al., 2008).

For our procedure, we utilise the MXU mode of FORS2 that allows slits to be cut individually and at any desired orientation into a mask by a laser. We pick up a particular target and start with a slit placed along the photometric major axis, as measured on spatially highly resolved images from the Hubble Space Telescope/Advanced Camera for Surveys (HST/ACS; Figure 1). The slit with width 1 arcsecond covers the full size of the galaxy in its mid-plane and extends much beyond it to allow an accurate sky subtraction (common slit lengths are 15–25 arcseconds). In the same manner, 20–30 more slits are placed on other targets across the full field of view of FORS2 (6.8 × 6.8 arcminutes), with, occasionally, even two or three objects falling into the same slit. Observations with such a mask will eventually yield rotation curves, as for our previous projects, with one spatial axis and one velocity axis by measuring the centre positions of an emission line row-by-row along the spatial profile of the two-dimensional galaxy spectrum (Böhm et al., 2004). In order to construct a velocity field with two spatial axes, we observe all targets twice more with different slit positions using two more masks. This time slits are offset by 1 arcsecond along the minor axis of the galaxy to either side of the first position, so that all three slit positions together correspond to a rectangular grid (Figure 1). In that way, the full extent of a galaxy is covered, which is particularly important for a TF (*viz.* undisturbed) galaxy, where we need to measure the flat part of the rotation curve, which is usually reached at about three disc scale lengths. At the redshifts of our targets (z = 0.1–1.0), this corresponds to angular sizes of about 3–6 arcseconds. The spatial resolution along the x-axis of our grid is given by the pixel size of the FORS2 CCD chips of 0.25 arcseconds. For the y-axis, we are restricted by the slit width of 1.0 arcsecond, which is a good compromise between minor loss of light falling out of the slit due to seeing, adequate spectral resolution (R = 1000), and spatial sampling in the y-direction.

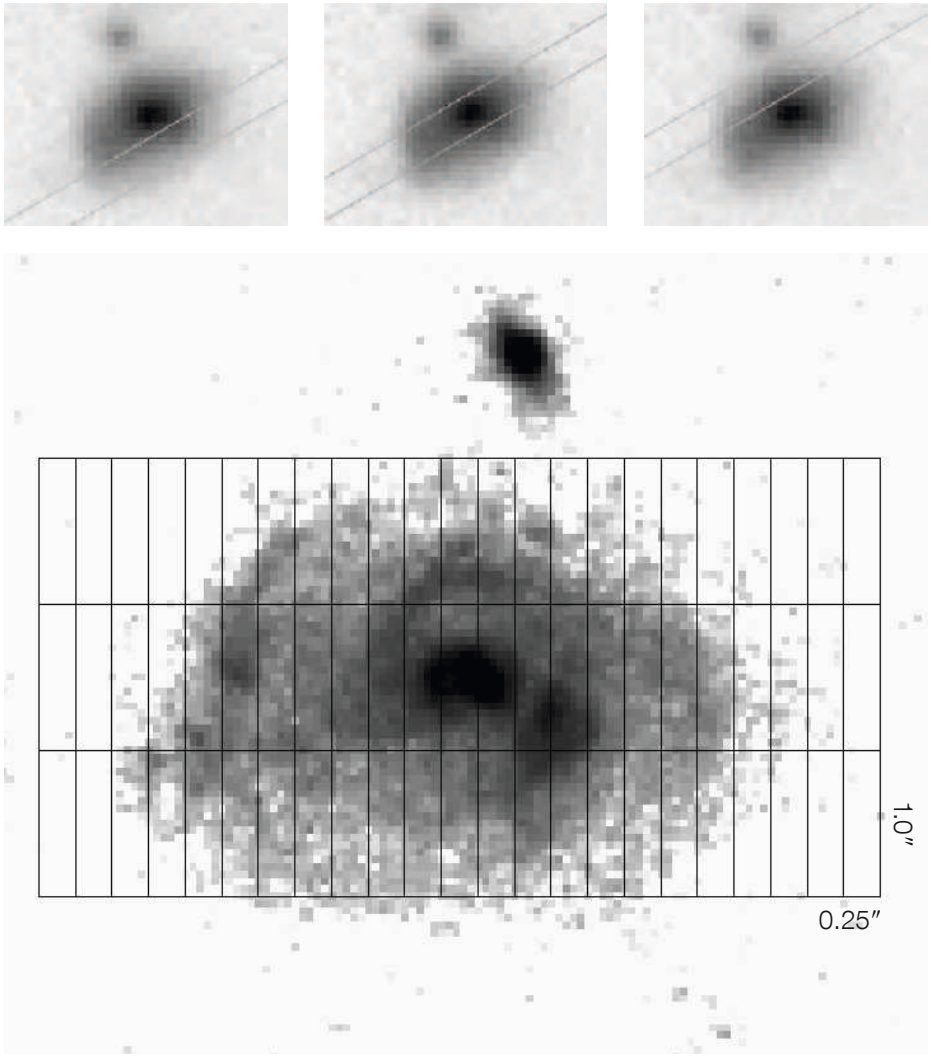

Figure 1. Our method for obtaining two-dimensional velocity fields with FORS2 is based on the observation of three different slit positions per target (upper). The combination of the measurements yields independent data points for a rectangular grid covering the whole galaxy (lower). From Kutdemir at al., 2008.

For the spectral element we use a high-throughput holographic VPH grism (600RI) that results in a long wavelength range (330 nm) projected onto the CCD. This has two advantages: for each galaxy several gas emission lines and many absorption lines of the stellar continuum are visible; all the absorption lines can be combined to derive the stellar rotation curve in addition to the gaseous one. Depending on the redshift of the object, emission lines from the blue [O II] line (at 372.7 nm) to the red Hα line (at 656.3 nm) are visible. While up to seven different lines can be observed in case of some field galaxies, most cluster members have four (Figure 2). This allows us to derive rotation curves and velocity fields in several independent ways and to check for consistency. In addition it also allows us to investigate possible dependencies

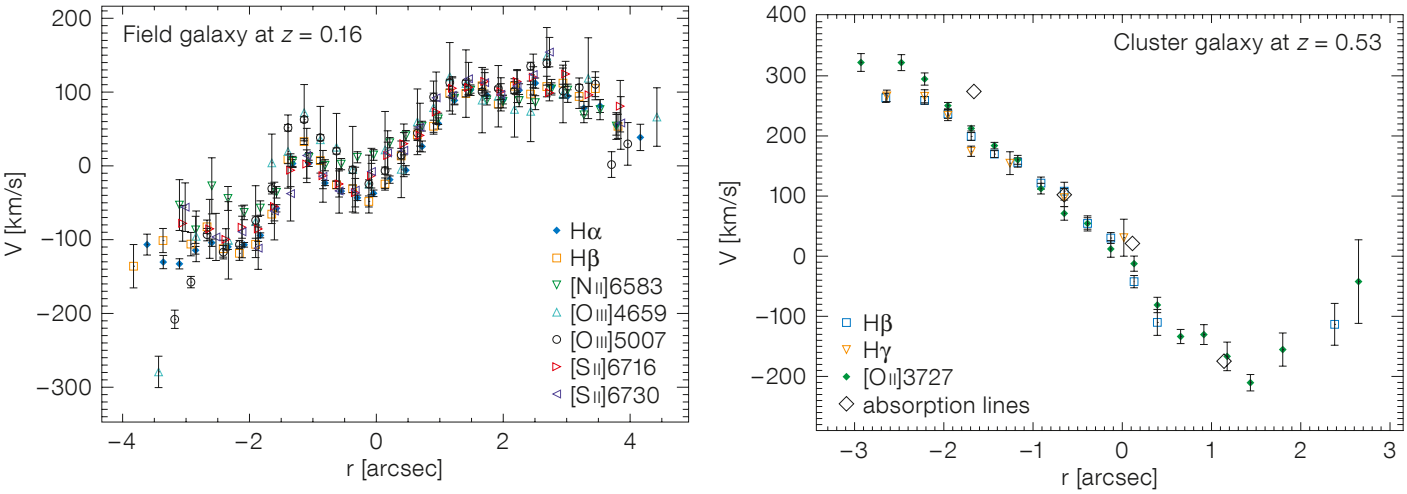

Figure 2. Two examples of rotation curves derived from the central slit. For some field galaxies up to seven different emission lines can be used independently to study the *gas* kinematics across a galaxy (left). For brighter galaxies, even *stellar* rotation curves can be measured by combining many absorption lines (right). From Kutdemir at al., 2008.

on the physical state of the gas clouds that emit the respective lines (all galaxies have both recombination and forbidden emission lines). From line ratios, we can then construct metallicity maps and assess a possible contribution from active galactic nuclei (AGN) activity in addition to star formation.

Despite the need for the observation with three masks in order to construct a velocity field, our method is still highly efficient. The VPH grism with its medium spectral resolution, together with the excellent optics of FORS2 mean that sufficient signal can be reached in an emission line to measure the line centres in each spectral (CCD) row accurately with 2.5 hours total integration time. This holds also for the outer regions of the galaxies, where the surface brightness drops to low values (from typically 22 V_{mag}/sq. arcsecond in the inner part to about 26 V_{mag}/sq. arcsecond). Therefore, we can obtain the necessary data for a large number of objects (20–30) within a total integration time of only 7.5 hours. For comparison, FLAMES observations with 15 IFUs of similar targets need integration times of 8–13 hours.

The standard reduction of the spectroscopic images produces a wavelength calibrated two-dimensional spectrum for each slit position of the mask separately. Thanks to the high stability of FORS, exposures of the same mask taken on different nights can be combined into a single deep spectrum. As for the determination of rotation curves, the wavelength of the centre position of a given emission line is measured along the spatial profile. Differences from a common systemic centre can then be translated into velocity space, applying Doppler's rule. The construction of the velocity field, VF, needs a very careful combination of the measurements from the three slit positions. So that we knew the exact position of the masks relative to each other, we also included a few stars with narrow slits perpendicular to each other. These stellar spectra are also used to determine the seeing during the exposure. In addition, for a third of the galaxies per mask the central slit position was taken, while the other two thirds had the off-centre positions, thus alleviating both mask acquisition during observations and mask combination in data reduction. To set up the VF, each position–velocity data point is then

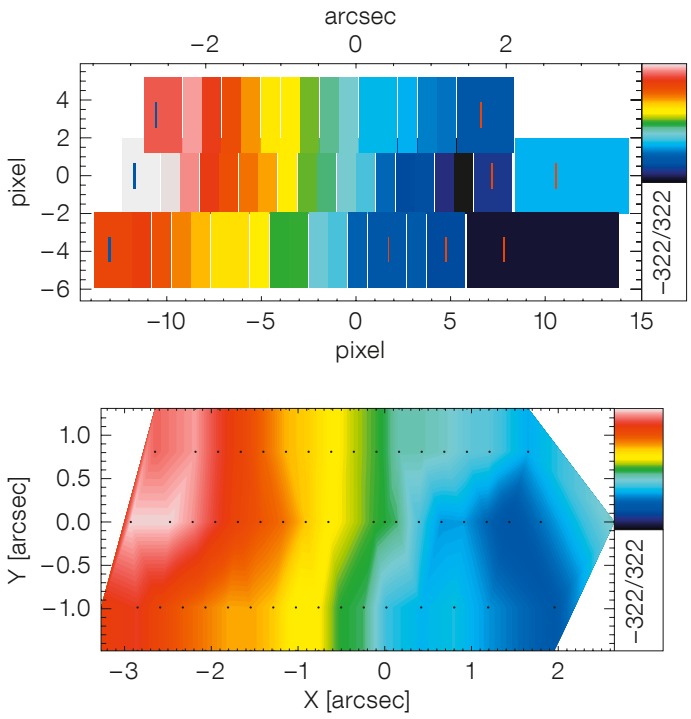

Figure 3. Example of an observed velocity field of a cluster spiral at z = 0.5 displayed in the upper panel as binned independent data points and in the lower panel linearily interpolated for visualisation purposes (from Kutdemir at al., 2008).

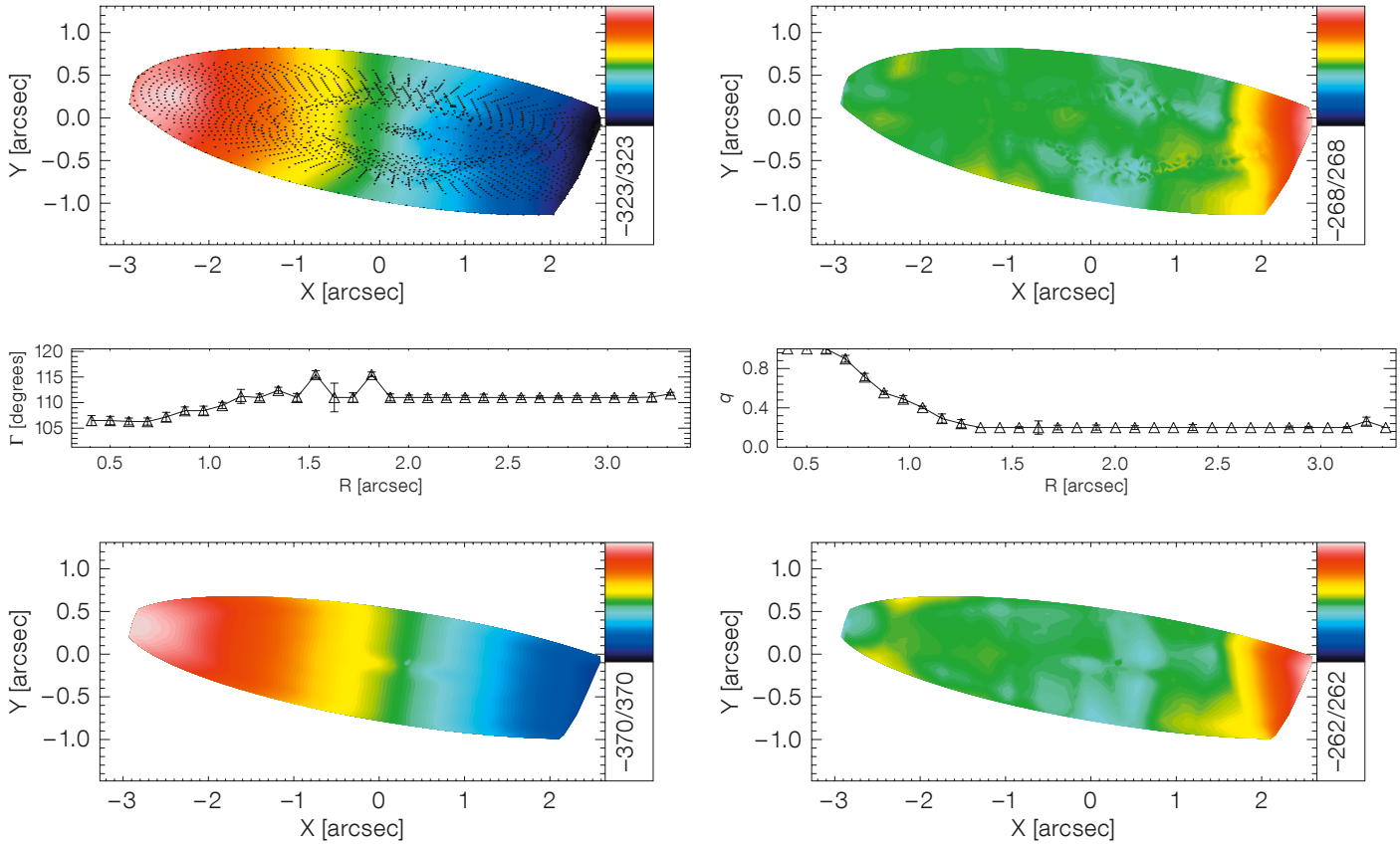

Figure 4. Velocity field of the galaxy in Figure 3 reconstructed by kinemetry with best-fitting ellipses overplotted (top left) and its residual map (top right) obtained by subtracting the model from the observed field. A model (bottom left) and its residual (bottom right) of the circular velocity component (rotation map) constructed for the average value of the kinematic position angle Γ and flattening q (shown in the middle panels as function of distance to the kinematic centre) (from Kutdemir at al., 2008).

calculated within a common coordinate system, whose origin was determined from the intensity maximum of the spatial profile around the emission line in the central slit and its respective wavelength. An example is shown in Figure 3.

Kinemetric analysis of velocity fields

Since our VFs cover a large fraction of a galaxy's extent with good spatial resolution, we can analyse them quantitatively in some detail. We use kinemetry (Krajnovic et al., 2006), originally developed for nearby galaxies observed with the SAURON 3D-spectrograph, whose VFs have much higher signal and resolve much smaller physical scales than is the case of our distant targets. In polar coordinates the velocity profile of a flat rotating disc can be described by a cosine function of the azimuthal angle. Best-fitting ellipses, along which the velocity profiles are extracted, can be determined as a function of radius. Deviations from these fits can be quantified by a harmonic Fourier expansion, whose coefficients can be interpreted in terms of physical parameters. While the first order reflects the bulk motion (the rotation), the third and fifth orders, for example, describe the correction to simple rotation and indicate separate kinematic components. For the reconstruction of the intrinsic velocity map, the free parameters are the flattening and the position angle of the ellipses, while their centres are fixed to a common origin. An example of a reconstructed velocity map with best-fitting ellipses overplotted is given in Figure 4. When, instead, the inclination and position angle are fixed to their average global value, a simple rotation field along the kinematic major axis can be modelled. Its residuals with respect to the observed VF may indicate non-circular velocity components like streaming motions along spiral arms or along a bar. Additional components such as a decoupled core can be recognised in such a residual map, or from an increase in the k_5 Fourier coefficient caused by twists in the position angle and flattening. A rotation curve is extracted from the observed VF along the kinematic major axis to determine V_{max} accurately, which may be different from the one derived from the curve along the central slit aligned with the photometric axis.

Simulations of interactions: structure and kinematics

One of the main goals of our project is to identify signatures of possible interaction events. Galaxies may be transformed from one type into another not only by merging or accretion, but also by other effects like ram-pressure stripping or harassment in the environment of a cluster or group. Open questions are still: which processes are efficient under what conditions and whether there is a

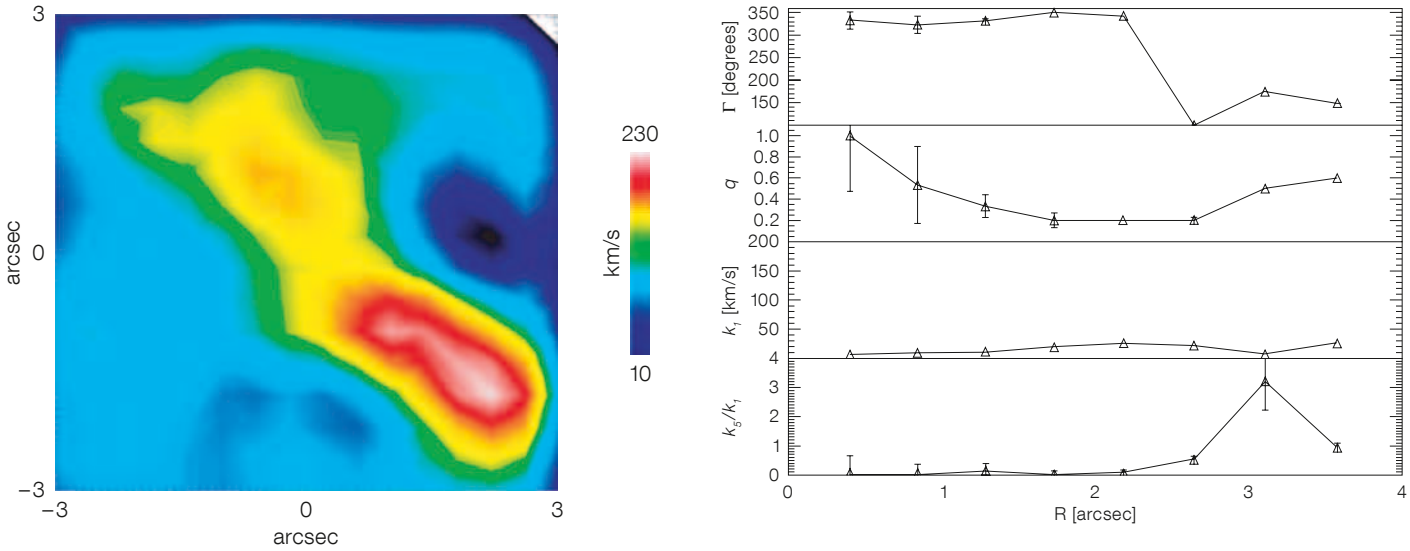

Figure 5. Velocity field of a simulated major merger as would be observed at $z = 0.1$ (left) and radial profiles of some parameters (kinematic position angle, flattening, first Fourier coefficient indicating the bulk motion and normalised fifth Fourier coefficient indicating separate kinematic components) determined by kinemetry (right). The case shown refers to a small galaxy that has penetrated a bigger one, seen 200 Myr after the event (from Kronberger at al., 2007).

dominant mechanism responsible for the abundance of elliptical galaxies in local rich clusters. In order to study systematically the distortions and irregularities in rotation curves and velocity fields caused by interaction phenomena, we performed N-body/smoothed-particle hydrodynamics (SPH) simulations and extracted both structural and kinematic information from the computer output in the same manner as from observational data. The numerical calculations were carried out for the three components — dark matter halo, stellar body and collisional gas clouds — of a galaxy and are based on the Gadget2 code (Springel, 2005) that incorporates hydrodynamic physics (and has explicit prescriptions for star formation and feedback).

So far, we have modelled minor mergers, major mergers, tidal interactions caused by fly-bys and ram-pressure stripping (Kronberger et al., 2007; 2008). There are large variations in the degree of distortions both in stellar structure and gas kinematics in the case of the first three of these processes, with the main dependencies being on the mass ratio of the galaxies, the geometry of the interaction in real space and the projection onto the sky plane (the viewing angle of the observations). In the case of a major merger, however, there is always a clear signal in the higher order coefficients of the Fourier decomposition of the kinemetry (Figure 5). Ram pressure by the intracluster medium, on the other hand, mainly affects the gas disc, pushing away the outer parts and creating distortions at the edge of VFs, while regular rotation can be maintained in the inner regions (Figure 6). In certain configurations, the gas disc can also be displaced from the centre of the stellar disc. During the stripping event, gas can also be compressed so that enhanced star formation is triggered, leading to changes in the stellar populations, too (Kapferer et al., 2009).

In addition, we utilise the simulations to investigate systematically how velocity fields and their characteristic parameters are influenced by the instrumental and observational setup (like spectral resolution, seeing) and for which cases artificial distortions can be induced. A major impact is caused by the decreasing spatial resolution of the spectra when galaxies are observed at higher and higher redshifts. Minor irregularities can be completely smeared out due to seeing and the resolution elements being too coarse.

Currently, we are in the process of analysing each observed galaxy individually. In the case of a regular VF, we perform a TF analysis deriving the rotation curve along the kinematic major axis. For irregular galaxies we examine both the VF and the stellar structure (as revealed on our HST/ACS images) and compare them to a suite of simulated events, taking into account the specific galaxy parameters, in order to pin down the specific interaction mechanism that caused the distortions.

Velocity fields of distant galaxies

The spectroscopic observations using the method presented were performed in Periods 74 and 75 in four different cluster fields (MS1008.1-1224 at $z = 0.30$, MS2137.3-2353 at $z = 0.31$, Cl0412-65 at $z = 0.51$ and MS0451.6-0305 at $z = 0.54$). The target galaxies were not only cluster members but also field galaxies in the background and foreground ($0.1 < z < 0.9$), so that we can investigate different environments. All cluster fields were imaged with ACS onboard HST, enabling an accurate assessment of the morphological structure of the galaxies as well. Our method presented here yielded velocity fields for 49 objects with good signal-to-noise appropriate for our kinemetric analysis. Out of these, there are 16 VFs suitable for investigation of possible interaction processes in rich clusters.

In addition to our detailed analysis with comparison to simulations, we also investigated average properties to assess the abundance of galaxies that have irregular kinematics, irrespective of any assumption of a particular interaction process. To

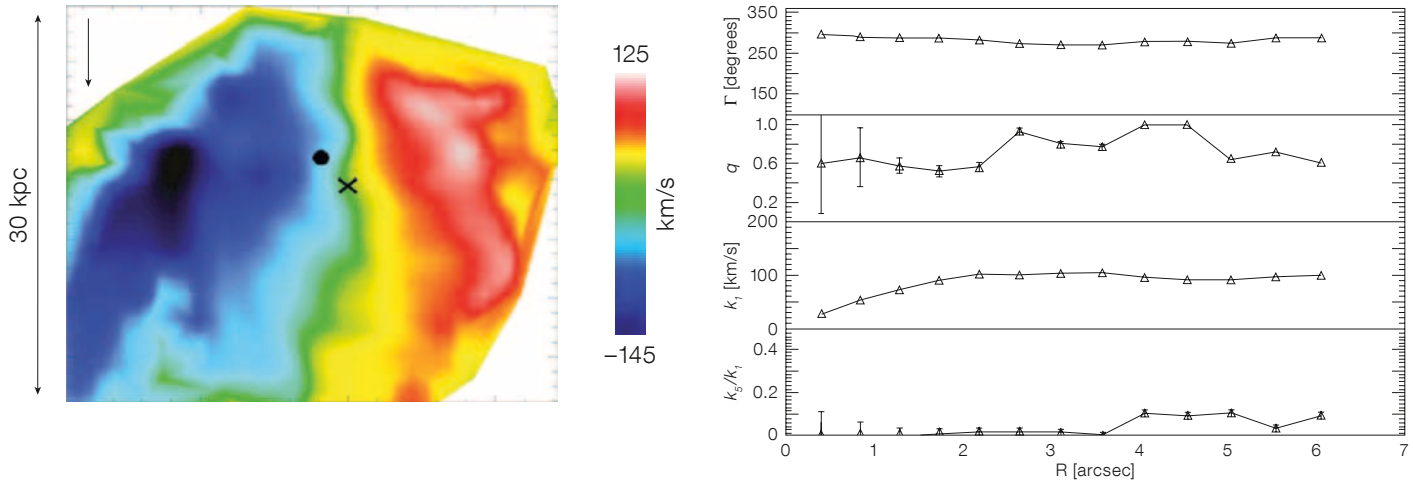

Figure 6. Velocity field of a simulated ram-pressure stripped galaxy as would be observed at $z = 0.1$ and radial profiles (kinematic position angle, flattening, first Fourier coefficient and normalised fifth Fourier coefficient) determined by kinemetry, as in Figure 5a. The case shown refers to one where edge-on ram pressure has already been in action for 400 Myr, with the black arrow indicating intracluster matter wind direction and the cross and circle indicating the kinematic and stellar disc respectively (from Kronberger at al., 2008).

that purpose, we quantify deviations from a simple smooth rotation field with three different indicators measured for each galaxy in the same way. The first two parameters we use are pure gas kinematic tracers: 1) σ_{PA}, the standard deviation of the kinematic position angles of the best-fitting ellipses found by kinemetry across a galaxy; and 2) $k_{3,5}/k_1$, an average value of higher order Fourier coefficients normalised by the rotation velocity. The third parameter compares the global velocity field determined by spectral lines emitted by the (warm) gas content of a galaxy to its morphological structure seen in the continuum light of the stars, given by $\Delta\varphi$, the mean difference between photometric and kinematic position angles across a galaxy. To find an appropriate limit of the value range, below which a galaxy can still be classified as undistorted, we measured the three parameters first for a local sample (taken from Daigle et al., 2006) of

Figure 7. Abundance of galaxies distributed according to our three irregularity parameters, with upper panels showing the local sample and bottom panels the distant, field (green hashed) and cluster (blue) galaxies. Galaxies are classified irregular if $\Delta\varphi > 25$, $k_{3,5}/k_1 > 0.15$ or $\sigma_{PA} > 20$ degrees (from Kutdemir at al., 2009).

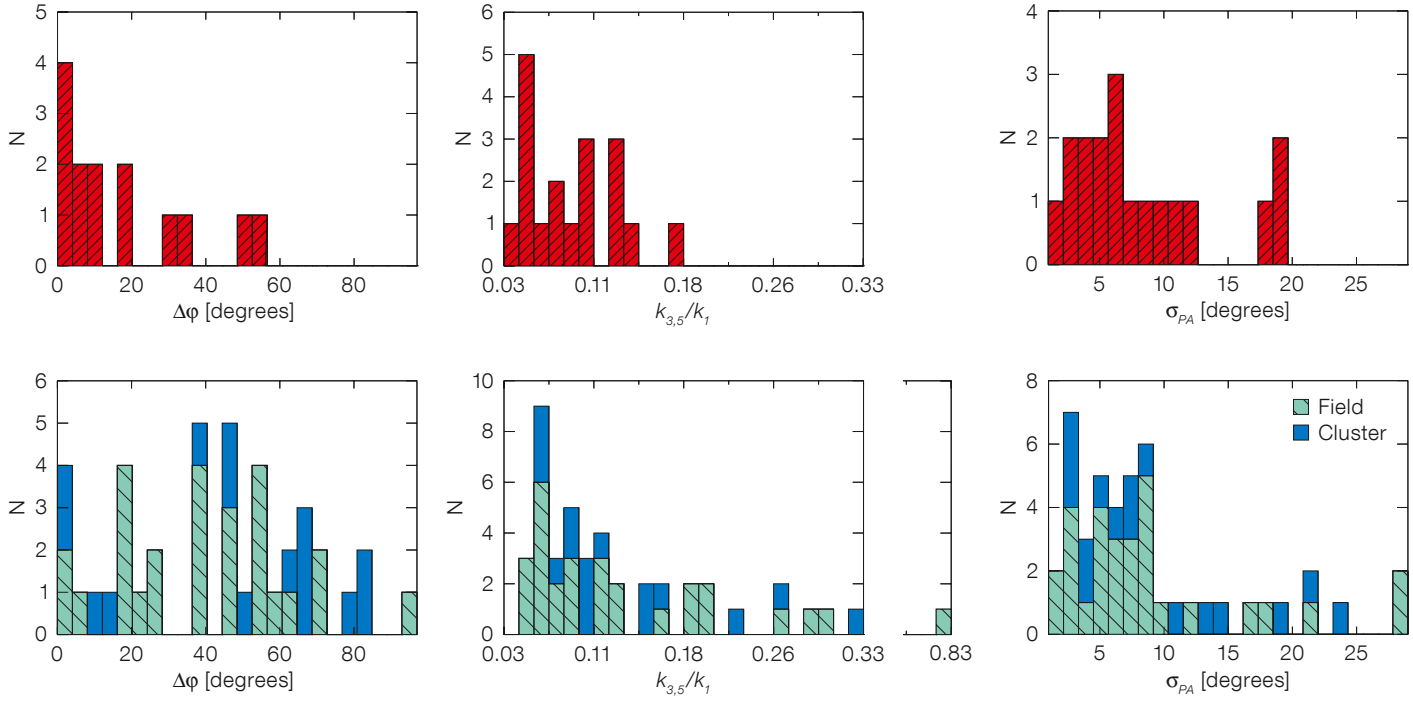

18 galaxies that have high resolution VFs (see Kutdemir et al., 2008).

For our distant sample, we find that the fraction of galaxies classified to be irregular according to the three indicators is not unique. For the two pure kinematic tracers we derive a much lower percentage (about 10 % and 30 %) than for the third parameter (about 70 %); see Figure 7 and Kutdemir et al. (2009). The parameters trace different signatures of external processes, but are also sensitive to intrinsic properties. For example, the presence of a bar misaligned with the disc's major axis can also cause a large offset between the gas field and the stellar component. In addition, peculiarities in a VF are more affected by a coarse spatial binning and could be "smeared out". By modelling resolution effects we found that the irregularity fractions we measure are lower limits only.

Furthermore, our simulations show that only strong interactions, like major mergers, induce large values of the kinematic tracers indicating large distortions with high significance. So most of our observed objects with smaller values of the irregularity parameters probably underwent more subtle events. This is presumably also the reason for the surprisingly similar abundance of peculiar galaxies in the field and cluster environment, no matter what indicator is chosen. Since we detect more irregular field galaxies at intermediate redshifts than in the local sample, we are probably witnessing the ongoing growth of their discs via accretion and minor mergers as predicted in CDM models. To clarify decisively the ongoing processes both for field and cluster galaxies, we will, in the near future, examine all available pieces of information for each galaxy (gas VFs, stellar rotation curves, morphologies and stellar populations) and compare them to our simulations.

Acknowledgements

This work was supported financially by Volkswagen-Stiftung (I/76 520), DFG (ZI 663/6), DLR (50OR0602, 50OR0404, 50OR0301) and the Kapteyn institute.

References

Böhm, A. et al. 2004, A&A, 420, 97
Böhm, A. & Ziegler, B. 2007, ApJ, 668, 846
Ferreras, I. et al. 2004, MNRAS, 355, 64
Daigle, O. et al. 2006, MNRAS, 367, 469
Jäger, K. et al. 2004, A&A, 422, 941
Kapferer, W. et al. 2009, A&A, 499, 87
Krajnovic, D. et al. 2006, MNRAS, 366, 787
Kronberger, T. et al. 2007, A&A, 473, 761
Kronberger, T. et al. 2008, A&A, 483, 783
Kutdemir, E. et al. 2008, A&A, 488, 117
Kutdemir, E. et al. 2009, A&A, submitted
Springel, W. 2005, MNRAS, 364, 1105
Tully, R. B. & Fisher, J. R. 1977, A&A, 54, 661
Ziegler, B. et al. 2003, ApJL, 598, 87

A typical Galactic HII region, the very well-known Eagle Nebula (NGC 6611), is shown in this composite of *B*, *V* and *R* images taken with the Wide Field Imager on the MPG/ESO 2.2-metre telescope. See ESO Photo Release 26/09 for more details.

Wandering in the Redshift Desert

Alvio Renzini[1]
Emanuele Daddi[2]

[1] INAF – Osservatorio Astronomico di Padova, Italy
[2] CEA, Saclay, France

The cosmic star formation rate, active galactic nuclei activity, galaxy growth, mass assembly and morphological differentiation all culminate at redshift $z \sim 2$. Yet, the redshift interval $1.4 < z < 3$ is harder to explore than both the closer and the more distant Universe. In spite of so much action taking place in this spacetime portion of the Universe, it has been dubbed the "redshift desert", as if very little was happening within its boundaries. The difficulties encountered in properly mapping the galaxy populations inhabiting the desert are illustrated in this paper, along with some possible remedies.

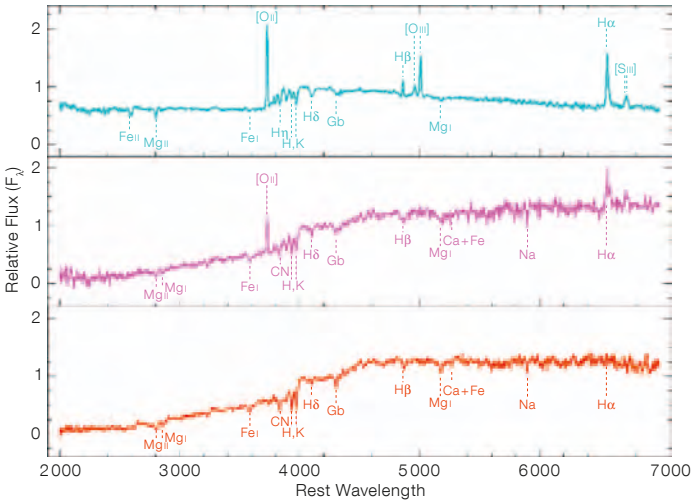

Figure 1. The template spectra of actively star-forming (top), moderately star-forming (middle) and passively evolving galaxies (bottom). From Mignoli et al., 2005.

Optical spectroscopy of $1.4 < z < 3$ galaxies

Figure 1 shows typical FORS2 spectra of actively star-forming, moderately star-forming, and passively evolving galaxies at $z \lesssim 1$ (Mignoli et al., 2005). The strongest, most easily recognisable features in these spectra are the [OII] 3727 Å line in emission, the CaII H&K doublet, and next to it the 4000 Å break. These are the features that allow spectroscopists to measure reliable redshifts even on relatively low signal-to-noise (S/N) spectra. Provided, of course, these features are included in the observed spectral range.

As redshift increases beyond $z \sim 1$ all these features become harder to recognise in observed spectra, as they enter a wavelength region where the sensitivity of CCDs starts to drop, detector fringing complicates life, and the sky deteriorates. At this point we are already in quite an arid environment (redshift-wise), though still manageable thanks to the collective power of our very large telescopes, routinely applied dithering patterns, and the like. But a little further out in redshift our preferred spectral features move beyond 1 μm, i.e., into the near-infrared, and we are in full desert.

Still, survival with optical spectrographs is hard, but not completely impossible. While we have lost, beyond 1 μm, the strong features, other, albeit less prominent, ones have entered our optical range coming from the restframe ultraviolet (UV). Just as opportunistic organisms still find their ecological niche in the driest desert, so we currently rely on weak, restframe UV features to explore the redshift desert. In the case of actively star-forming galaxies at $z \gtrsim 1.4$, these are several narrow absorption lines across the UV continuum, most of which originate in the interstellar medium of these galaxies (see Figure 2). In the case of passively evolving elliptical galaxies at $z > 1.4$, the strongest feature in the observed optical spectral range is a characteristic feature at 2600–2800 Å, due to neutral and singly ionised magnesium and iron (see Figure 3). Thanks to these features, we can survive in the desert, but it is not an easy life.

First of all, it is quite awkward to use narrow, weak absorption lines to obtain

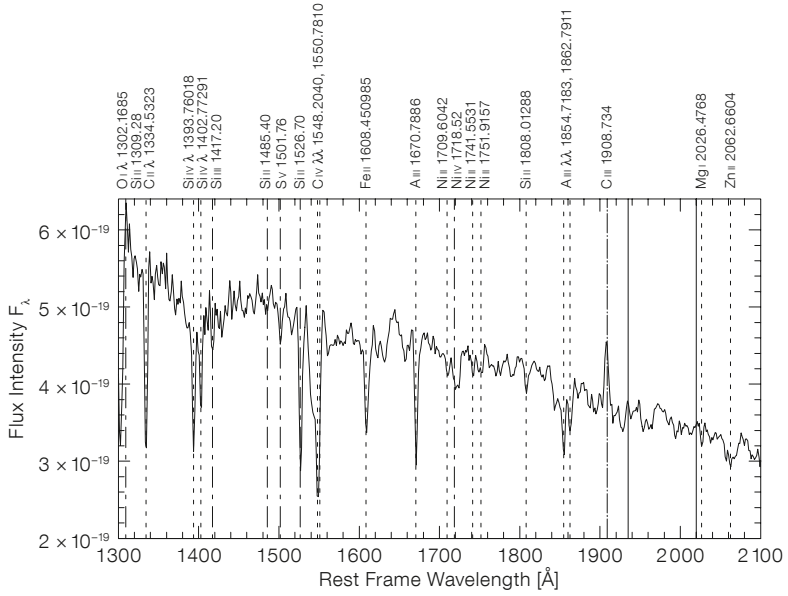

Figure 2. The co-added FORS2 spectrum of 75 star-forming galaxies at $z \sim 2$, corresponding to 1652.5 hours of integration (from Halliday et al., 2008). The main spectral features are indicated, including the weak blend of FeIII lines that originate in the photosphere of the OB stars responsible for the UV continuum.

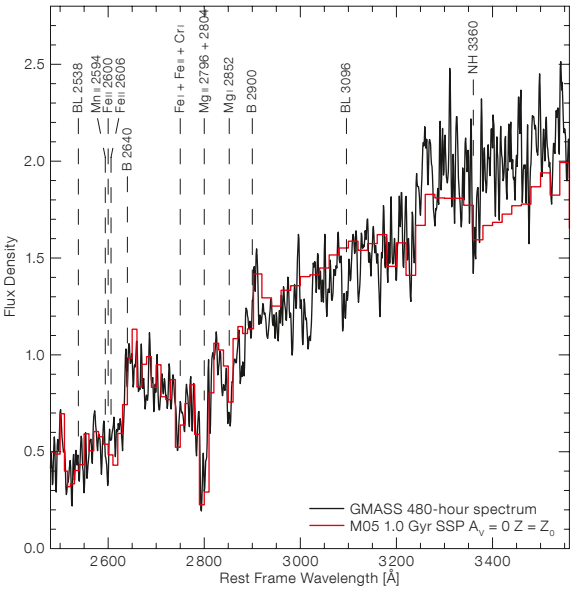

Figure 3. The co-added FORS2 spectrum of 13 passively evolving galaxies at $z \sim 1.6$, corresponding to 480 hours of integration (from Cimatti et al., 2008). The main spectral features are indicated, along with the synthetic spectrum of a 10 Gyr old, solar metallicity stellar population model (Maraston et al., 2005).

redshifts of star-forming galaxies that have strong emission lines elsewhere in their spectrum, or absorptions on a very faint UV continuum for galaxies that are intrinsically very red. These are indeed the cases shown in Figues 2 and 3! But this is not the whole story. In order to make the fairly good S/N spectra shown in these figures from the GMASS Large Programme, Cimatti et al. (2008) had to co-add the spectra of several galaxies, each integrated from a minimum of 30 to a maximum of 60 hours. Thus, the spectrum of star-forming galaxies in Figure 2 is the result of co-adding 75 spectra of individual galaxies for a total integration time of 1652.5 hours (!). Similarly, the spectrum of passive galaxies in Figure 3 was obtained by co-adding the spectra of 13 galaxies, for a total integration time of 480 hours (!). Clearly, journeys in the redshift desert take time nowadays.

In the case of star-forming galaxies a little relief may be offered by Ly-α, if the spectrograph is efficient enough in the UV. Indeed, even if not in emission, Ly-α is such a strong feature that it helps a lot in getting redshifts. However, in a spectrograph such as e.g., VIMOS, Ly-α does not enter before $z \sim 1.8$, hence the range $1.4 < z < 1.8$ is perhaps the harshest part of the redshift desert.

Drawbacks

For quite a few years we have known that at $z \sim 2$ galaxies with star formation rates (SFR) as high as some ~ 100 $M_\odot$ yr^{-1} are quite common, and, by analogy with the rare objects at $z \sim 0$ with similar SFRs, many of us believed they were caught in a merger-driven starburst. It was quite a surprise when one of these galaxies (BzK-15504 at $z = 2.38$) did not show any sign of ongoing merging, but on SINFONI 3D spectroscopy looked like a rather ordered rotating disc (Genzel et al., 2006). But still, its many clumps and a high velocity dispersion make it (like many others, see Förster-Schreiber et al., 2009) quite different from local disc galaxies.

That high SFR in $z \sim 2$ galaxies does not necessarily imply starburst activity became clear from a study of galaxies in the GOODS fields (Daddi et al., 2007a). Figure 4 shows the SFR *v.* stellar mass, M^*, for galaxies at $1.4 \lesssim z \lesssim 2.5$ in the GOODS-South field, where a tight correlation is apparent between SFR and stellar mass. Only a few galaxies are far away from the correlation, most notably a relatively small number of passive galaxies (with undetectable SFR), conventionally placed at the bottom of Figure 4. Among star-forming galaxies, the small dispersion of the SFR for given M^* demonstrates that these objects cannot have been caught in a special, starburst moment of their existence. Rather, they must sustain such high SFRs for a major fraction of the time interval between $z = 2.5$ and $z = 1.4$, i.e. for some 10^9 yr instead of the order of one dynamical time (~ 10^8 yr) typical of starbursts.

In parallel with this observational evidence, theorists are shifting their interest from (major) mergers as the main mechanism to grow galaxies, to continuous cold stream accretion of baryons, hence turned into stars (Deckel et al., 2009). Clearly a continuous, albeit fluctuating SFR such as in these models is far more akin to the evidence revealed by Figure 4, compared to a scenario in which star formation proceeds through a

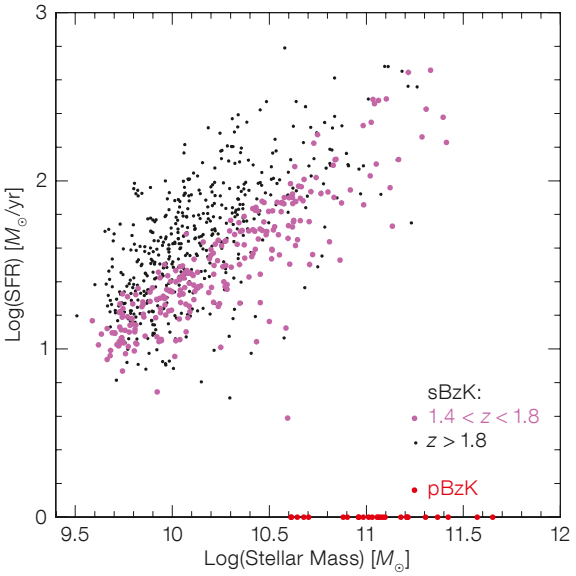

Figure 4. The SFR in $M_\odot$ yr^{-1} *v.* stellar mass for actively star-forming galaxies galaxies (sBzK) in the GOODS-South field and with spectroscopic or photometric redshifts in the range $1.4 < z < 2.5$ (adapted from Daddi et al., 2007a). Passively evolving galaxies (with SFR ~ 0, dubbed pBzKs from Daddi et al., 2004) are conventionally plotted at the bottom as red dots.

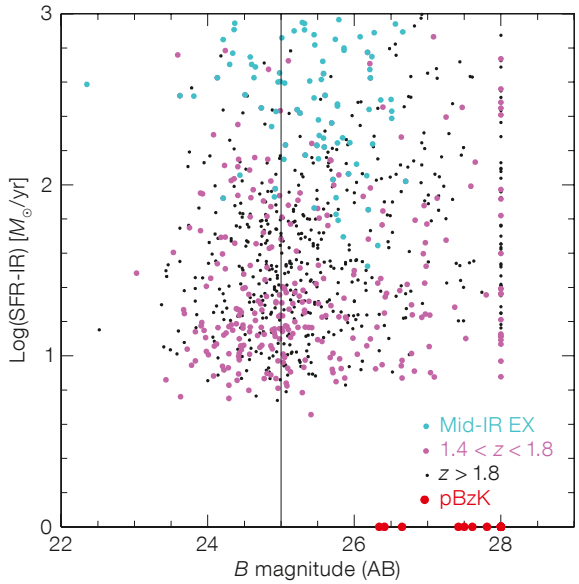

Figure 5. The SFR (here measured from the 24-μm flux as in Daddi et al., 2007a) *v.* the *B* magnitude for $1.4 < z < 2.5$ galaxies in the GOODS-South field. The cyan dots denote galaxies with excess mid-infrared (IR) emission, that according to Daddi et al. (2007b) may be due to a buried, Compton-thick active galactic nucleus (AGN), in which case the SFR may have been overestimated. The vertical line marks the current practical limit of what is doable with the VIMOS instrument.

series of short starbursts interleaved by long periods of reduced activity. This is not to say that major mergers do not play a role. They certainly exist, and can lead to real, giant starbursts corresponding to SFRs as high as ~ 1000 $M_\odot$ yr^{-1}, currently identified with submillimetre galaxies (e.g., Tacconi et al., 2008).

This paradigm shift, from mergers to cold streams, adds flavour to a thorough exploration of the redshift desert, an enterprise which is at the core of the zCOSMOS-Deep project (Lilly et al., 2007), the largest ongoing spectroscopic survey of the desert. This survey is targeting star-forming galaxies whose spectrum is pretty much like that shown in Figure 2, and does so with VIMOS for objects down to *B* magnitudes ~ 25 with 5-hour integrations. The success rate of zCOSMOS-Deep (i.e., the fraction of targets for which a reliable redshift is obtained) is ~ 2/3 (Lilly et al., in preparation), not bad at all for objects in the desert! Still, we wonder what we get, and what we miss.

Figure 5 shows the SFR *v.* *B* magnitude for the same $1.4 < z < 2.5$ GOODS galaxies shown in Figure 4. Clearly, the vast majority of actively star-forming galaxies in the desert are fainter than $B = 25$ mag, and they include several among the most active galaxies (here and elsewhere magnitudes are in the AB system). Those brighter than $B = 25$ mag account for just ~ 16 % of the global SFR of the whole sample, hence ~ 84 % of it remains out of reach. But why is the *B* magnitude (i.e., the restframe UV) such a poor indicator of SFR? This is so because lots of gas is needed to sustain high SFRs, but gas is accompanied by dust, and dust is a potent absorber of UV radiation.

Figure 6 shows the dust reddening E(B–V) for the same set of GOODS galaxies as Figure 5, as a function of SFR (from Greggio et al., 2008). Indeed, the star-forming galaxies with the highest star formation rates are also those with the most extinction, which makes it difficult to obtain redshifts from *B*-band spectroscopy. Such a strong correlation of extinction and SFR has been recently quantitatively confirmed using the dust-free 1.4 GHz flux as a SFR indicator (Pannella et al., 2009). What is said for the SFR also holds true for the stellar mass. Figure 7 shows M^* *v.* *B* magnitude, and again most of the stellar mass is in galaxies fainter than $B = 25$ mag, including many among the most massive galaxies.

Usually, when extinction bothers us it helps to go into the near-infrared. Figures 8 and 9 are analogous to the previous two figures, but SFR and M^* are now plotted *v.* the *J*-band magnitude instead of the *B*-band. Clearly, whereas a $B < 25$ mag selection misses most of the SFR and most of the stellar mass at $z \sim 2$, a $J < 24$ mag selection would pick up most of them. In particular, note that most of the highest star formation and most massive galaxies are fainter than $B = 25$ mag, but are instead among the brightest in the *J*-band. Thus, a $B < 25$ mag selection picks up a fair number of massive, star-forming galaxies at $z \sim 2$, but misses the majority of them, and in particular may miss several of the most massive and most star-forming ones.

It is worth emphasising that a comparison of Figures 7, 8 and 9 shows that all passive galaxies (the pBzKs of Daddi et al., 2004) are among the faintest objects in the *B*-band, but are among the brightest ones in the *J*-band. Being fainter than $B = 25$ mag, all passive

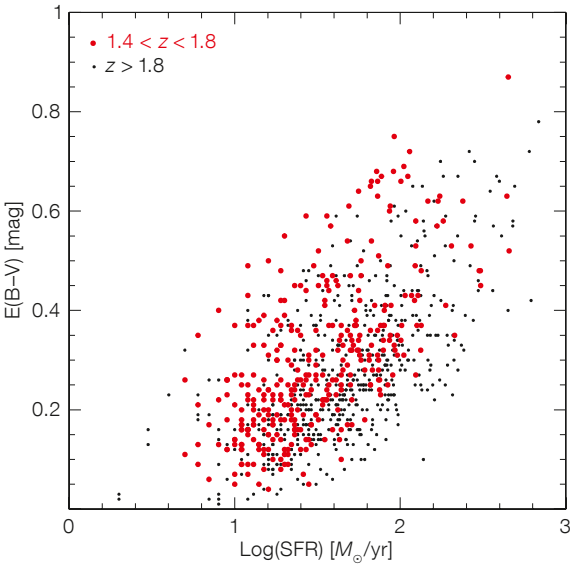

Figure 6. The global reddening E(B–V) derived from the slope of the rest-frame UV continuum as a function of the star formation rate for the same objects shown in Figure 5.

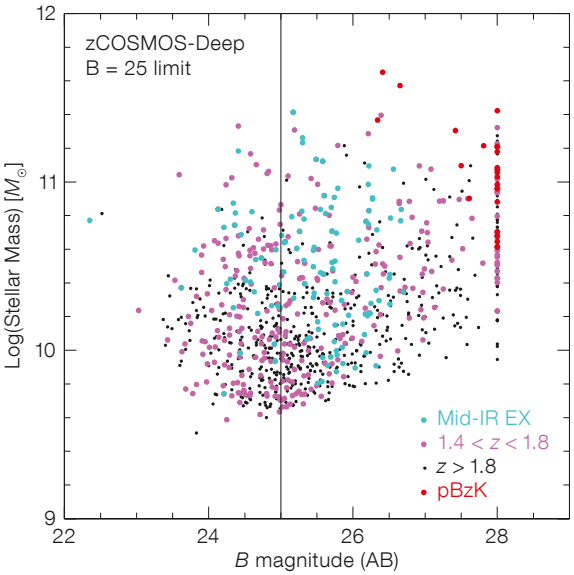

Figure 7. The stellar mass *v. B* magnitude for the same objects shown in Figure 5.

galaxies at $z > 1.4$ are automatically excluded from e.g., the zCOSMOS survey. Now, there are over 3000 such galaxies in the COSMOS field (McCracken et al., 2009), and if we wanted to make, over the whole COSMOS field (7200 arcminute^2), the same effort that GMASS did on one FORS2 field of view (49 arcminute^2), investing over 100 hours of VLT time, then it would take well over 15000 hours (!) of telescope time. Passive galaxies at $z > 1.4$ are the most massive galaxies at these redshifts, and they likely mark the highest density peaks in the large-scale structure, but we suspect that this argument would not be sufficient for the Observing Programmes Committee to recommend the allocation of over 1500 VLT nights to such a project ...

With reference to the COSMOS field, using COSMOS data for 30866 star-forming galaxies Figures 10 and 11 further illustrate the differences between *B*-band and *J*-band limited samples of $z \sim 2$ galaxies. Galaxies are first selected with the BzK criterion of Daddi et al. (2004) from the COSMOS *K*-band catalogue (McCracken et al., 2009), which is complete down to $K = 23.5$ mag. Then multi-band photometric redshifts from Ilbert et al. (2009) are used. Notice that the full range of masses and SFRs are still sampled for a selection down to a limiting magnitude as bright as $J = 22$–23 mag. In Figures 8–11 the vertical line at $J = 24$ mag is meant for objects that would be detected with S/N = 5 with 10-hour integrations with the FMOS *J*-band spectrograph at the SUBARU telescope (Kimura et al., 2003). This may well be a rather optimistic limit for a robust detection of the continuum and the absorption lines of passive galaxies. But for star-forming galaxies, the [O II] emission line would help greatly in measuring redshifts, hence a $J = 24$ mag limit may not be a mere dream for such objects.

Remedies

We understand that many may prefer to leave deserts as uncontaminated as possible, rather than crowded by swarms of all-inclusive tourists. But, what options do we have if we really want to colonise the redshift desert fully?

One possibility would be to use VIMOS with much longer integrations compared to the 5 hours currently invested by the zCOSMOS project, i.e., $\gtrsim$ 30 hr as used for the GMASS project. But before doing so, VIMOS would have to be made at least as efficient as FORS2 in the red, a good thing that may happen anyway. With respect to field of view, VIMOS is like 4 FORS units, hence doing all the COSMOS pBzKs (and along with them a much larger number of star-forming galaxies in the desert) would take about a quarter of the time we have estimated above for FORS2, i.e., some 350 VLT nights. This still looks like a lot of time, yet is somewhat more affordable than a mere FORS2 brute force effort. After all, VIMOS was conceived and built primarily for making large redshift surveys, hence, why not this one? But, how many years are 350 nights? We can scale from zCOSMOS, whose 640 hours (~ 75 nights) were reckoned to complete the project in four semesters. Suppose (a big if) VIMOS could be used for zCOSMOS whenever the COSMOS field is +/−4 hours from the meridian. But because of bad weather, competition from projects working on objects at the same right ascension, and instrument downtime, it is now taking five years to finish

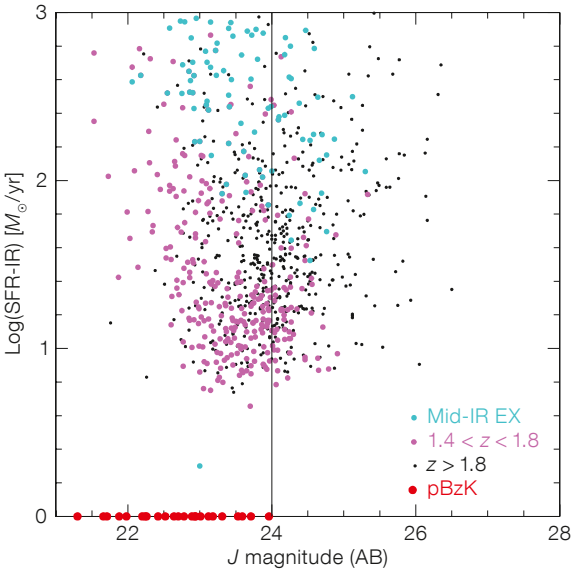

Figure 8. The same as in Figure 5, but now plotted *v.* the *J* magnitude. The vertical line at *J*(AB) = 24 mag marks the limit expected for reaching S/N = 5 with 10-hour integration with the FMOS *J*-band spectrograph at the SUBARU Telescope.

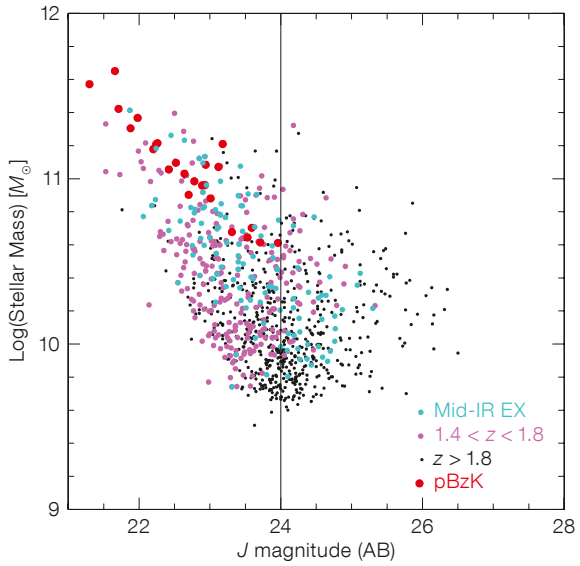

Figure 9. The same as in Figure 7, but now plotted against the *J*-band magnitude.

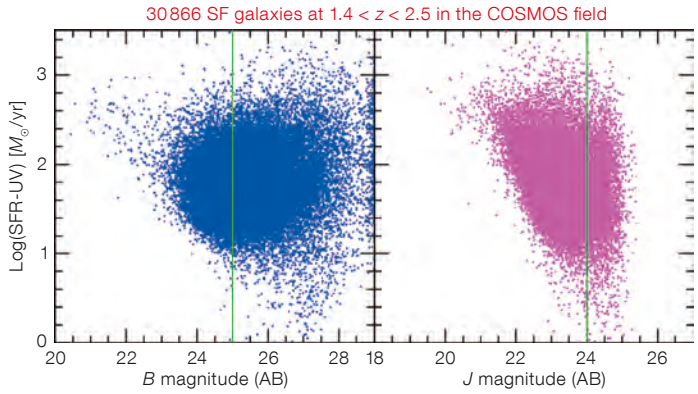

Figure 10. The SFR from the UV diagnostics for SF galaxies at $1.4 < z < 2.5$ in the COSMOS field *v.* their *B*-band magnitude (left) and their *J*-band magnitude (right). A plume of objects brighter than $B \sim 22$ mag are likely to be AGN.

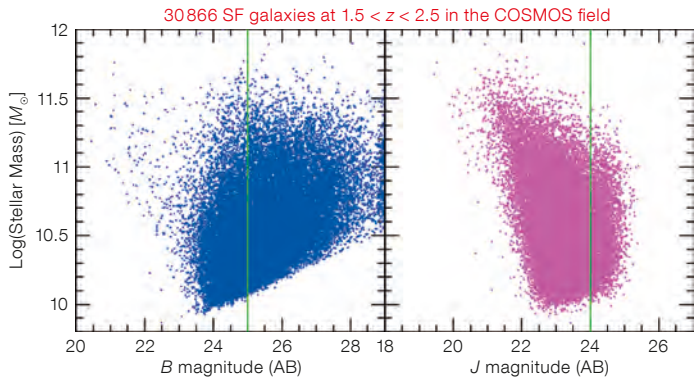

Figure 11. The same as in Figure 10, but now the stellar mass *v.* the *B*- and *J*-band magnitudes are plotted.

zCOSMOS. By the same token, it would then take ~ 25 years for an upgraded VIMOS to do justice to the COSMOS field alone.

Thus, what we would really need is a high-multiplex instrument able to sample the strongest spectral features of galaxies in the $1.4 < z < 2.5$ desert, i.e., [O II] 3727 Å for the overwhelming population of star-forming galaxies, and Ca II H&K and the 4000 Å break for the passive ones. All these features fall in the *J*-band for the galaxies in the desert, thus a cryogenic instrument would not be necessary. Without having to bother about the thermal background, a room temperature instrument could then cover wide fields in a single telescope pointing. A preliminary knowledge of the distribution of the [O II] line flux for star-forming galaxies in the desert would be critical for properly planning a spectroscopic survey targeting them. Such information is not yet to hand.

The surface density of these objects for the full COSMOS sample down to $K \sim 23.5$ mag is 4 per arcminute, or ~ 1 per arcminute for the brighter portion down to $J = 22$. Thus, the ideal VLT instrument would be one able to exploit fully the largest field of view of the VLT (i.e., ~ 500 arcminute^2 at the Nasmyth focus) with a multiplex $\gtrsim 1$ arcminute^{-2}, or ~ 500 objects over the whole field. This can be achieved only with a fibre-fed *zJ*-band spectrograph, not too different from the FMOS instrument on SUBARU. A *camel* of this species may offer the best, short-term possibility of wandering in the redshift desert.

References

Cimatti, A. et al. 2008, A&A, 482, 21
Daddi, E. et al. 2004, ApJ, 617, 746
Daddi, E. et al. 2007a, ApJ, 670, 156
Daddi, E. et al. 2007b, ApJ, 670, 173
Deckel, A. et al. 2009, Nature, 457, 451
Föster-Schreiber, N. M. et al. 2009, ApJ, submitted (arXiv0903.1872)
Genzel, R. et al. 2006, Nature, 442, 786
Greggio, L. et al. 2008, MNRAS, 388, 829
Halliday, C. et al. 2008, A&A, 479, 417
Kimura, M. et al. 2003, SPIE, 4841, 974
Lilly, S. J. et al. 2007, ApJS, 172, 70
Maraston, C. 2005, MNRAS, 362, 799
McCracken, H. J. et al. 2009, ApJ, submitted
Mignoli, M. et al. 2005, A&A, 437, 883
Pannella, M. et al. 2009, ApJ, 698, L116
Tacconi, L. J. et al. 2008, ApJ, 680, 246

ESO Director General Tim de Zeeuw being interviewed on the Brazilian national evening news programme *Jornal Nacional* about the E-ELT during the XXVIIth IAU General Assembly.

At its peak the *ESOHour* at the XXVIIth IAU General Assembly attracted more people than could fit into ESO's exhibition stand (see article on p. 55).

Health, Safety and Performance in High Altitude Observatories: A Sustainable Approach

Michael Böcker[1]
Joachim Vogt[2]
Oliver Christ[2]
Alice Müller-Leonhardt[2]

[1] ESO
[2] Technische Universität Darmstadt, Germany

The research project "Optimising Performance, Health and Safety in High Altitude Observatories" was initiated by ESO to establish an approach to promote the well-being of staff working at its high altitude observatories, and in particular at the Antiplano de Chajnantor. A survey by a questionnaire given to both workers and visitors was employed to assess the effects of working conditions at high altitude. Earlier articles have outlined the project and reported early results. The final results and conclusions are presented, together with a concept for sustainable development to improve the performance, health and safety at high altitude employing Critical Incident Stress Management.

Innovative ground-based submillimetre astronomical observatories like the Atacama Large Millimeter/submillimeter Array (ALMA) and the Atacama Pathfinder EXperiment (APEX) take advantage of the very low natural levels of atmospheric water vapour at very high altitude sites to attain high sensitivity in the submillimetre wavelength range. As these and other similar ground-based facilities come into operation, more people will be exposed to high altitude conditions.

The research project "Optimising Performance, Health and Safety in High Altitude Observatories" was initiated by ESO from an organisational psychology perspective to establish a sustainable development programme for the well-being of its staff in special environments. The major objective is to consider the effects of high altitude on those people who will be required to work above 5050 m altitude at Llano de Chajnantor, the site of ALMA and APEX. The final goal of the project is to acquire and promote knowledge in the field of human activity at high altitude observatories, which then will be utilised to help in planning observatory operations.

In addition to the scientific challenge for the astronomical community presented by APEX and ALMA, there is the challenge for the executive organisations to take sufficient care of staff and equipment. This is especially true if sensitive work has to be performed at high altitude (above 3000 m). A good example is the operation of the ALMA transport vehicles: ALMA staff must move the antennas across the Chajnantor Altiplano over distances from 150 metres to 15 kilometres using these specialised transport vehicles (see Kraus et al., 2008). The weight of the antennas (about 100 tons), their delicacy and the hostile, high altitude environment impose severe constraints on the use and functionality of the transport vehicles and the technical equipment in general, as well as on the drivers and supporting staff. Amongst other manoeuvres, staff have to position the antennas to an accuracy of a few millimetres or move the antennas slowly for maintenance and repair from the Array Operations Site (AOS) at 5050 m altitude to the Operations Support Facilities (OSF) at 2900 m, via a 12-metre wide and 28 kilometre-long road — a 3 to 5 hour drive at 8 km/h.

While a great deal of knowledge has been acquired about the biomedical changes at high altitude and under low oxygen conditions, there is little knowledge available about the psychological changes. Furthermore, there are conflicting results on the effects of high altitude, adding emphasis to the importance of the project. So as to develop an adequate preventive health and safety process systematically, a questionnaire was developed and distributed to staff working for ALMA and APEX, or visiting the sites, and 28 questionnaires were returned by visitors and workers. As has already been summarised (Böcker et al., 2008), the results from the questionnaire indicated that working conditions at high altitude are better than expected. The visitors/workers reported neither major psychosomatic complaints nor impairments in abilities and work behaviour or performance (see Figure 1 for a diagrammatic summary of the questionnaire results). The participants reported moderate to slight limitations with respect to their tasks at low altitude workplaces. Planning and teamwork activities were slightly impaired, while manual and other tasks were moderately impaired. Teamwork could have a social activation function, in that it reduces fatigue and attention problems that might be induced by high altitude conditions and travel jet lag. Workers tended to report more limitations than visitors, especially for complex mental tasks, such as computer programming. Concentration problems, fatigue, reduction of their usual activities, shortness of breath on exertion (see Figure 1) were the complaints reported to occur on average slightly more often. Other complaints that have been reported by mountaineers, such as nausea, vomiting and severe sleep difficulties, were not experienced at all by the ESO site workers and visitors.

The regular workers generally report slightly more problems at high altitude, but received more benefit from preparatory documents/tools than visitors, although these results were not statistically significant. The experience of workers appears to be a good training for effective functioning at high altitude. However, cultural differences (optimism of local staff and workers as opposed to the critical outlook of the visiting scientist) and adaption to the difficult working conditions probably also play a role; for activities involving selective attention (concentration) and technical understanding of equipment, the differences were statistically significant. Two functions stood out from the questionnaire results as showing a tendency to be impaired at high altitude: perceptual speed and attention span (see Figure 2). Occupational Safety and Health (OSH) programmes could consider this result and try to address perception and attention problems. Workers reported slightly more impairment than visitors.

High altitude safety and health issues were generally considered seriously by visitors and also by the local and international staff working at the site. Serious incidents could result if individuals are unprepared for high altitude activities and in cases where the standard preparation procedures are not followed for whatever

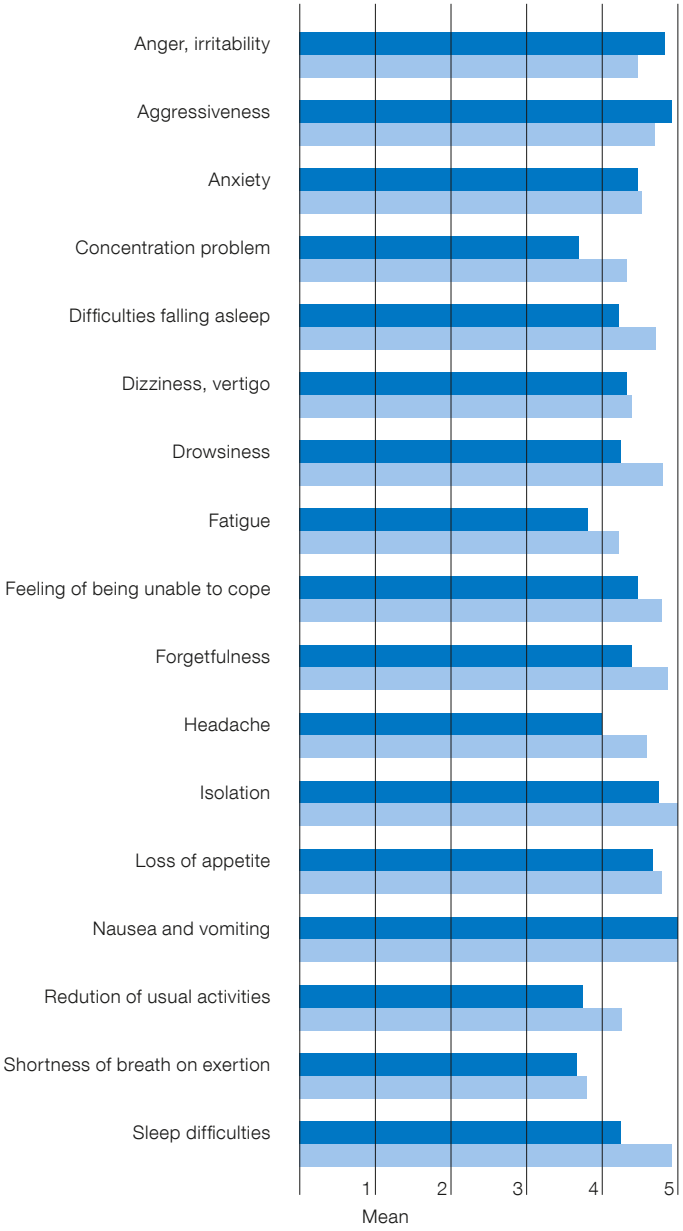

Figure 1. Summary of questionnaire returns showing average scores for physical and psychological complaints (scale: 1 extreme; 5 absent).

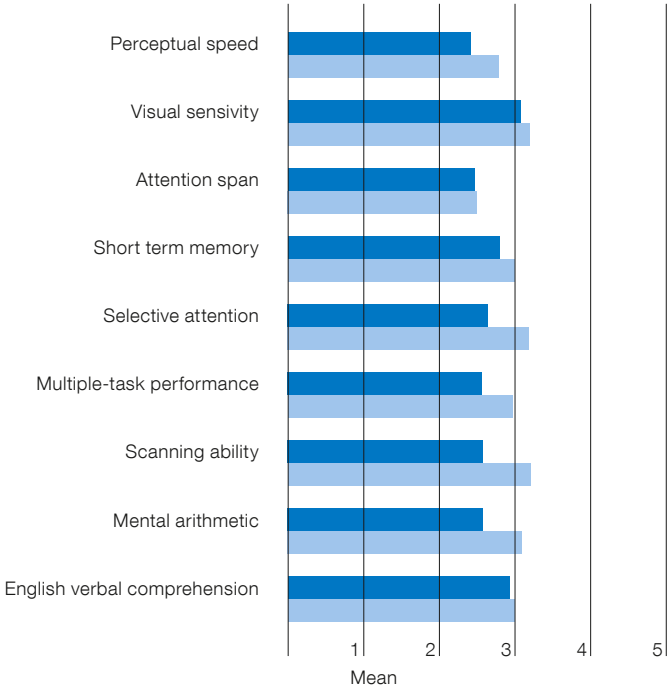

Figure 2. Ratings of abilities at high altitude from the questionnaire results (scale: 1 strongly impaired; 5 greatly improved).

reason. A decent amount of safety consciousness and consideration of the negative environmental conditions prevalent at high altitude sites are a necessity.

The questionnaire results indicated some areas worthy of further study and that could be given more support in OSH programmes, such as concentration/attention problems, under-arousal and reduced capacity. Measures to improve work conditions, organisation and human behaviour, safety and health consciousness at high altitude sites must be developed.

A sustainable development approach

From an organisational and personal development viewpoint, a comprehensive analysis should be carried out. This analysis should include psychological/team factors, because in other high altitude environments with established good team cultures, like APEX, fewer accidents seem to occur. In order to investigate psychological or team factors in the area of health awareness, a theory-based and empirically validated framework is needed to outline the process describing behavioural change. From nearly one hundred years of motivation and action research, it is known that behaviour modification is difficult and requires more than just information and insight. The overlap between what we think is right and what we actually act on is less than 30 % (Six, 1992).

The Health Action Process Approach (HAPA model; Schwarzer, 2008) is suggested as a basis for behavioural development. This model explicitly considers the volitional phase of action. But before such a person-centred framework is developed, a systemic approach to the personal, situational and organisational factors has to be taken into account to facilitate a broader view of optimising human and organisational performance. The adoption, initiation and maintenance of health behaviour are processes of motivation, volition and action (Schwarzer, 2008). Motivation means we must make people want to behave safely and in a healthy manner. Volition means we must increase their self-awareness of the consequences of unsafe actions and increase their belief in safe behaviour. Action is largely an individual's responsibility, but they should be properly

Malpractice	No. of workers recorded	Abuses %
Speeding	463	14
Drugs	38	4
Alcohol	35	13

Table 1. ALMA driving malpractice (driving too fast or after drinking alcohol or taking drugs) statistics recorded in a randomly chosen month.

supported in their self-management by tools, procedures and safety leadership.

An observatory site is a web of complex human relations under challenging conditions. The good intentions of staff with regard to safety do not guarantee the corresponding safe actions. Consideration of the accident statistics at ALMA demonstrates that, in spite of information campaigns, practical training, additional speed signs and increase of speed controls, vehicle speeding, for example, remains a problem. Although driving and drinking is proscribed at the observatory sites, it still remains a problem as the statistics in Table 1 demonstrate.

However, good intentions alone do not necessarily guarantee the corresponding right actions. Important factors are how hard a person will try to put an intention into practice and how long he or she will persist. Psychological distractions such as unforeseen circumstances may influence the maintenance of goals because of changing the self-efficacy (e.g., stressful incidents). Also work organisation practices can have a major influence. In future, ALMA will operate round the clock, so shift work will need to be considered in terms of matters of health, safety and performance of staff.

A major driver of the negative effects of shift work on employees is the desynchronisation of the circadian rhythm (body clock), both in biological and social respects. Due to the lack of adjustment of the body, the person has to work against its demands. Studies show that the error rate during night shift work is higher than for day shift and, as a consequence, productivity is lower, with a higher accident rate than during daytime. The most important social areas affected by shift work are partnership, family life and leisure time. Working shifts at a high altitude in the Atacama desert, far away from the social support of the family, with a reduced social life and possible jet lag due to overseas travel (for visiting scientists and engineers) can increase the risk of accidents.

Hence, at the prevention level, knowledge about critical behaviour and risk factors is essential. One efficient and certified programme for a sustainable development in organisations is Critical Incident Stress Management[1] (CISM), which facilitates a professional handling of accidents, near misses and critical incidents. Although CISM is conceived as an intervention after such negative occurrences, our experience demonstrates that CISM supports the prevention of problems and also facilitates innovation (Mosmann, 2009), as well as the development of a sustainable communication and safety culture. It is generally assumed that using CISM as a mutual basis for activities stabilises intercultural teams or networks. The physical (high altitude, etc.) and social stress factors (absence from family, etc.) at the high altitude Chajnantor site can promote maladaptive behaviour, such as the overestimation of abilities or drinking that can compromise safety. Prevention works on the basis of the culture that CISM fosters in communication and safety management. The professional intervention, prevention and implementation of CISM also imply positive business and economic benefits (Vogt & Pennig, 2006).

Conclusions

The recommendation for high altitude observatories is to integrate adequate occupational health and safety programmes early and to begin a process of personnel and organisational development quickly. Otherwise the physical and social stress factors at the high altitude observing site can facilitate maladaptive behaviour such as an overestimation of abilities, drinking or taking drugs, thus compromising safety. Adaptive coping by individuals must be promoted. In order to ensure this, a proper programme must be put in place, based on a scientific and standardised approach. One very efficient method is Critical Incident Stress Management.

References

Böcker, M. & Vogt, J. 2007, The Messenger, 127, 64

Böcker, M., Vogt, J. & Nolle-Gössner, T. 2008, The Messenger, 133, 49

Kraus, M. et al. 2008, The Messenger, 132, 23

Mosmann, H. 2009, Master's Thesis, University of Saarbrücken, Germany

Schwarzer, R. 2008, Applied Psychology: An International Review, 57, 1

Six, B. 1992, in Beiträge des 7. Hamburger Symposiums zur Methodologie der Sozialpsychologie, *Einstellung und Verhalten*, ed. Witte, E. H., (Braunschweig), 21

Vogt, J. & Pennig, S. 2006, in *Critical Incident Stress Management in Aviation,* ed. Leonhardt, H. & Vogt, J., (Aldershot: Ashgate), 153

Links

[1] http://www.icisf.org

Report on the Workshop

Impact of ALMA on Spanish Extragalactic Astronomy

held at the Instituto de Astrofísica de Andalucía, Consejo Superior de Investigaciones Científicas (CSIC), Granada, Spain, 11–13 February 2009

Lourdes Verdes-Montenegro[1]

[1] Instituto de Astrofísica de Andalucía, CSIC, Granada, Spain

In order to prepare the Spanish extragalactic community for the impact of ALMA science, a meeting with participation of non-radio astronomers was held to introduce the ALMA capabilities and to explore the synergies with optical and infrared facilities.

The Atacama Large Millimeter/submillimeter Array (ALMA) will be an extraordinarily complex and powerful instrument for the study of the (sub)millimetre window in the extragalactic field. A panchromatic approach to its exploitation will be a key to the success of the project and therefore the active involvement of those outside the radio astronomy community is highly desirable. To this purpose, more than 70 Spanish extragalactic astronomers from 13 Spanish research centres, either already involved or potentially interested in the ALMA project, met in Granada, together with some invited international specialists in the field. The scientific organising committee, chaired by Lourdes Verdes-Montenegro and Josefa Masegosa from the Instituto de Astrofísica de Andalucía (IAA–CSIC), aimed at involving most of the Spanish extragalactic community in ALMA, with a strong contingent of non-radio astronomers. The scientific programme was designed to exploit the complementarities between the radio and non-radio communities, exploring how ALMA could enhance the research of those astronomers currently less familiar with the project, as well as how synergies with other wavelengths could benefit the radio astronomers. A total of 36 talks were presented at the workshop, while eight young researchers contributed with posters describing their PhD thesis work in the context of ALMA. The contributions can be consulted on the conference web page[1].

Introduction to the ALMA project

This first session was opened by Jesús Martin Pintado, representing the RIA (Red de Infrestructura en Astronomia) ALMA working group, and by the European ALMA Project Scientist Leonardo Testi, who presented the status of the ALMA project. Support activities for Spanish astronomers by the IRAM node were presented by Philippe Salome and complemented by the talks from the three Spanish groups developing applications to exploit ALMA. In particular, Jesus Martín Pintado introduced MADCUBA (Madrid Data Cube Analysis), a tool for advanced datacube analysis, José Miquel Girart presented ARTIST (Adaptable Radiative Innovations for Submillimeter Telescopes), a next-generation model suite for comprehensive multi-dimensional radiative transfer calculations of dust and line emission, as well as their polarisation, while Lourdes Verdes-Montenegro presented the development of a new VO-compliant GIPSY package fully compatible with ALMA datacubes. Tommy Wiklind closed this first section with a vision of representative scientific cases for ALMA, explaining how the large increase in both sensitivity and angular resolution, compared with existing facilities, will allow detailed studies of the molecular gas and dust content of both nearby and distant galaxies. For the most distant galaxies ALMA will also be able to study the ionised gas component through fine-structure lines.

Nearby galaxies — detailed studies

The topic was reviewed by Elias Brinks, with particular emphasis on the prediction of the star formation rate density, from the THINGS (The HI Nearby Galaxy Survey) project. The study of the content, distribution and kinematics of interstellar gas is a key to understanding the origin and maintenance of active galactic nuclei (AGN). Santiago García-Burillo provided a complete molecular line perspective of AGN feeding, while Sergio Martín presented the strength of unbiased spectral line surveys to understand the main heating mechanisms of the interstellar medium. The information that can be obtained from maser lines of water vapour to trace the gas around AGNs was discussed by José Cernicharo. ALMA will allow high excitation maser lines of water vapour to be observed in the submillimetre domain.

Environment

The long-standing debate of "nature versus nurture" was revisited by David Sanders. He discussed plans for observations with ALMA that will be critical for a proper understanding of the important role played by dense molecular gas in fuelling both starburst and AGN activity in ultraluminous infrared galaxies, powerful radiogalaxies and optically selected quasars in the local Universe, most of them strongly interacting. Daniel Espada emphasised the bias of most studies on molecular gas towards interacting systems, due to the lack of sensitive instruments in the millimetre/submillimetre range, describing how the multi-wavelength study of a large sample of isolated galaxies performed by AMIGA (Analysis of the Interstellar Medium of Isolated GAlaxies) project will contribute towards establishing a reference for future ALMA environmental studies.

High-*z* systems and cosmology

The unique capabilities of ALMA, that will further understanding of the formation and build-up of the highest mass/most luminous galaxies and AGN in the early Universe, were emphasised by Nick Scoville, who summarised the current observations in this area, including the COSMOS project. Both Min Yun and Pablo Pérez-González emphasised how ALMA could complete the panchromatic view of galaxy formation and mass build-up, bridging the knowledge gap presently caused by wavelength-dependent limitations. The current understanding of the spatial distribution of the dust in nearby star-forming galaxies was summarised by Armando Gil de Paz, who discussed the detectability of redshifted [CII]150-μm emission with ALMA, as well as current efforts to provide a calibration of this line as a measure of the star formation rate in galaxies using Herschel.

ALMA will be able to detect Cosmic Microwave Background (CMB) anisotrop-

ies at arcsecond angular scales, allowing the characterisation and separation of some of the secondary effects in the CMB, such as the Sunyaev–Zeldovich and Ostriker–Vishniak effects. Those observations could probe the reionisation epoch, the nature of the dark energy and allow the study of high redshift galaxy clusters and protoclusters, as explained by José Antonio Rubiño.

Preparing for ALMA — synergies

The final session of the conference was designed explicitly to promote synergies between the radio and non-radio astronomers, with the aim of preparing for challenging projects with ALMA. Survey projects with the strong involvement of the Spanish community, which would provide the best targets for ALMA studies, were reviewed. Narciso Benítez presented preliminary results from the ALHAMBRA (Advancer Large Homogeneous Area Medium-Band Redshift Astronomical) survey and introduced the future Javalambre/PAU (Physics of the Accelerating Universe) survey, which will cover the full northern sky with 40 medium band filters. Jordi Cepa summarised some of the surveys proposed by the OSIRIS instrument at the 10.4-metre GranTeCan (GTC) telescope, Marc Balcells presented the near-infrared spectroscopy of z = 1–2.5 galaxies to be performed by the GOYA (Galaxy Origins and Young Assembly) project with the GTC/EMIR instrument and Nieves Castro-Rodríguez reviewed Herschel and Spitzer cosmological surveys.

With ALMA approaching operations in the next few years, it is clear that the various millimetre and submillimetre facilities must be already preparing the first science targets. Single-dish far-infrared to millimetre facilities were reviewed by David Hughes, while Paul T. P. Ho focused on the interferometric ones, showing how the SubMillimeter Array (SMA) is preparing specifically for higher frequency studies in the ALMA era. Antonio Alberdi presented the sensitivity improvements that could be obtained if a phased array with a large number of antennas working at millimetre and submillimetre wavelengths like ALMA is used as an element of the VLBI array, while José-Carlos Guirado identified various scenarios where the synergy between ALMA and the Square Kilometre Array (SKA) may optimise their scientific output, as complementary instruments in frequency coverage and maximum resolution. Javier Goicoechea summarised the design concept behind SAFARI, a European imaging far-infrared spectrometer for the SPICA mission covering the 30–210 μm band, and highlighted science questions that it will be possible to address with SPICA/SAFARI that will complement ALMA capabilities.

Complementarities between ALMA and existing forthcoming X-ray observatories, which together can help to disentangle the contribution of star formation and supermassive black hole growth to the bolometric luminosity of AGN and luminous infrared galaxies, were presented by Francisco Carrera. Special interest was raised by the talk by José-Miguel Rodríguez-Espinosa, who showed the status of the Spanish GTC telescope, which has just entered operations, alerting the community to the excellent opportunities that the GTC offers to start preparing programmes for ALMA observations, as well as providing instrumental possibilities to follow up ALMA discoveries.

Acknowledgements

The workshop was supported by the Spanish Astronomy Infrastructures Network (RIA) and by the CSIC.

Links

[1] http://riastronomia.es/opencms/opencms/Workshops/R20081201.html

---

Report on the ESO Workshop

E-ELT Design Reference Mission and Science Plan

held at ESO Garching, Germany, 26–28 May 2009

Isobel Hook[1,2]
Jo Liske[3]
Daniela Villegas[3]
Markus Kissler-Patig[3]

[1] Department of Astrophysics, University of Oxford, United Kingdom
[2] INAF Osservatorio di Roma, Italy
[3] ESO

ESO hosted a dedicated workshop on the European Extremely Large Telescope (E-ELT) Design Reference Mission (DRM) and the Design Reference Science Plan (DRSP). The main aim of this three-day workshop was to exchange information and ideas with the scientific community on the status of the E-ELT and in particular on the development of the E-ELT science case through simulations.

Bringing together interested members of the community, various instrument study teams, members of the Science Working Group and the E-ELT Science Office at ESO, the focus of the workshop was to provide all interested parties with a platform for open exchange and critical assessment of the results of E-ELT performance simulations. In addition, the workshop provided an opportunity to present and discuss the E-ELT DRSP,

The participants at the E-ELT Design Reference Mission and Science Plan workshop assembled in the grounds of ESO Headquarters.

and to encourage the community to provide input to this wide-ranging survey of the scientific aspirations for the E-ELT. The workshop was timed to take place shortly before the deadline for DRSP submissions.

This was the second DRM workshop funded by the FP7 programme, E-ELT Preparatory Phase. The first took place in May 2008 and focused on simulation tools and methods, rather than results. This year's workshop attracted 83 registered participants (up from 34 last year), which we are happy to interpret as a reflection of the community's rising interest in the E-ELT.

The introductory session covered the E-ELT project status, a summary of the science case and the DRM, and a summary of the methods and aims of the DRSP, including a live demo on how to complete the online submission form.

This introduction was followed by presentations grouped into sessions based on four broad science themes: Stars and Planets, Galactic Centre and Black Holes, Resolved Stellar Populations and High Redshift Universe, each being closed by an open discussion. On the second day there was also a session on instrumentation and observing techniques. All presentations are available from the workshop web page[1].

In addition to covering the key, well-established E-ELT science cases and instrument studies, the presentations and discussion sessions included themes that had not been covered in depth previously, such as opportunities for high-impact science from high-precision astrometry, polarimetry and high-time-resolution observations.

Overall, the workshop was perceived as being very lively and interesting. It provided very valuable input to the E-ELT project on its way to completing the detailed design phase by the end of 2010.

Acknowledgements

The organisers would like to thank Samantha Milligan for logistical support. They are also most grateful for support by the European Community within the frame of the FP7 grant (Contract INFRA-2.2.1.28) European Extremely Large Telescope Preparation.

Links

[1] http://www.eso.org/sci/facilities/eelt/science/drm/workshop09/

Report on the ESO Workshop

Imaging at the E-ELT

held at ESO Garching, Germany, 29 May 2009

Magda Arnaboldi[1]
Sandro D'Odorico[1]

[1] ESO

The aim of this one-day workshop, part of the FP7-funded programme to prepare for the European Extremely Large Telescope, was to bring together members of the community working on wide-field imagers on 4–8-metre-class telescopes and on instruments and science cases related to imaging at the E-ELT, exploring complementarities and synergies between the two communities.

The workshop was organised as part of the FP7 programme "Preparing for the construction of the European Extremely Large Telescope (E-ELT)", within the Work

Package 6000 “Networks of Nodes of Expertise”. The goal of the network “Wide Field Imaging at the E-ELT; from GLAO to diffraction limit” is to identify the parameter space of the upgrade path in the area of wide-field imaging (WFI) at the E-ELT, within the framework set by the scientific requirements and the E-ELT instrument studies already in place. Using WFI at the E-ELT we intend to go beyond those applications that require very high Strehl ratios on single sources over a very small field, such as those required, for example, by the imaging of planets. The workshop followed the three-day workshop on the E-ELT Design Reference Mission and Design Reference Science Plan (Hook et al., p. 51). The programme and presentations are available at the workshop web page[1].

The workshop covered four main topics: the current WFI projects on 4–8-metre-class telescopes; the performance and limitations for E-ELT imaging; the current plans for wide-field imaging at future large telescopes, including the expected performance in imaging of the US Thirty Metre Telescope (TMT) and the James Webb Space Telescope (JWST); and a dedicated session on future prospects with imaging at the E-ELT.

WFI projects on 4–8-metre-class telescopes

The first session covered the overview of the current status of the existing wide-field imagers, up to 8-metre-class facilities, the requirements for current instrumentation and the scientific goals. Gavin Dalton presented a brief overview of the Visible and Infrared Survey Telescope for Astronomy (VISTA) system, information on the commissioning process, and an outline of the public surveys that form the major part of the first phase of VISTA science operations (see also Arnaboldi et al., 2007, for a presentation of the ESO public survey projects). VISTA is a 4-metre wide-field telescope with a 1.7-degree field of view 64 Mpix infrared camera (see Emerson et al., 2006, for a more extensive overview).

A stimulating overview of the Hyper-Suprime Cam (HSC) project was given by Satoshi Miyazaki from the National Astronomical Observatory of Japan. HSC is the Subaru next generation wide-field camera. This project represents the upgrade of the 10-year-old (and very successful imager) Suprime-Cam (SC) on the Subaru 8.2-metre telescope. The goal is to expand the field of view (FoV) to 1.5 degrees in diameter, while maintaining the same image quality as for SC in *r*-, *i*-, *z*-, *Y*-bands. It implies that the instrumental point spread function (PSF) is less than 0.4 arcsecond full width at half maximum (FWHM) and could reach even higher quantum efficiencies for the CCD detectors in the red. These constraints are set by the weak-lensing survey requirements, which aim at taking full advantage of the excellent image quality and the wide FoV.

Roberto Ragazzoni reported on the Large Binocular Telescope (LBT) wide-field imager project, the commissioning of the cameras and early science results. These 23 × 23 arcminute cameras can image simultaneously in ultraviolet and in optical wavelengths with peak performance of 0.4 arcsecond FWHM in the *U*-band and 0.5 arcsecond FWHM in the *V*-band. The high throughput enables a limiting magnitude of 25.6 AB mag in the *Z*-band in 3 hours exposure. There are now more than 20 papers either submitted or accepted coming from the early science with LBT imaging.

The transition to discussing imaging with the next generation telescopes was laid by the scientific overview of Jarle Brinchmann on the deep extragalactic imaging surveys and the expectations of the new facilities. In his comprehensive overview, Brinchmann outlined the dramatic advances in extragalactic research in the last couple of decades, and how deep imaging has been essential to this evolution. A comprehensive overview of deep fields is available[2]. The strong evolution in extragalactic research is expected to continue in the coming decades with the development of very wide-field imagers on 8-metre-class telescopes as well as wide-field imagers on the next generation of 30–40-metre-class telescopes. It is clear that a major advance for these large telescopes is in their improved spatial resolution over limited field of view (FoV), which will be of major interest for a wide range of extragalactic research fields. With current-day adaptive optics (AO) technology it is unlikely that this kind of instrument will reach a large enough FoV to become a true survey instrument. Brinchmann argued that a camera with a lower order AO correction, but much larger FoV than those currently foreseen would be of significant scientific interest for deep extragalactic surveys and as a fast imager of faint transient phenomena, as high-*z* supernovae and gamma-ray bursts. The current evaluation that emerges from a comparison in mapping speed with HSC on Subaru at optical wavelengths and NIRSPEC on JWST indicates that an imager with a FoV of 15 arcminutes on the side, sensitive from 0.35–1.5 μm and designed to take advantage of higher order AO correction with 50 % ensquared energy in 0.1 arcseconds at ~ 1 μm would be an ideal match; see Figure 1 for an illustration of such effective synergies.

The performance and limitations of E-ELT imaging

This session included an overview of AO simulations at the E-ELT by Miska Le Louarn and a presentation by Gavin Dalton on the detectors for imaging — optical and near-infrared (NIR), with a forward-look towards technology developments that may have significant impact on the feasibility of wide-field imaging with ELTs. Le Louarn presented in particular the results of simulations for Ground Layer Adaptive Optics (GLAO). The goals of GLAO are to improve the seeing on a “wide” FoV, rather than reaching the diffraction limit, by correcting for the atmospheric turbulence averaged on many natural stars and/or laser guide stars. “Wide” field in this case means fields from 5 to 7 arcminutes. Simulations in the *K*-band show that there can be up to 50 % gain in image quality with respect to the natural seeing with three natural guide stars (NGS). The need for three NGSs and constraints on their magnitudes restrict the sky coverage to about 50 %; this may improve with higher efficiencies and fainter stars. The sky coverage can increase by using three laser guide stars, but this imposes more load on the operational aspects of GLAO.

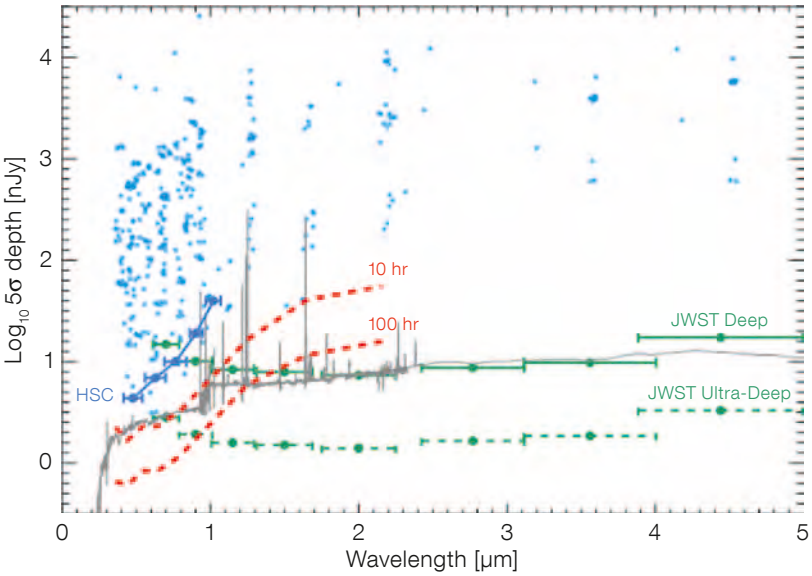

Figure 1. The depth of extragalactic fields as a function of the wavelength of observation. This is contrasted with the nominal goals of the JWST Deep and Ultra-Deep surveys (in green, from Gardner et al., 2006), as well as the depth one might be able to reach with an 8-metre-class telescope in 50 hrs, here represented by HSC (blue). This is compared with a typical spectral energy distribution of a star-forming galaxy at $z = 1.5$ (in grey), normalised to the JWST Deep target depth at 2 μm. Note that while such a star-forming galaxy will be easily detected in the near-infrared by JWST, it will be fainter in the optical than an 8-metre-class telescope is expected to reach in 50 hrs. However in 10 hours with the E-ELT it will be possible to detect it in the optical (upper red dashed line) and a 100-hour exposure with the E-ELT will complement the depth of the JWST Ultra-Deep field in the optical (lower red dashed line). From J. Brinchmann's contribution to the FP7 report of the Network "Wide Field Imaging at the E-ELT; from GLAO to diffraction limit".

Plans for imaging with the next generation telescopes

Luc Simard presented an overview of the instrument suite being developed for the TMT and Simon Lilly gave a presentation on the status of the James Webb Space Telescope and the NIRCAM camera. In the case of TMT, there are two instruments that work in the visible and are seeing-limited, the Wide Field Optical Spectrometer (WFOS) and the High resolution Optical Spectrometer (HROS). The FoV of the former is 40.5 arcminute^2. The gain in this case is a factor 14 with respect to 8-metre-class telescopes, while it becomes 200 for high-contrast AO observations of unresolved sources, but still allows the scientific cases such as intergalactic medium tomography and the stellar archeology in the local Universe to be pursued. The AO-driven imagers, like IRIS and the Planet Formation Instrument (PFI), are targeting 15 × 15 arcsecond FoV and 2-arcsecond radius, respectively.

Imaging at the E-ELT

MICADO, described by Renato Falomo, is the imaging camera for the multi-conjugate adaptive optics system for the E-ELT. The goal of the consortium building MICADO (PI Reinhard Genzel) is to design a simple and robust instrument that can address as much of the primary NIR science as possible, in time for first light at the E-ELT. MICADO will work from 0.8 to 2.5 μm, and cover a FoV of 53 × 53 arcseconds. The pixel scale is 3 milliarcseconds (mas), with a PSF FWHM of 6 mas (*J*-Band) and 10 mas (*Ks*-band). Main scientific drivers for the instrument design are the Galactic Centre, the study of the resolved stellar population beyond the Local Group and the study of galaxy morphology in the high redshift Universe. The multi-conjugate adaptive optics (MCAO) module for the E-ELT is MAORY, and Paolo Ciliegi discussed the results of PSF simulations. The FoV of MAORY is 150 arcseconds in diameter, and it can support the diffraction limit (DL) requirement of MICADO very well. Ciliegi commented that if the target area for a wide-field imager on the E-ELT is 5 × 5 arcminutes, then the technology required is GLAO, and one moves away from the diffraction-limited MCAO space. Olivier Le Fevre showed the wide-field imaging possibilities with OPTIMOS, which envisages a 7 × 7 arcminute FoV, with wavelength coverage from 0.37 to 1.4 μm, and 0.05-arcsecond pixels. This instrument is primarily a multi-object spectrometer using up to 500 multi-slits in the optical and 170 in the NIR. Operation of such an instrument is foreseen in natural seeing or GLAO.

In addition to the technical presentations, two short contributions on science cases with the E-ELT were also included: one on the resolved stellar populations in the Virgo cluster by Magda Arnaboldi and the other on resolved starburst clusters near and far, by Andrea Stolte.

Prospects

The scientific programme of the one-day workshop ended with a lively discussion on the prospects for imaging with the E-ELT and the role of an imager covering the full scientific field of the telescope. While it became clear that the instrument suite at first light would aim to exploit the largest advantage in terms of sensitivity with respect to an 8-metre-class telescope and JWST, i.e. operation at the diffraction limit over fields less than 1 arcminute, the outcome of this one-day workshop indicates that GLAO is a promising technique. If successfully implemented over a FoV of several square arcminutes, it would naturally complement the first light instrument suite of the E-ELT and the capabilities of JWST, even if the latter retains a performance advantage because of the reduced sky background.

References

Arnaboldi, M. et al. 2007, The Messenger, 127, 28
Emerson, J., McPherson, A. & Sutherland, W. 2006, The Messenger, 126, 41
Gardner, J. et al. 2006, Spa. Sci. Reviews, 123, 485

Links

[1] http://www.eso.org/sci/facilities/eelt/fp7-elt-pub/wfi_workshop/index.html
[2] http://www.strw.leidenuniv.nl/~jarle/Surveys/DeepFields

ESO at the XXVIIth IAU General Assembly

Lars Lindberg Christensen[1]

[1] ESO

The General Assembly of the International Astronomical Union (IAU) is held every three years and is one of the largest astronomical conferences in the world. The XXVIIth General Assembly was held this year in Rio de Janeiro in Brazil from 3 to 14 August and had 2109 registered attendees from all around the world. It is the first time that an IAU General Assembly has been held in Brazil. In the last decade, astronomy in Brazil has experienced a period of major growth and development triggered by significant investments from the Brazilian government. The astronomical community has grown to almost 200 astronomers and in 2008 they were responsible for nearly 2 % of the total number of astronomical scientific papers in the world, which is impressive for a developing nation.

More than 50 ESO staff including the Director General, Tim de Zeeuw, attended various parts of the two-week-long meeting. On the science side the participants attended six Symposia, sixteen Joint Discussions and ten Special Sessions and heard a balanced mix of review talks and cutting-edge presentations. On the outreach and press side ESO had an impressive exhibition stand (see Figure 1), and the IAU Press Office and the office for the International Year of Astronomy 2009 were also staffed partly by ESO personnel. The Press Office hosted more than 80 members of the press, mainly from Brazil, and more than 50 interviews were set up.

At the ESO stand it was decided to host a social event on some of the afternoons. The *ESOHour* quickly became quite an attraction (see the lower photograph on the Astronomical News section page, p. 46). One can only guess whether the popularity was due to the impressive display of large ESO pictures or the supply of great Brazilian food and drink ...

Five Resolutions were approved by vote at the Closing Ceremony of the General Assembly including a decadal plan for the global development of astronomy called "The Strategic Plan: Astronomy for the Developing World", which is seen as a successor to the International Year of Astronomy 2009.

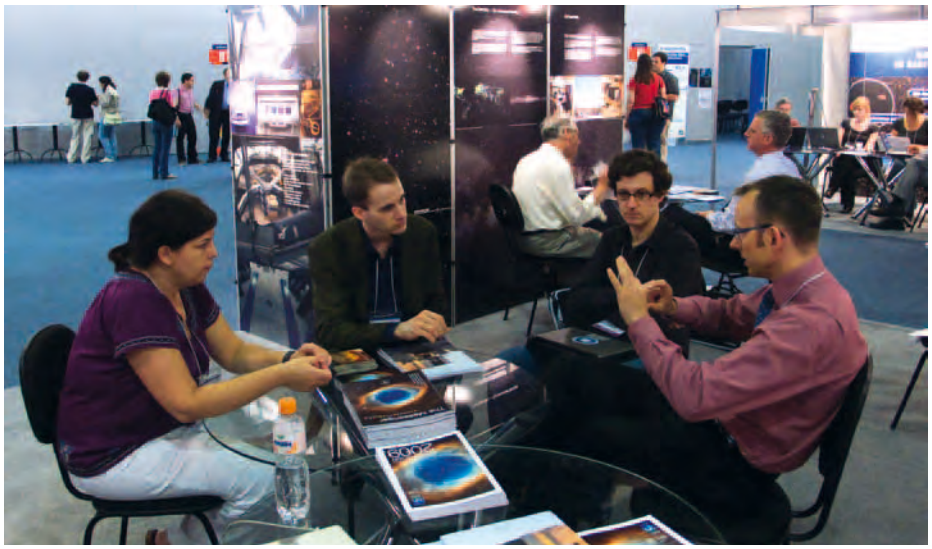

Figure 1. The ESO stand at the IAU General Assembly was often a focal point for intense discussions and meetings.

The IAU General Assembly was embraced by the local authorities and media, and the resultant press coverage was impressive (see Figure 2). Several of the articles and television programmes featured ESO's telescopes prominently. Director General Tim de Zeeuw for instance appeared on the Brazilian national evening news programme *Jornal Nacional* with a long segment about the E-ELT (see the upper photograph on the Astronomical News section page, p. 46). *Jornal Nacional* is seen by between 40 and 50 million viewers.

Figure 2. The IAU General Assembly and ESO were also visible in the Rio streets. Large signs were posted in the Maracanã football stadium during the Sunday game, and advertisements for parallel outreach events (shown here presenting ALMA) were posted on billboards on the pavement.

Report on the

2009 ESO Fellows Symposium

held at ESO Garching, Germany, 8–10 June 2009

Eric Emsellem[1]
Michael West[1]
Bruno Leibundgut[1]

[1] ESO

The fourth ESO Fellows Symposium took place in Garching from 8–10 June 2009. This year's symposium brought together 28 ESO Fellows from Chile and Germany to meet their colleagues from across the ocean, discuss their research and provide feedback on ESO's Fellowship programme. This year's symposium also included training workshops to enhance the practical skills of ESO Fellows in today's competitive job market.

Like many international organisations, ESO has a geographically distributed staff separated by thousands of kilometres. Regular scientific exchanges between ESO offices in Germany and Chile are essential to bridge physical and cultural differences, and to ensure that the two sites work together as a coherent organisation. The ESO Fellows Symposia are an important component of this effort, bringing together Fellows from Chile and Germany to share their research, stimulate new scientific collaborations, build personal connections and discuss issues of common interest. These biennial gatherings originated from a desire, expressed by past Fellows, to have a more unified Fellowship programme.

The 2009 Fellows Symposium took place at ESO Headquarters in Garching. During the three-day event, each Fellow gave a 20-minute overview of his or her current research interests and activities. These presentations covered many areas of modern astrophysics — both observational and theoretical — and spanned the electromagnetic spectrum from gamma rays to radio waves. A number of staff astronomers, students and visitors from ESO Garching also attended the talks, curious to learn more about the Fellows' research. Many of these talks were followed by numerous questions from interested participants.

An important new component of this year's symposium was the inclusion of training workshops to aid the career development of ESO Fellows. These workshops, led by experts from outside ESO and organised with the help of ESO's Human Resources department, focused on three important areas: job interview skills; time management strategies; and techniques for giving effective presentations. The information and insights gleaned from these training sessions, which included opportunities to practice what was learned, will undoubtedly prove useful for Fellows as they compete for jobs and pursue careers at observatories, universities or elsewhere in the future.

Social interactions have always been a key part of the ESO Fellows Symposia, and this year was no exception. Coffee breaks and lunches provided opportunities for Fellows to get to know each other better in an informal setting, and the highlight was an enjoyable Symposium dinner at the famous Ratskeller restaurant, located on Marienplatz in the heart of Munich. As the evening finished and the final goodbyes were said, thoughts were turning already to the next ESO Fellows Symposium, which should take place in Santiago in 2011.

Participants at the 2009 ESO Fellows Symposium in Garching.

Report on the

2009 Joint Observatories Science Retreat in Chile

held at Hotel de la Bahia, La Serena, Chile, 9–10 July 2009

Michael West[1]

[1] ESO

In Chile, an old tradition has been revived with a new twist. Recently, more than 50 astronomers from ESO, ALMA, Gemini, CTIO, Las Campanas and SOAR participated in a two-day Joint Observatories Science Retreat that was held in La Serena. The goal of this event was to bring together astronomers from all the major international observatories in Chile to share their science, to discuss common interests and to stimulate new research collaborations.

Chile is home to many of the world's leading astronomical observatories, including ESO's La Silla Paranal Observatory and the Atacama Large Millimeter/submillimeter Array (ALMA). In the past, the international observatories in Chile held regular meetings, usually focused on specific scientific topics. Unfortunately, such meetings ceased several years ago and consequently an important opportunity for observatory astronomers in Chile to interact with each other was lost. Today, despite their relative proximity, many observatory astronomers in Chile do not know their neighbours at the other observatories.

With the goal of increasing scientific interactions between the observatories, representatives from ESO, Gemini, and the Cerro Tololo Inter-American Observatory (CTIO) worked together to organise a unique gathering of observatory astronomers from across Chile. More than 50 astronomers — nearly one third of them from ESO — participated in a two-day science retreat held 9–10 July at the Hotel de la Bahia on La Serena's scenic main beach. In the spirit of making this a special meeting of the observatories, distinct from other meetings that bring together the wider astronomical community in Chile, participation was limited to observatory astronomers only.

The 2009 Joint Observatories Science Retreat featured ten-minute talks in which each participant described his or her research interests and ongoing projects, plus thirty-minute talks by observatory directors (among them Andreas Kaufer from ESO and Thijs de Graauw from ALMA) with the latest news from the observatories. The breadth and depth of the research activities being pursued by observatory astronomers in Chile were impressive, as were the many exciting developments reported by the observatory directors.

Yet perhaps even more important than the presentations were the opportunities for observatory astronomers to meet and chat informally. Social activities included a welcoming cocktail party, ample time for lunch and coffee breaks each day, and a conference dinner at one of La Serena's seaside restaurants, where the seeds of future research collaborations were planted in the company of new friends, fine food and good wine.

This gathering of kindred spirits also attracted media attention in Chile, with the country's two largest newspapers publishing articles that noted the benefits of social networking as a way for observatory astronomers to share information with their neighbours.

The 2009 Joint Observatories Science Retreat was a great success, with a strong consensus among participants that they should be continued in the future. Plans are already underway for the 2010 meeting, which will take place in Santiago and hence should allow for an even greater degree of participation by ESO and ALMA astronomers.

Credit: H. Ochoa and L. Opazo/CTIO

Participants at the 2009 Joint Observatories Science Retreat in La Serena, Chile

News from the ESO Science Archive Facility

Nausicaa Delmotte[1]
(for the ESO archive team)

[1] ESO

The latest developments from the archive are presented. Information is provided to the astronomical community on new data releases and services.

PI data packages

ESO Principal Investigators (PIs) can retrieve their raw data online while the data are still protected during their proprietary period. It is now possible to retrieve, in addition to the raw science files, the corresponding data package containing raw and master calibrations, science data products and ancillary information (processing logs, excerpts from the relevant observing logs, etc.). PI data packages containing this additional content are available for VLT/VLTI service mode runs active in P83 (the current period) and beyond. To obtain earlier or other raw data that are still covered by the proprietary period, PIs may use the normal ESO archive request form[1].

This online service[2] requires authentication through the ESO User Portal (Tacconi-Garman, 2007) for evaluation of the user credentials. Documentation and Frequently Asked Questions about this newly released service are also available online.

New data releases

The July release of the X-shooter Commissioning data includes a total of 4594 files collected over 24 nights split into four commissioning periods. The first two commissioning runs were with the UV-B and VIS-R arms only, while the third and fourth runs were with the UV-B, VIS-R and NIR arms.

Public HARPS data packages produced by the automatic HARPS pipeline developed by the Observatoire Astronomique de l'Université de Genève were released in June through the ESO Science Archive Facility. Each data package consists of a number of related files: an extracted and flat-fielded 2D spectrum; an extracted, flat-fielded, de-blazed, wavelength calibrated and order merged 1D spectrum; cross-correlation function; integrated guiding image (when available); and 1D bisector. The packages cover the first six years of operation (2003–2008). As a comparison, the initial release in January 2008 consisted of packages covering the first four years of HARPS operations (2003–2006). No modifications were made to the original release packages from the 2008 release.

The VIMOS imaging data release version 1.0 of the Great Observatories Origins Deep Survey (GOODS) was released in April. This data release, covering the Chandra Deep Field South, contains the co-added images in *U*-band from the ESO Large Programme 168.A-0485 (PI Cesarsky) which had been obtained in service mode observations between mid-2004 and late 2006. Also included in this data release is a co-added image in *R*-band obtained from data retrieved from the ESO archive. A full description of the data reduction steps can be found in an accompanying publication (Nonino et al., 2009).

Contact

For more information about the ESO archive, the new data releases, or to subscribe to the archive RSS feed in order to be informed about the latest archive developments, see the archive web page[3]. For any questions or comments on the ESO archive, contact us at archive@eso.org.

References

Nonino, M. et al. 2009, ApJS, 183, 244
Tacconi-Garman, L. E. 2007, The Messenger, 130, 54

Links

[1] http://archive.eso.org/eso/eso_archive_main.html
[2] http://www.eso.org/requestHandler/pipacks
[3] http://archive.eso.org/

Corrigendum

In the Report on the ESO Workshop on Wide-Field Spectroscopic Surveys by Melnick et al. in the last issue of *The Messenger* (No. 136, p. 64-68), there were a couple of errors in the paragraph concerning exploitation of Gaia data (p. 66, right hand column).

Gaia was conceived from the beginning as an astrometric instrument with both a multi-colour photometer and a low dispersion slitless spectrograph.

The telescopes on Gaia are 1.45 m × 0.5 m (not ~ 50 cm diameter) and will allow radial velocities to be measured for stars brighter than V = 17 mag.

The HERMES survey on the AAT will not routinely obtain spectroscopy of the fainter (V ≳ 15 mag) Gaia sources.

Fellows at ESO

Silvia Leurini

I studied physics at the Universita' di Cagliari, in sunny Sardinia, where I was raised, but I was soon fascinated by astronomy, probably because I found it, and still do, the most romantic and philosophical branch of physics.

I then moved to Bonn, where I obtained my PhD under the supervision of Karl Menten at the Max-Planck-Institut für Radioastronomie. During this period I started working on massive star formation, mostly through spectroscopic observations at millimetre wavelengths. Thanks to this, I gathered extensive observational experience and visited beautiful countries with millimetre-wavelength telescopes, such as Spain, Hawaii and Australia. I finished my PhD at the end of 2004, when the APEX project was in its final commissioning phase. Therefore I decided to stay in Bonn as a postdoc and took part in the APEX project. I was so fascinated by the Atacama desert and by the challenge of working at 5000 m altitude to observe at high frequency, that in 2006 I decided to stay in Germany, despite the weather, and took up a fellowship at ESO in Garching in order to be directly involved in the next project in the Atacama, ALMA.

Since arriving in Garching I have continued my work in star formation, but I have expanded my studies to shorter wavelengths. For my functional work I joined the ESO ALMA team as European User Support specialist for the Common Astronomy Software Applications (CASA) package. I also had the unique opportunity to work at the ALMA Test Facility in New Mexico on testing of the ALMA prototype antennas.

ESO offers an incredibly stimulating scientific atmosphere with many seminars and lively discussions at morning coffee. The diversity of research carried out by ESO researchers is something that will be hard to match anywhere else. I will be sad to leave Garching behind, but I am excited about moving on to the next chapter of my career. I will join the Max-Planck-Institut für Radioastronomie in Bonn as a staff member — back to a research institute where radio astronomy is not an exception!

Masayuki Tanaka

I did my undergraduate studies at the Tohoku University, which is in the northern part of the main island of Japan. After that, I moved to the University of Tokyo to start my PhD there. My thesis research focused on observations of distant galaxy clusters using the Subaru 8.2-metre telescope. After receiving my PhD, I moved to Germany and started my first postdoc at ESO.

This is the first time I have worked at an international institute. I am quite impressed by the wide range of science covered at ESO and the neighbouring institutes, and I find ESO a very stimulating environment. It is great to have so many seminars and visitors every week in Garching. Soon after arriving at ESO, I started new collaborations with people at ESO and the local institutes.

I have continued to work on galaxy clusters, but the focus has shifted to high redshift clusters, particularly those at $z > 1$. When I started my fellowship, I could not imagine that I would be working on $z \sim 2$ galaxies. The VLT has excellent instruments for this work, and I am fortunate to have access to the VLT to further my science.

I am a VLT user, and, at the same time, I am a VLT astronomer. I am one of the relatively few Garching fellows who are brave enough to take up functional duties on Paranal and I have spent quite a bit of time on the mountain. Paranal is an amazing place in many respects — beautiful sunsets with the green flash, an amazing night sky, world-leading telescopes, hard-working people, scary earthquakes, incredibly sweet desserts at the cafeteria, etc., etc.. It is great experience for me to operate the VLT for so many nights.

Later this year, I will go back to Tokyo to take a small step forward in my career. I am very excited to move on to the next chapter in my life. But it will be sad to leave the Biergartens behind, but my friend told me that there is an Oktoberfest in Tokyo. I shall wear Lederhosen and say "Prost" in Tokyo!

Announcement of the ESO Workshop

Galaxy Clusters in the Early Universe

9–12 November 2009, Pucón, Chile

Galaxy clusters at high redshifts provide important constraints on cosmological parameters, such as the dark energy equation of state, the amplitude of the power spectrum of primordial density fluctuations from which structure on all scales arose, and the amount of dark matter in the Universe. Moreover, high-redshift clusters also serve as unique laboratories for studying environmental influences on galaxy formation and evolution in the early Universe. Consequently, the search for distant galaxy clusters is a very active field at present, with the number of known high-redshift clusters or proto-clusters increasing rapidly.

The goal of the four-day workshop is to bring together theoreticians and observational astronomers working at different wavelengths to summarise the current state of knowledge of galaxy clusters at redshifts $z > 1$. Among the topics that will be discussed are:

1. Cluster evolution over a Hubble Time
2. Numerical simulations and semi-analytical models of cluster formation and evolution
3. Techniques for finding clusters at early epochs
4. Multi-wavelength views of clusters and their constituents
5. High-z clusters as cosmological probes

The conference will be held in Pucón, a picturesque town in the Lakes region of Southern Chile. Pucón is situated on the shore of Lago Villarrica, within sight of the volcano of the same name. Numerous national parks, glaciers, rivers, lakes and mineral springs are all close by.

The deadline for registration and abstract submission is 30 September 2009.

Scientific Organising Committee: Felipe Barrientos (Pontificia Universidad Católica de Chile), Gabriella De Lucia (Osservatorio Astronomico di Trieste), Michelle Doherty (ESO), Alastair Edge (University of Durham), Gus Evrard (University of Michigan), Percy Gomez (Gemini Observatory), Marc Huertas (ESO), Leopoldo Infante (Pontificia Universidad Católica de Chile), Tadayukiu Kodama (National Astronomical Observatory of Japan), Chris Lidman (Oskar Klein Centre, Stockholm), Simona Mei (Observatoire de Paris-Meudon), George Miley (Leiden University), Emanuela Pompei (ESO), Kathy Romer (University of Sussex), Piero Rosati (ESO), Ricardo Schiavon (Gemini Observatory), Alice Shapley (University of California, Los Angeles), Adam Stanford (University of California, Davis and IGPP) and Michael West (ESO).

More information is available at the conference website http://www.eso.org/sci/meetings/GCEU2009/.

Announcement of the ESO Workshop

The Origin and Fate of the Sun: Evolution of Solar-mass Stars Observed with High Angular Resolution

2–5 March 2010, Garching, Germany

The goal of the workshop is to review recent results on solar-mass stars obtained with infrared and millimetre interferometers, and to discuss their importance for our understanding of stellar evolution from star formation to stellar end products. The workshop will concentrate on the mass range from approximately 0.5 to 2 solar masses and discussions will centre on what new results for one stage of stellar evolution imply for the next stage. One of the aims is to bring interferometric results into the context of our knowledge based on other observational techniques, and with theory. The workshop will also include prospects for second generation instruments at the VLTI and with ALMA. Interferometry experts and non-interferometrists alike are welcome to attend the workshop, bringing together different perspectives.

More details can be found at http://www.eso.org/sci/meetings/stars2010/.


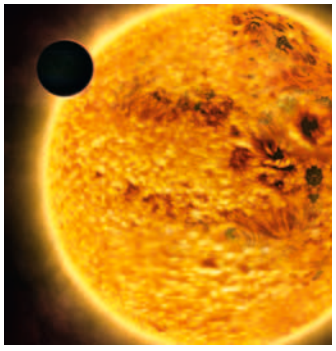
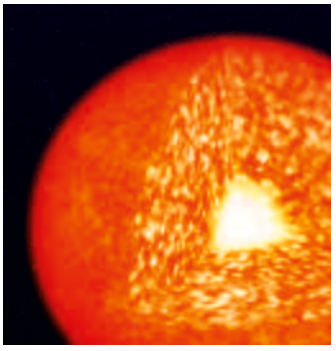


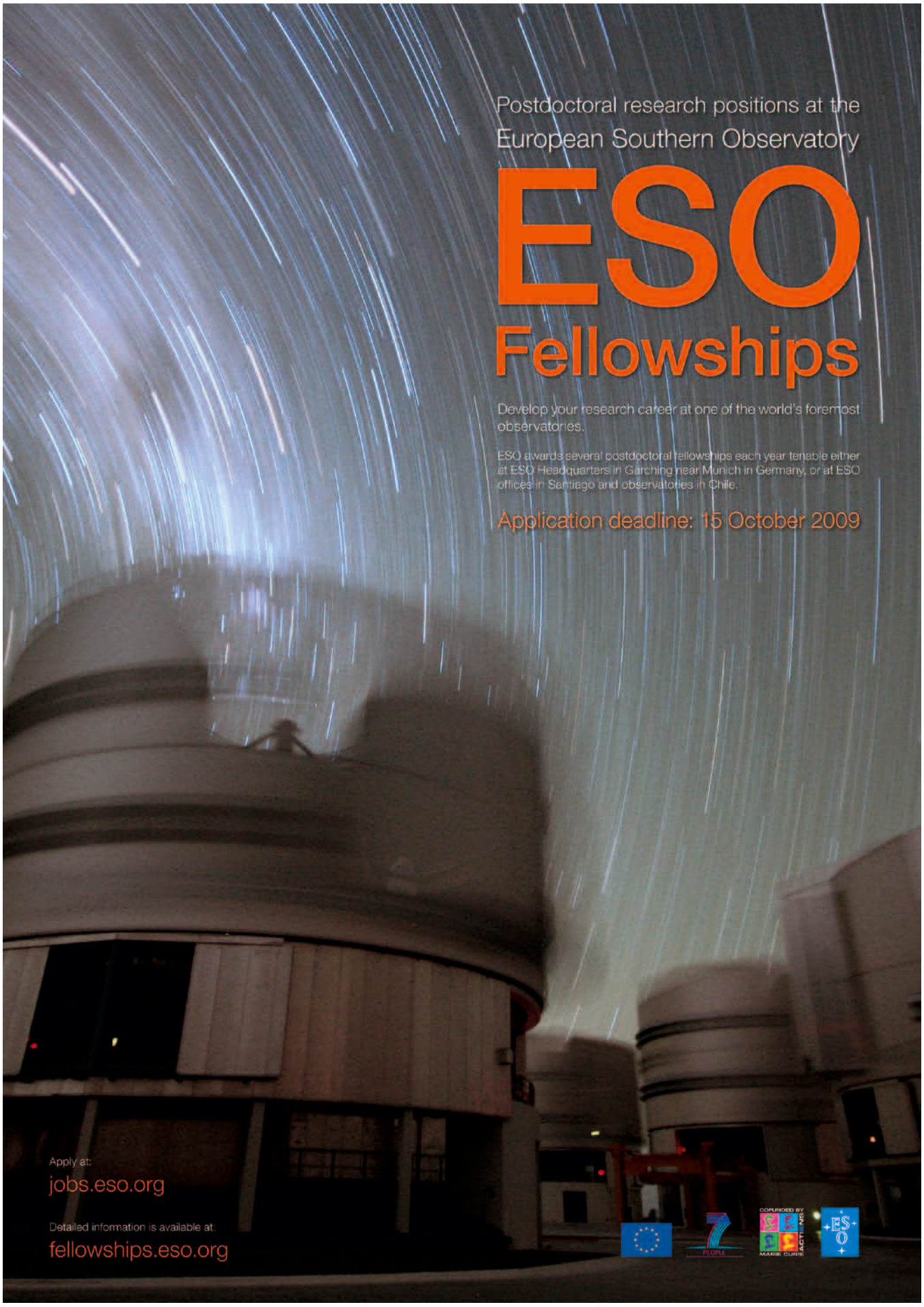

Credit: G. Lombardi/ESO


Postdoctoral research positions
ESO ALMA Fellowships
Develop your research career and gain experience in mm and sub-mm astronomy with ALMA at the beginning of its operations.
With ALMA becoming operational soon, ESO awards ALMA Fellowships – funded by the Marie-Curie COFUND Programme of the European Community. The selected candidates may choose to work at one of the European institutes hosting an ALMA Regional Centre node (Bologna, Bonn, Grenoble, Leiden, Manchester, Onsala), or at ESO in Garching, and enhance their research in close contact with ALMA experts.
Applications deadline: 1 November 2009
Apply at:
jobs.eso.org
Detailed information is available at:
fellowships.eso.org
PEOPLE
MARIE CURIE ACTIONS
ESO

ESO and EDP Sciences Sign New Contract for *Astronomy and Astrophysics*

A new contract for the publication of the scientific journal *Astronomy and Astrophysics* (A&A) was signed on 29 May 2009 with EDP Sciences (EDPS) by Tim de Zeeuw, ESO Director General, and Jean-Marc Quilbé, Managing Director of EDPS, at ESO Headquarters. "It is a great pleasure for the Board to announce that the contract for the production of A&A from January 2010 has been signed at ESO with EDP Sciences. Thus, for a renewed period, EDPS will continue as the publisher of A&A," said Georges Meynet, Chairman of the Board of Directors of A&A. The Board is in charge of managing the journal. It consists of representatives of A&A's 23 member countries plus ESO, which has handled the legal matters of A&A since the journal was established in 1969.

Tim de Zeeuw, ESO Director General, (left) is shown signing the contract for A&A publication in the presence of, from left to right, Jean-Marc Quilbé, Managing Director of EDP Sciences, Georges Meynet, Chairman of the Board of Directors of A&A and Klaas de Boer, Vice-Chairman of the Board of Directors of A&A.

"*Astronomy & Astrophysics* is owned by and operated for the astronomical community, and it is important that we make sure that we have the best available publisher for the journal," said Tim de Zeeuw. "EDPS is excited to be continuing as the publisher of this major journal of astronomy, which is an important vehicle for the dissemination and archiving of high quality science results," said Jean-Marc Quilbé.

Personnel Movements

Arrivals (1 July–30 September 2009)

Europe	
Bhatia, Ravinder (GB)	System Engineer
Bramich, Daniel (GB)	Astronomer
Correia, Joana (P)	Certified Accountant
De Silva, Malcolm (GB)	Contract Officer
Gerlin, Francesca (I)	Student
Gonzalez, Oscar (RCH)	Student
Humphreys, Elizabeth (GB)	ARC Astronomer
Ives, Derek (GB)	Engineer
Kotamäki, Miikka (FIN)	Mechanical Engineer
Montironi, Katia (I)	Administrative Assistant
Oliveras, Ester (E)	Accountant
Rino, Bruno (P)	Software Engineer
Schleicher, Dominik (D)	Fellow
Tischer, Helmut (D)	Software Engineer
Van Der Swaelmen, Mathieu (F)	Student
Young, Peter (AUS)	Software Engineer

Chile	
Acuña, Margarita (RCH)	Administrative Assistant
Di Cesare, Maria Alejandra (RA)	Operations Astronomer
Emmerich, Alejandra (RCH)	Secretary
Girard, Julien H. V. (F)	Operations Astronomer
Patru, Fabien (F)	Fellow
Sánchez-Janssen, Rubén (E)	Fellow
Siringo, Giorgio (I)	Operations Astronomer
Snow, William (USA)	System Engineer
Wagg, Jeffrey (CDN)	Fellow

Departures (1 July–30 September 2009)

Europe	
Böcker, Michael (D)	Safety Engineer
Castro, Sandra Maria (BR)	Software Engineer
Chen, Kuan Chung (TW)	Unpaid Associate
Chereau, Fabien (F)	Software Engineer
Christensen, Lise Bech (DK)	Fellow
Dietrich, Jörg (D)	Fellow
Eder, Brigitta (A)	Student
Galametz, Audrey (F)	Student
Jaffe Ribbi, Yara Lorena (VE)	Student
James, Gaël (F)	Fellow
Kammermaier, Katharina (D)	HR Officer
Leurini, Silvia (I)	Fellow
Monnet, Guy (F)	Senior Astronomer
Stanke, Thomas (D)	Fellow
Ventimiglia-Werner, Giulia (I)	Student
Zheng, Zheng (CN)	Student

Chile	
Cortes, Jose Ignacio (RCH)	Telescope Instruments Operator
Miranda, Jorge (RCH)	Telescope Instruments Operator
Molina, Faviola (VE)	Operations Astronomer
Molina, Juan (RCH)	Driver
Saldias, Antonio (RCH)	Safety Officer

ESO, the European Southern Observatory, is the foremost intergovernmental astronomy organisation in Europe. It is supported by 14 countries: Austria, Belgium, the Czech Republic, Denmark, France, Finland, Germany, Italy, the Netherlands, Portugal, Spain, Sweden, Switzerland and the United Kingdom. ESO's programme is focused on the design, construction and operation of powerful ground-based observing facilities. ESO operates three observatories in Chile: at La Silla, at Paranal, site of the Very Large Telescope, and at Llano de Chajnantor. ESO is the European partner in the Atacama Large Millimeter/submillimeter Array (ALMA) under construction at Chajnantor. Currently ESO is engaged in the design of the 42-metre European Extremely Large Telescope.

The Messenger is published, in hardcopy and electronic form, four times a year: in March, June, September and December. ESO produces and distributes a wide variety of media connected to its activities. For further information, including postal subscription to The Messenger, contact the ESO education and Public Outreach Department at the following address:

ESO Headquarters
Karl-Schwarzschild-Straße 2
85748 Garching bei München
Germany
Phone +49 89 320 06-0
Fax +49 89 320 23 62
information@eso.org
www.eso.org

The Messenger:
Editor: Jeremy R. Walsh
Design, Layout, Typesetting:
Jutta Boxheimer
www.eso.org/messenger/

Printed by Peschke Druck
Schatzbogen 35, 81805 München
Germany

ISSN 0722-6691

Contents

Front Cover: The edge-on spiral galaxy NGC 3190 (Hubble type Sa at a distance of 22 Mpc) is shown in a VLT FORS1 colour composite formed from images in *B*, *V*, *R* and *I* filters. This galaxy had two supernovae in 2002, SN2002bo (an unusual Type 1a) and SN 2002cv (a heavily dust-obscured but otherwise normal Type 1a supernova). See ESO Press Photo 17/06 for more details.